Title
Ion Transport and Limiting Current in Conventional and Novel Polymer Electrolytes

Author
Hoffman, Zachary

Publication Date
2023

Peer reviewed|Thesis/dissertation

Ion Transport and Limiting Current in Conventional and Novel Polymer Electrolytes

By

Zachary Hoffman

A dissertation submitted in partial satisfaction of the

requirements for the degree of

Doctor of Philosophy

in

Chemical Engineering

in the

Graduate Division

of the

University of California, Berkeley

Committee in charge:

Professor Nitash P. Balsara, Chair
Professor Bryan D. McCloskey
Professor Naomi S. Ginsberg

Summer 2023

Ion Transport and Limiting Current in Conventional and Novel Polymer Electrolytes

Abstract

Ion Transport and Limiting Current in Conventional and Novel Polymer Electrolytes

By

Zachary Hoffman

Doctor of Philosophy in Chemical Engineering

University of California, Berkeley

Professor Nitash P. Balsara, Chair

Lithium-ion batteries are essential for the decarbonization of our power generation systems and electrification of the transportation sector. Their popularity stems from their impressive characteristics, including high energy density, low rates of self-discharge, and high cell voltage. However, the performance of these batteries is starting to reach a plateau. To enable the next generation of lithium-ion batteries, high energy electrodes such as lithium metal and silicon anodes are needed. Conventional battery electrolytes, consisting of a lithium salt dissolved in mixtures of organic solvents, are unstable against these electrode materials. A compelling alternative comes in the form of polymer electrolytes, which offer enhanced safety and greater chemical stability.

This dissertation focuses on understanding ion transport within polymer electrolytes, including a conventional polymer electrolyte and novel polymer electrolytes. Full electrochemical characterization, following Newman's concentrated solution theory, allows for the measurement of transport parameters that provide a full description of ion transport in an electrolyte. Using concentrated solution theory, predictions of salt concentration profiles can be made. These are useful for understanding the conditions under which an electrolyte can stably operate. With higher amounts of current applied to an electrolyte, salt concentration gradients can grow until the salt is depleted at the cathode. The current density at which that occurs is known as the limiting current, which is an important parameter to judge the practical limitations of an electrolyte and its utility in battery systems.

Chapters 2, 3, and 4 present studies on ion transport in a conventional homopolymer electrolyte, LiTFSI salt dissolved in poly(ethylene oxide) (PEO). These works build on our understanding of ion transport in a model system that has been well characterized. In Chapter 2, the ion transport properties of PEO/LiTFSI electrolytes are measured across a wide range of salt concentration at three temperatures of interest. Included in this work is a

full description of the experiments and calculations required for full electrochemical characterization. The dependence of the ion transport properties on temperature varies with each property, and thus predicting the effect of temperature on overall performance is impossible without the results of our full characterization study. Chapter 3 provides a comparison of salt concentration profiles predicted from concentrated solution theory with those measured using *operando* Raman spectroscopy. In Chapter 4, theoretical predictions are made of electrolyte performance at current densities above the limiting current density and are compared to experimental measurements.

Chapters 5 and 6 focus on potential next-generation polymer electrolytes. PEO has been the benchmark polymer electrolyte material since its discovery, and it is of utmost importance to discover new polymers for battery electrolytes. In Chapter 5, the dependence of the limiting current density on electrolyte thickness is measured for a conventional and a single-ion-conducting block copolymer. Chapter 6 presents the results of full electrochemical characterization of a novel homopolymer electrolyte, and these results are compared to those of PEO electrolytes.

"We are on Earth to take care of life. We are on Earth to take care of each other."

- Xiye Bastida

Contents

List of Figures

List of Tables

Acknowledgments

I want to express my deep appreciation for my advisor, Nitash Balsara. Nitash, you taught me so much about polymers, electrochemistry, and how to be an independent researcher. Your passion for science is contagious, and the joy you get from working with the group has continued to inspire me. Through the many challenges I have faced over my studies, you supported me and advocated for me fervently, sometimes more than I was able to. The culture you have created within your group is incredibly special, and I think this reflects not only on your ability to assemble an amazing group of researchers but also how you treat them.

During my time in the Balsara Lab, the post-docs have been essential to keeping the group running smoothly, both scientifically and culturally. Hee Jeung, while we overlapped for only a short time, I was impressed by your kindness, positivity, and scientific drive. Youngwoo, you were one of the hardest workers I've seen during my graduate studies. You balanced work and family, all while being present for many group activities. Louise, you have been one of my biggest mentors, and I can never repay the limitless advice and perspective you have offered me. Your presence was felt everywhere in the group: providing scientific input, leading the charge on happy hours, checking in with group members to make sure everyone was included and taken care of, and of course the amazing food and drinks you shared with us. Xiaopeng, you were a passionate researcher and brought a lot of energy to lab social events. Saheli, you have been a constant source of scientific knowledge and support, and your selflessness with your time has helped so many people push their projects forward. While much of the work and effort you put into the group may not have been noticed by all, there were times where it felt like you were single-handedly keeping the group afloat. David, I have always been inspired by your insightful questions and wealth of knowledge in many different research spaces. You have always been happy to help with anything in lab, and you've never shied away from participating in whatever adventures the group undertakes. Jaeyong, you've been a close friend and collaborator towards the end of my time in the group. Your work ethic never ceases to amaze me with your long hours (typically preceded or followed by major social events). You are a fast learner and always eager to help. It has been such a pleasure working closely with you, and I wish you the best in whatever you decide to do after your post-doc.

Deep, you were an important mentor to me inside and outside of the lab. I appreciate how quick you were to befriend me and your willingness to offer your time and knowledge to me. My first few years would never have been as fun without you. Jackie, your dedication to detailed and careful science is something that the rest of the group could only strive to match. Your joy and kindness made me feel welcome in the group, and I will always appreciate that. Whitney, you were a dedicated leader in our group who was never afraid to take on responsibility. I was always impressed with your leadership skills, and I'm confident they are serving you well in your own research group. You were one of the hardest workers

in the group, while also never forgetting the importance of having fun.

Gumi, you brought so much positivity and joy to any event you were a part of, and you never had any trouble bringing up the energy of the group. You provided great advice whether it was about science or getting through graduate school. Mike, you are an incredible scientist and innovator, and one of the smartest people I know. You were quick to speak of the successes of others before your own, but your intelligence, passion, and abilities are unmatched. I look forward to the many successes and accomplishments that await you in your future.

Kevin, you are a great runner, teammate, baker, collaborator, mentor, and friend. I couldn't have asked for a better lab mate to share B33 with. There was never a dull moment going through graduate school with you, and I'm thankful we were able to spend as much time together as we did. Lorena, you were a friend to everyone in the lab and provided more support than you probably ever realized. You were never afraid to step up when someone needed to be a leader. I was constantly impressed with your ability to balance work and your many leadership roles, and how you always took whatever life threw at you in stride.

I will always be grateful that I was able to spend all 5 years of my Ph.D. with my fellow Balsara Boys. I couldn't imagine anyone else I would have rather gone through this journey with. Alec, I've enjoyed all the time we spent together, between Edwards house, our many climbing sessions, happy hours, frisbee, and countless adventures throughout the bay. Our friendship has been a pillar of my grad school experience, and you've always been someone I can go to for advice or to vent about the many annoyances of grad school. Neel, you are a caring friend and always ready to lend a hand. Your ability to always find something to laugh about has brought a lot of joy during my time at Berkeley. You are someone I could always go to when I was feeling overwhelmed or down.

Darby and Morgan, I feel confident that you both will continue to be excellent leaders in the lab as you finish your time at Berkeley. Darby, your dedication to effectively communicating the deeper meaning of your results has been inspiring. I've enjoyed our conversations about electrochemistry, book club, and life. While you never joined us full time in B33, I always appreciated your visits. Morgan, you've had such a strong presence in our group, and I've really respected how good you are about calling people out for their own benefit. You're a natural leader, and I hope you'll continue to stay true to your values.

Karim, you've had to overcome some difficult challenges already and your resilience has been admirable. You have challenged me to look at the world in new ways, and our conversations have always given me new insights and perspectives. Some of your music tastes will always puzzle me, but I hope you continue to follow your own path, no matter what. Vivaan, you have exceeded all my expectations for a fellow Georgia Tech graduate. Your dedication to science has been apparent to everyone around you, and I'm sure it will serve you well in

the future. You have kept the welcoming spirit of our lab alive and well, and the younger students are lucky to have your leadership.

Emily, you've shown strong leadership skills that will only grow with time, and I'm glad you joined our squad in B33. I'm sure you will continue to make the group an enjoyable environment to work in. Lily, you're quickly becoming familiar with many systems and techniques in our lab, and I look forward to the future work you will accomplish. Michael, you have clearly demonstrated an aptitude and dedication to research during the time you have been in the lab. I have no doubt that your future work in the group will be impressive. I've appreciated our time playing, watching, and talking about soccer.

I had the great opportunity to mentor an undergraduate researcher, Sean, who was a pleasure to work with. You were dedicated to the work, and I was impressed with how self-sufficient you became during your time in our lab. I look forward to your many future accomplishments.

I learned a lot from my collaborators outside of the group. Without Dr. Madeleine Gordon and Prof. Jeff Urban, the work in Chapter 3 would not have been possible. Dr. Aashutosh Mistry and Prof. Venkat Srinivasan have been indispensable to our lab and have helped deepen our fundamental understanding of ion transport. It has been a privilege to work with you. I'd also like to acknowledge the tremendous amount of administrative support that Joseph Nolan and Carlet Altamirano have provided over my time at Berkeley.

I am extremely grateful for the people I have lived with during my Ph.D. Justin and Kwasi, I enjoyed our year living together a lot, and I'm glad we've continued to stay friends even after I "abandoned" you. I hope your final year of graduate school is enjoyable, and I'm looking forward to future reunions. I could not have asked for better people to share my time at Edwards house with than Alec, Francis, Josh, Matt C., Nathan, and Zach. You all have been some of my closest friends at Berkeley, and graduate school wouldn't have been nearly as fun without all of you.

I'm thankful for my friends outside of Berkeley for their support and love over the years. Austin, Connor, Liz, Matt F., Sydney, Andy, Chris, Listya, and Sree, you all have been there for me time after time throughout the years. Your encouragement has helped me stay motivated, and I will always be appreciative of your constant loyalty.

I would like to thank my family; without them I would not be who I am today. Mom and Dad, you have supported me no matter what, and you've have always pushed me to be the best I can be. You both have provided me with endless guidance and perspective, and your insights have helped me overcome countless challenges over the years. Ben, your texts throughout my Ph.D. have always helped me feel closer to home, even if I don't always respond. Thank you for all the help you've given me over the years. Anna, thank you for the advice and support you've given me. Our conversations have been of great help at challenging times during my Ph.D.

Lastly, I would like to thank my partner, Julia. You have been my biggest advocate, and your positivity and joy have always brightened my day, no matter how down I am. I'm so grateful for all the memories we've made together and all those to come.

1: Introduction

1.1 Motivation

Our planet is currently experiencing a significant rise in temperatures, at a rate of 0.2°C per decade. Projections indicate that global temperatures will surpass 1.5 °C above preindustrial levels by 2037.[1,2] This rise in global temperatures can have cataclysmic effects on our planet, including the melting of ice sheets and glaciers, widespread damage to forests, extreme weather events, and destruction of coral reefs.[3–7] While we can only estimate the extent of global warming and the effects it will have, the risks to our planet and our species are substantial. Although there is geopolitical momentum to address these risks, changes in administrations along with a lack of actionable plans from some nations paints a grim picture for our future.[8–10] Therefore, it is imperative to develop technical solutions to tackle the global emissions problem.

In recent years, approximately 50% of global CO_2 emissions have been attributed to the electricity generation and transportation sectors.[2,11] Effective implementation of energy storage solutions can significantly reduce emissions in these sectors. In the transportation sector, the use of energy storage solutions such as batteries eliminates the need for fossil fuel combustion, resulting in substantial emissions reductions.[12] While renewable energy sources are being integrated into our power grid, they may not always meet short-term power demands. This challenge can be addressed by employing grid-level energy storage solutions, which, when combined with renewable energy sources, can result in up to 90% emissions reductions depending on location.[13,14] Lithium-ion batteries are the most common energy storage solution used today, including in electric vehicles. This is primarily due to their exceptional energy density, low self-discharge rates, and high cell voltage. However, to enable the broader use of electric vehicles and effective integration of batteries into our energy generation sector, there is a need for improved battery performance.

A typical lithium-ion battery consists of three components: a graphite anode, a transition metal oxide cathode, and an electrolyte. Conventional battery electrolytes are comprised of a lithium salt dissolved in a mixture of organic solvents within a porous separator. These electrolytes are used for their excellent performance and good contact with electrode surfaces.[15] However, their flammability poses significant safety risks in situations where a battery may be punctured or experience thermal runaway.[16] As a result, there is considerable interest in exploring alternative electrolyte materials that can replace these conventional liquid electrolytes.

1.2 Polymer Electrolytes

The study of polymer electrolytes dates back to 1973 when Fenton et al. first discovered the ability of poly(ethylene oxide) (PEO) to form stable complexes with metal salts.[17] Then in

1983, Armand et al. first discussed the potential of polymers for battery electrolyte materials in 1983.[17,18] Polymer electrolytes offer several advantages over conventional liquid electrolytes including improved safety due to their chemical stability and non-flammability.They also have the potential to inhibit the growth of lithium dendrites, which can short circuit a cell.[19–21] However, the performance of these electrolytes is not competitive with current liquid electrolytes. For instance, PEO's conductivity at elevated temperatures is an order of magnitude lower than that of liquid electrolytes at room temperature.[22,23] Despite this, the potential of polymer electrolytes is significant, driving research on polymer materials that can replace current electrolytes.

One of the major benefits of polymer electrolytes lies in their chemical stability.[20,24] This makes them suitable for use with a lithium metal or silicon anode, which can improve the energy density of a battery compared to current graphite anodes.[24–26] However, the growth of lithium dendrites remains a concern for lithium metal anodes, particularly with homopolymer electrolytes like PEO. To address this, block copolymer electrolytes combine polymers with different properties, such as good ion transport from PEO and mechanical rigidity from polystyrene or polyhedral oligomeric silsesquioxane.[27–31] While these block copolymers are briefly discussed later on, the primary focus of this work is on the study of homopolymer electrolytes.

1.3 Ion Transport

Following the work of Onsager, ion transport within a binary electrolyte can be completely described with three transport coefficients, in addition to a single thermodynamic parameter, as dictated by the Gibbs-Duhem relation.[32,33] This preliminary work by Onsager was influential, however the coefficients could not be easily measured. Newman's concentrated solution theory offers a framework to describe ion transport with experimentally determinable transport parameters.[33] These parameters are conductivity, salt diffusion coefficient, cationic transference number with respect to the solvent velocity, and thermodynamic factor. The transference number and thermodynamic factor are derived parameters requiring five separate experiments, which will be discussed later. Once the four parameters are determined, concentrated solution theory enables the prediction of salt concentration gradients within an electrolyte.[28,34] These gradients are of practical significance, and they result in concentration overpotentials. Additionally, they can lead to depletion of salt at the negative electrode or precipitation of salt at the positive electrode, ultimately resulting in cell failure.[35–37]

Conductivity measures an electrolyte's ability to transport charge, including both cations and anions. The salt diffusion coefficient provides a timescale for the relaxation of concentration gradients within an electrolyte. Three additional measurements are required to determine the derived parameters: current fraction, electric potential from concentration cells, and density of the electrolyte. The current fraction is the ratio of the steady state current and the initial

current in response to a constant potential. The electric potential from concentration cells relates salt concentration gradients to electric potential gradients in the absence of applied current or electric potential. Finally, measurements of the density of an electrolyte as a function of salt concentration are required. Upon completion of these measurements, the derived parameters can be calculated using equations developed by Newman. The cationic transference number with respect to the solvent velocity is the fraction of current carried by the cation. Different reference frames can be used to describe the transference number, but in this work, we utilize the solvent reference frame.[38,39] The thermodynamic factor measures the dependence of the mean molal activity coefficient of the salt on salt concentration. In this study, we report the methods used to complete full electrochemical characterization, and present results for PEO electrolytes along with a novel homopolymer electrolyte.

While providing a comprehensive description of ion transport in electrolytes is important, the measurements are typically conducted at small current densities that do not reflect the conditions experienced by an electrolyte within a battery. To better understand electrolyte performance at practical current densities, the limiting current must be measured. The limiting current is the maximum current density an electrolyte can sustain before the salt is depleted at the negative electrode or the solubility limit of the electrolyte is exceeded at the positive electrode.

1.4 Structure of the Dissertation

This dissertation presents measurements of ion transport properties and limiting current of polymer electrolytes.

Chapter 2 presents the full electrochemical characterization of PEO electrolytes across a range of salt concentrations and temperatures. These results are used to model salt concentration profiles within the electrolyte at the temperatures of interest, and concentration polarization was significantly larger at the lowest temperature. Chapter 3 contains a comparison of salt concentration profiles modeled with concentrated solution theory and experimentally measured using *operando* Raman spectroscopy in PEO electrolytes. The concentration polarization measured experimentally was smaller than predicted with theory. Chapter 4 includes measurements of the Sand's time of a PEO electrolyte, which are compared to those predicted using concentrated solution theory. With these values of Sand's time, the limiting current of the electrolyte is estimated. Chapter 5 investigates the limiting current measured in a conventional block copolymer and a comparable single-ion-conducting block copolymer. The limiting current of the conventional block copolymer electrolyte linearly depends on the electrolyte thickness, while the limiting current density of the single-ion-conducting block copolymer was independent of the electrolyte thickness. Chapter 6 presents the full electrochemical characterization of a beyond-PEO polymer electrolyte. We find the cationic transference number of this electrolyte is greater than in PEO, resulting significantly lower

concentration polarization within the electrolyte, and thus a lower value of the limiting current density.

2: Temperature and Concentration Dependence of the Ionic Transport Properties of Poly(Ethylene Oxide) Electrolytes*

2.1 Abstract

Even though batteries operate at different temperatures depending on their use and state of charge, little work has been done to understand the effects of temperature on the ionic transport properties of the electrolyte. The temperature dependence of these properties is important for predicting how the performance of the battery will change as a function of temperature, along with gaining fundamental insights into the underpinnings of ion transport in these electrolytes. In this study we provide the first investigation of the effect of temperature on conductivity, salt diffusion coefficient, transference number, and the thermodynamic factor of a model polymer electrolyte: lithium bis(trifluoromethanesulfonyl)imide (LiTFSI) salt dissolved in poly(ethylene oxide) (PEO). These properties were measured at 70, 90, and 110 °C. As expected, we see monotonic increases in conductivity and diffusion with increasing temperature. Additionally, monotonic dependencies on temperature were obtained for the transference number and the thermodynamic factor. One presumes that concentration polarization decreases with increasing temperature due to more rapid ion transport. We use concentrated solution theory to predict concentration polarization in lithium-PEO/LiTFSI-lithium symmetric cells and thereby quantify the effect of temperature on concentration polarization.

2.2 Introduction

Conventional lithium ion batteries use liquid electrolytes which are mixtures of organic solvents, mainly cyclic and linear carbonates, and a lithium salt. There is considerable interest in replacing organic solvents with a polymer to address issues related to energy density and safety.[19] Polymer electrolytes are stable against lithium metal; replacing the graphite in lithium ion batteries with lithium metal results in an increase in theoretical energy density.[40,41] Polymer electrolytes are also less flammable than organic solvents, improving safety.[42]

Ion transport in electrolytes is inherently complex due to the presence of two strongly interacting charged species. The thermodynamic factor and three transport parameters, conductivity, salt diffusion coefficient, and the transference number, govern ionic transport in these

*This chapter is adapted from work reported in Hoffman, Z. J.; Shah, D. B.; Balsara, N. P. *Solid State Ionics*, **2021**, 370, 115751.

systems. In spite of the commercial importance of carbonate-based electrolytes and the fact that they have been studied since 1958[43], there are few studies on the temperature dependence of the properties that govern ion transport.[23,44,45] Such studies are important for two reasons. First, batteries are operated at different temperatures based on ambient conditions and state of health of the battery.[46] Second, temperature dependent measurements provide fundamental insight that cannot be gleaned from measurements at a fixed temperature.

Mixtures of poly(ethylene oxide) (PEO) and bis(trifluoromethanesulfonyl)imide lithium salt (LiTFSI) are commonly used polymer electrolytes. While there are numerous reports of the dependence of conductivity on temperature[47–50], there is little work on the temperature dependence of the other relevant properties.[51,52] The objective of this paper is to present measurements of all the properties that affect ion transport in PEO/LiTFSI mixtures as a function of temperature

2.3 Experimental Methods

2.3.1 Electrolyte Preparation

Electrolytes for most of the measurements reported in this paper were prepared by adding LiTFSI salt (Sigma Aldrich) to 10 kg/mol PEO with a dispersity of 1.03 (Sigma Aldrich), then dissolving in tetrahydrofuran (THF). The mixtures were stirred at 60 °C until completely dissolved, dried on a hotplate for at least 12 hours to evaporate the THF, and then dried at 90 °C under vacuum to remove any residual solvent. These procedures were previously reported by our group[36,48]. Electrolytes were produced with salt concentrations of r values from 0.02 to 0.3, where r is the ratio of lithium ions to ethylene oxide moieties ($r = [\mathrm{Li}^+]/[\mathrm{EO}]$). The density of our electrolytes, ρ, was assumed to follow that previously measured in our group for PEO samples of 5 and 35 kg/mol[48,53], and was used to calculate the molar salt concentration, c, using the equation

$$c = \frac{\rho r}{M_{EO} + r M_{EO}} \tag{2.1}$$

with M_{EO} and M_{salt} being 44.05 g/mol and 287.09 g/mol, respectively. In our calculations we also use m, the molality of the electrolyte, which is calculated using

$$m = \frac{r}{M_{EO}}. \tag{2.2}$$

Values for c, ρ, and m for the range of salt concentrations of interest can be found in Reference 48.

We found that concentration cells made with 10 kg/mol PEO at 110 °C gave irreproducible results, presumably due to the liquid like nature of this polymer at 110 °C. We therefore

made electrolytes using the same process described above but with 275 kg/mol PEO for constructing these cells. Gao and Balsara have shown that electrochemical properties show no discernible dependence on molecular weight.[22]

2.3.2 Electrochemical Characterization

Preparation of electrochemical cells was done in an argon-filled VAC glovebox with water and oxygen levels below 1 ppm.

Conductivity cells were constructed by filling a silicone spacer (McMaster-Carr) with a thickness of 508 μm and inner diameter of 3.175 mm with the electrolyte and pressing a 200 μm stainless-steel shim (MTI Corporation) blocking electrode on each side of the spacer. Nickel current collectors (MTI Corporation) were attached to the cell using Kapton tape. The cells were then vacuum sealed inside aluminum laminated pouch material (MTI Corporation) before being removed from the glovebox.

The conductivity cells were annealed for 2 hours at 90 °C.The temperature was controlled with a custom built heating stage. Using a Biologic VMP3 potentiostat, ac impedance spectroscopy was performed with an amplitude of 60 mV, and a frequency range of 1 MHz to 1 Hz. After these measurements were made, the cells were brought back into the glove box for deconstruction and the final thickness of the electrolyte was measured.

The conductivity (κ) was calculated using Equation 2.3

$$\kappa = \frac{L}{R_b A_E}, \tag{2.3}$$

where L is the thickness of the separator, A_E is the electrochemically active area of the electrolyte, and R_b is the bulk resistance of the electrolyte, which is found by fitting the conductivity data to an equivalent circuit.

Lithium symmetric cells were used to perform both current fraction and restricted diffusion experiments. 508 μm thick silicone spacer material with an inner diameter of 3.175 mm was filled with electrolyte, and lithium foil (MTI corporation) of measured thicknesses ranging from 180 to 350 μm was pressed on each side of the spacer material, followed by 200 μm thick stainless steel shims. Nickel current collectors were adhered to the stack using Kapton tape. The stacks were sealed in laminated aluminum pouch material, and then removed from the glovebox.

The lithium symmetric cells were first annealed for 3 hours at 90 °C and then conditioned with 4 cycles of ± 0.02 mA/cm^2, each for 5 hours. This conditioning was performed to ensure the formation of a stable interfacial region indicated by consistent values of a cell's interfacial resistance and its potential response to each cycle. The cells were then subjected

to a constant +10 mV for 20 minutes followed by an impedance measurement and then this was repeated to observe the changes in resistances as the system reached a steady state current. This process was replicated for -10 mV, +20 mV, and -20 mV. The current fraction (ρ_+) is calculated by comparing the steady state current (i_{ss}) and the initial current density (i_0). In ideal electrolytes this relation can be simply written as

$$\rho_+ = \frac{i_{ss}}{i_0}, \tag{2.4}$$

In polymer electrolytes it is necessary to account for the potential drop cause by the electrode/electrolyte interface which results in

$$\rho_+ = \frac{i_{ss}(\Delta V - i_0 R_{i,0})}{i_0(\Delta V - i_{ss} R_{i,ss})}, \tag{2.5}$$

as developed by Bruce and Vincent[54], where ΔV is the applied potential, and $R_{i,0}$ and $R_{i,ss}$ are the initial and steady state interfacial impedance values measured using impedance spectroscopy, respectively. Practically, it is challenging to measure i_0 accurately without sufficiently fast sampling rates. Instead, we use a calculated initial current i_Ω which can be determined from easily measured parameters using

$$i_\Omega = \frac{\Delta V}{R_{b,0} + R_{i,0}}, \tag{2.6}$$

where $R_{b,0}$ is the initial resistance of the bulk. Combining Eqs. 2.5 and 2.6 gives

$$\rho_+ = \frac{i_{ss}(\Delta V - i_\Omega R_{i,0})}{i_\Omega(\Delta V - i_{ss} R_{i,ss})}. \tag{2.7}$$

At the end of the current fraction experiments restricted diffusion experiments are performed, where the cells were allowed to relax for 3 hours.[55] This relaxation of the potential in the cell can be fit to

$$U(t) = k_0 + ae^{-bt}, \tag{2.8}$$

where k_0 is the fitted offset voltage, and a and b are fit parameters. Using b, the salt diffusion coefficient can be found using the formula

$$D = \frac{L^2 b}{\pi^2}. \tag{2.9}$$

These fits are performed while increasing the lower bounds of time so that the nondimensional number α, according to

$$\alpha = \frac{Dt}{L^2}, \tag{2.10}$$

reaches a value above 0.05, as established by Thompson and Newman.[56] Concentration cells were used to measure the open circuit potential produced from the concentration gradient

between two electrolytes with different amounts of LiTFSI. The cell design was based on procedures outlined in Reference 48. 508 μm thick silicone spacer material was cut into rectangular shapes with an internal channel of about 2.5 cm by 3 mm. The silicone channels were placed on a similarly sized rectangle of nickel foil to act as a base. Electrolyte was then placed into each half of the channel, with one half always containing the reference electrolyte (r = 0.06, ln$m$ = 0.31). Lithium foil was placed on the ends of the channel, and nickel current collectors were attached to the lithium foil. A rectangle of silicone spacer material was then placed on top of the cell to maintain the construction of the cell during sealing and to help ensure there was enough pressure within the cell to prevent leakage of the electrolyte. The cells were then sealed inside laminated aluminum pouch material and brought to the temperature of interest using a heating stage. The voltage was measured until it reached a plateau, at which point the average potential was measured and recorded as the open circuit potential of that salt concentration (U).

For conductivity cells, and lithium symmetric cells, the average value of at least three measurements is reported with the standard deviation as the error bar. The error for the transference number was calculated using the equation

$$(\delta t_+^0)^2 = \left(\frac{dt_+^0}{d\rho_+}\right)^2 \delta {\rho_+}^2 + \left(\frac{dt_+^0}{d\kappa}\right)^2 \delta\kappa^2 + \left(\frac{dt_+^0}{dD}\right)^2 \delta D^2 + \left(\frac{dt_+^0}{d\frac{dU}{d\ln m}}\right)^2 \delta \left[\frac{dU}{d\ln m}\right]^2, \qquad (2.11)$$

where δt_+^0 indicates the error of the transference number, and $\delta\rho_+$, $\delta\kappa$, δD, and $\delta[dU/d\ln m]$ are the values of error for each parameter. The same general equation was used to calculate the error of the thermodynamic factor.

2.4 Results and Discussions

Figure 2.1a shows the conductivity of PEO/LiTFSI electrolytes as a function of temperature for the seven different electrolytes. Conductivity, κ, increases monotonically with temperature as expected, but this increase depends on salt concentration. It is customary to use the Vogel-Tamman-Fulcher equation to describe the temperature dependence of conductivity:

$$\kappa(T) = A\left[exp\left(-\frac{E_a}{R(T - T_g + 50)}\right)\right], \qquad (2.12)$$

where A and E_a are parameters found by fitting the experimental data, R is the universal gas constant, and T_g is the glass transition temperature of the electrolyte. The glass transition temperature of PEO/LiTFSI electrolytes was taken from the work of Perrier et al. and Pesko et al.[49,57] The lines in Figure 2.1b represent these fits, and the dependence of T_g, A, and E_a are given in Table 2.1. VTF analysis assumes that ion transport is governed by segmental relaxation and the VTF parameters quantify this relaxation. In Figure 2.1b we plot κ as a function of $1000/(T - T_g + 50)$ on a semi-log plot. These plots are linear, which is

consistent with the literature.[49,50] While the slopes obtained at different salt concentrations are similar, the intercepts are not. This implies that T_g is not the only parameter that affects conductivity. For a given value of $1000/(T-T_g+50)$ the maximum conductivity is obtained at a salt concentration of $r = 0.12$.

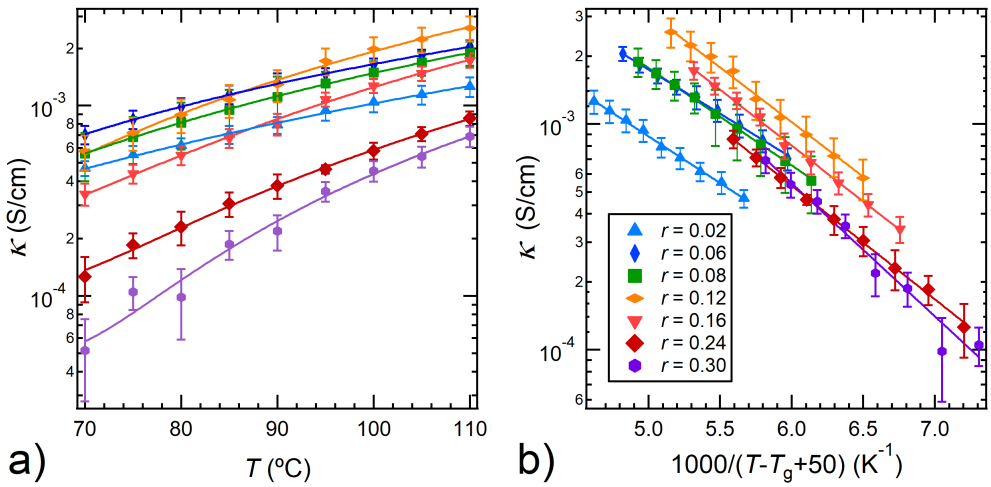

Figure 2.1: (a) Conductivity of PEO/LiTFSI electrolytes as a function of temperature, T, and polynomial fits of the data. (b) Vogel-Tammann-Fulcher plot of conductivity of the electrolytes, T_g is the glass transition temperature of each electrolyte, and it depends on salt concentration. Salt concentration, r, for each data set is given in the legend

An alternative approach for examining electrolyte conductivity was proposed by Mongcopa et al.

$$\kappa(r) = K(T)r\left[exp\left(-\frac{r}{r_{max}(T)}\right),\right] \tag{2.13}$$

where $K(T)$ is a temperature dependent constant that is related to the extent of salt dissociation, and the term within the square brackets represents frictional interactions between the salt ions and the polymer.[58] Equation 2.13 has two temperature dependent fitting parameters. It can readily be seen that the parameter relating to the frictional interactions, $r_{max}(T)$, coincides with the salt concentration at which the conductivity is maximized.

In Figure 2.2a, we plot conductivity as a function of r at different temperatures. The curves in Figure 2.2a are fits of Equation 2.13 with $K(T)$ and $r_{max}(T)$ as fitting parameters. Both parameters are linear functions of T:

$$K(T) = (9.90 \times 10^{-4})T - (3.95 \times 10^{-2}) \tag{2.14}$$

$$r_{max}(T) = (6.69 \times 10^{-4})T - (1.30 \times 10^{-2}) \tag{2.15}$$

An important parameter is the value of the maximum conductivity obtained at each temperature, κ_{max}. We use fits of Equation 2.13 to determine κ_{max} and these results are shown in Figure 2.2c. κ_{max} increases by about a factor of 3 when temperature is increased from 70 to 110 °C.

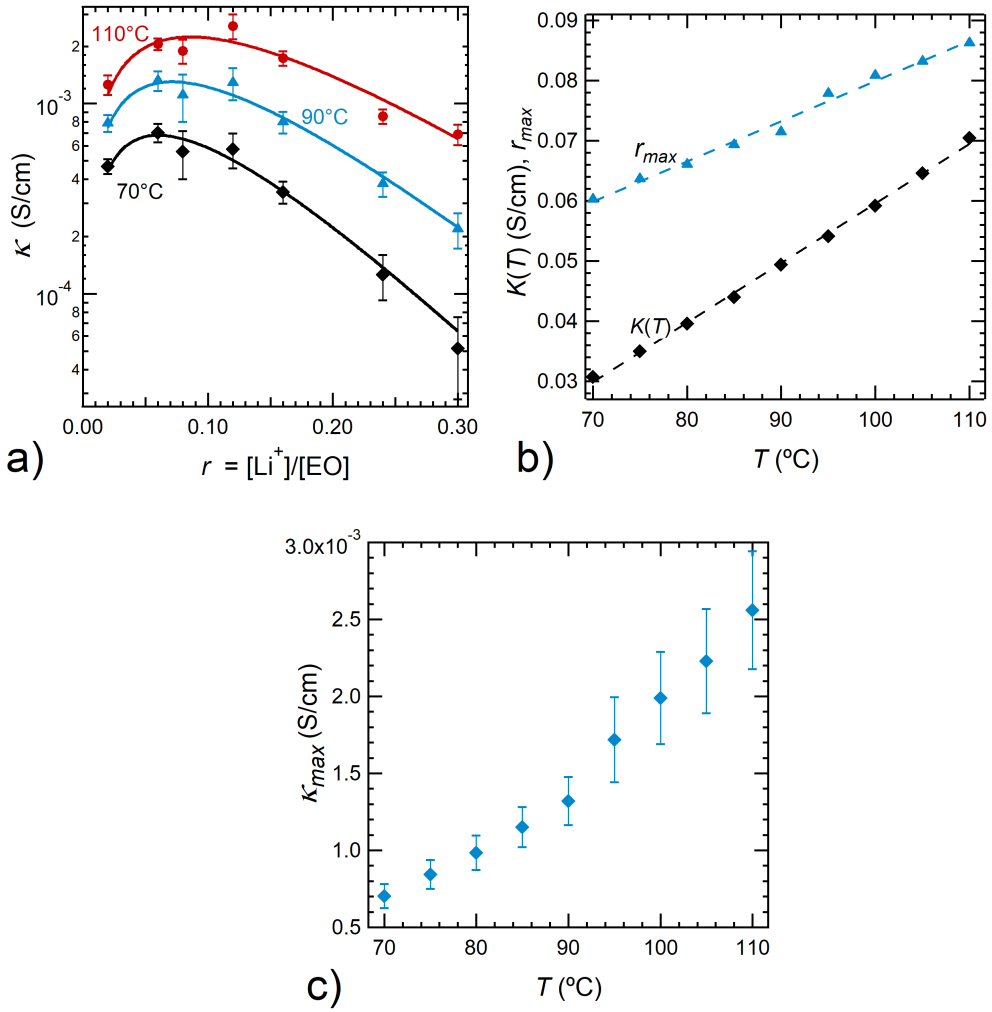

Figure 2.2: (a) Conductivity of PEO/LiTFSI electrolytes as a function of salt concentration, r, at 70, 90, and 110 °C. (b) The fit parameters $K(T)$, and r_{max} from Equation 2.13 plotted as a function of temperature. r_{max} is the salt concentration at which conductivity is maximized, and $K(T)$ is the prefactor in Equation 2.13. (c) The maximum value of conductivity, κ_{max}, plotted as a function of temperature, T.

Figure 2.3a shows the mutual salt diffusion coefficient (D) measured using restricted diffusion experiments, as a function of r and T. In general, we see that D decreases as r increases. The trend is approximately linear at all temperatures; Figure 2.3a shows linear fits through the data.

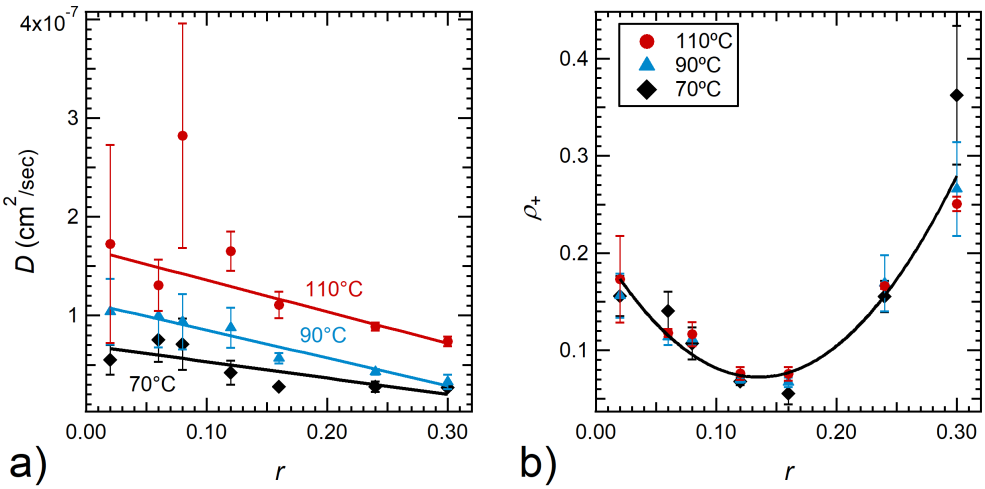

Figure 2.3: (a) Salt diffusion coefficient and (b) current fraction as a function of salt concentration, r, at 70, 90, and 110 °C. Fits of the data are included as solid lines. All the current fraction data have been fit to a single curve.

The slopes and intercepts respectively of the data are: -1.658×10^{-7} cm^2/s and 6.979×10^{-8} cm^2/s at 70 °C, -2.816×10^{-7} cm^2/s and 1.133×10^{-7} cm^2/s at 90 °C, and -3.205×10^{-7} cm^2/s and 1.679×10^{-7} cm^2/s at 110 °C.

At a given salt concentration, the diffusion coefficient increases by about a factor of 3 when temperature is increased from 70 to 110 °C. In this respect, we see similarities between the temperature dependencies of conductivity (Figure 2.2a) and diffusion coefficients (Figure 2.3a).

Figure 2.3b shows the current fraction (ρ_+) measured by the Bruce-Vincent method as a function of r and T. Unlike κ and D, ρ_+ is, to a reasonable approximation, independent of temperature between 70 and 110 °C. This is consistent with previous studies in the literature.[51,52] The curve in Figure 2.3b, is a polynomial fit through all three data sets:

$$\rho_+(r) = 7.632r^2 - 2.063r + 0.212. \tag{2.16}$$

The conductivity of an electrolyte reflects the mobility of both the cation and the anion. In most batteries, only the cation participates in the reactions occurring within the electrodes.

The symmetric lithium-lithium cell is the simplest construct to study the efficacy of an electrolyte in batteries. The ratio of the current density and the applied potential gradient can be regarded as an effective conductivity. In the limit of small applied potentials, this effective conductivity is equal to the product $\kappa\rho_+$.[33,59–61]

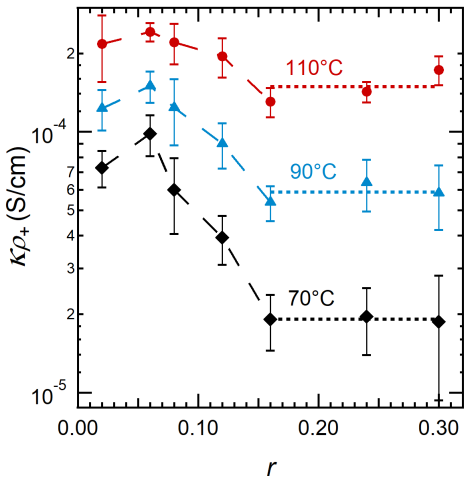

Figure 2.4: The product of the current fraction and the conductivity of the electrolytes, $\kappa\rho_+$. as a function of salt concentration, r, at 70, 90, and 110 °C. This product may be regarded as the effective conductivity in the limit of small applied potentials.

In Figure 2.4 we plot $\kappa\rho_+$ as a function of r for three different temperatures. The general features of the dependence of $\kappa\rho_+$ on r are similar at all temperatures. In the low concentration regime, $0 < r \leq 0.16$, $\kappa\rho_+$ approaches a maximum at $r = 0.06$, irrespective of temperature. Note that this salt concentration differs substantially from the salt concentration for which κ is maximized. In this low concentration regime, the decrease in conductivity with increasing salt concentration is steepest at 70 °C; $\kappa\rho_+$ at $r = 0.16$ is a factor of 5 smaller than that at $r = 0.06$. This decrease is significantly lower at 110 °C, where $\kappa\rho_+$ at $r = 0.16$ is only a factor of 2 smaller than that at $r = 0.06$. There is an abrupt change in the dependence of $\kappa\rho_+$ on r at $r = 0.16$. In the high salt concentration regime, $0.16 \leq r \geq 0.30$, $\kappa\rho_+$ is independent of r. In other words, the decrease in κ with increasing r in this regime is compensated for by an increase in ρ_+. Computer simulations have established that in the dilute limit, lithium ions are coordinated by six oxygen atoms.[62,63] At $r = 1/6 = 0.166$, all the oxygen atoms in the system are coordinated with lithium ions. It is interesting that the division between the two regimes seen in Figure 2.4 occurs at this value of r.

The final experiment required for completing the full electrochemical characterization of PEO/LiTFSI mixtures is the measurement of the open circuit potential, U, with the use of concentration cells. In these cells, a reference electrolyte with $r = 0.06$ ($\ln m = 0.31$) is

brought in contact with electrolytes of varying concentrations. It is customary to present such data on a plot of U versus $\ln m$.[64] The data obtained are shown in Figure 2.5, along with previously published data obtained from a PEO sample with a molecular weight of 275 kg/mol at 90 °C.[65] All data sets are similar: the slope of U versus $\ln m$ is small when $\ln m$ is less than zero compared to when $\ln m$ is greater than zero. We use a single 4th order polynomial to fit all the data in Figure 2.5:

$$U(\ln m) = -8.62(\ln m)^3 - 29.95(\ln m)^2 - 56.46(\ln m) - 20.56. \tag{2.17}$$

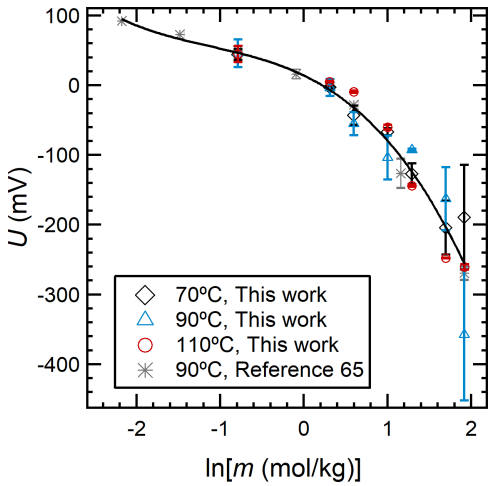

Figure 2.5: Open-circuit potential across concentration cells (U) plotted as a function of the natural logarithm of the molality of salt in the electrolyte ($\ln m$). In addition to data measured in this study, we have included data from Reference 65. All data sets were fit to a single curve shown in the figure.

Conductivity of an electrolyte can be measured in both conductivity cells (blocking electrodes) and lithium symmetric cells (nonblocking electrodes). In Figure 2.6 we compare these measurements for our PEO/ LiTFSI mixtures. The solid and dashed curves in Figure 2.6 represent fits of Equation 2.13 through these data. In general, the nonblocking conductivity is slightly lower than the blocking conductivity. At $r = 0.30$ however, significantly lower nonblocking conductivities are obtained at 70 and 90 °C. We note in passing that in many systems there are much more significant differences between blocking and nonblocking conductivities.[66]

The measurement of D, κ, ρ_+, and U as a function of salt concentration enables calculation of the cationic transference number with respect to the solvent, t_+^0, and the thermodynamic

factor, T_f, using the following equations,

$$t_+^0 = 1 + \left(\frac{1}{\rho_+} - 1\right) \frac{FDc}{\kappa} \left(\frac{d\ln m}{dU}\right), \tag{2.18}$$

$$T_f = 1 + \frac{d\ln\gamma_\pm}{d\ln m} = \frac{\kappa}{\nu RTDc\left(\frac{1}{\rho_+} - 1\right)} \left(\frac{dU}{d\ln m}\right)^2. \tag{2.19}$$

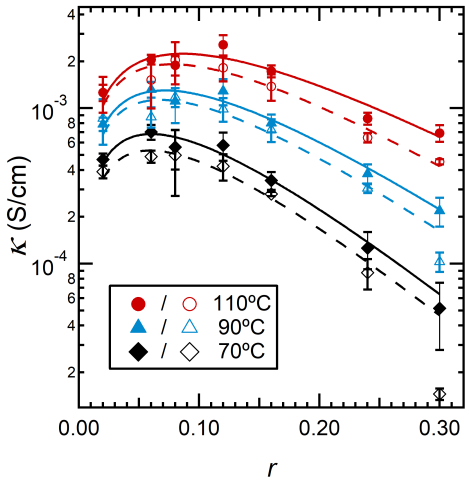

Figure 2.6: Conductivity measured with blocking and nonblocking electrodes, plotted as a function of r at 70, 90, and 110 °C. The solid curves are fits of the blocking conductivity data, represented by filled points, and the dashed curves are fits of the nonblocking conductivity, represented by hollow points.

In these equations, c is the concentration of lithium ions in the electrolyte (moles/L), and $dU/d\ln m$ is the derivative of the curve of U vs $\ln m$. We use Equations 2.13-2.17 along with the linear equations describing the diffusion coefficient noted previously to calculate the transference number and thermodynamic factor at different salt concentrations, and the results are shown in Figures 2.7a and 2.7b. The dependence of t_+^0 on r is similar at all temperatures with the minimum at $r = 0.16$, the salt concentration at which all of the oxygens in the PEO chains are coordinated with lithium. The transference number at this concentration is negative, implying the presence of negatively charged clusters, consistent with previous studies on PEO/LiTFSI.[48,65] The transference number at a given salt concentration increases when the temperature is changed from 70 to 90 °C. The same is true when changing the temperature from 90 to 110 °C, but the increase is much smaller. There are relatively few systems where the rigorously defined t_+^0 is defined explicitly. In conventional lithium-ion battery electrolytes comprising mixtures of ethylene carbonate, dimethyl

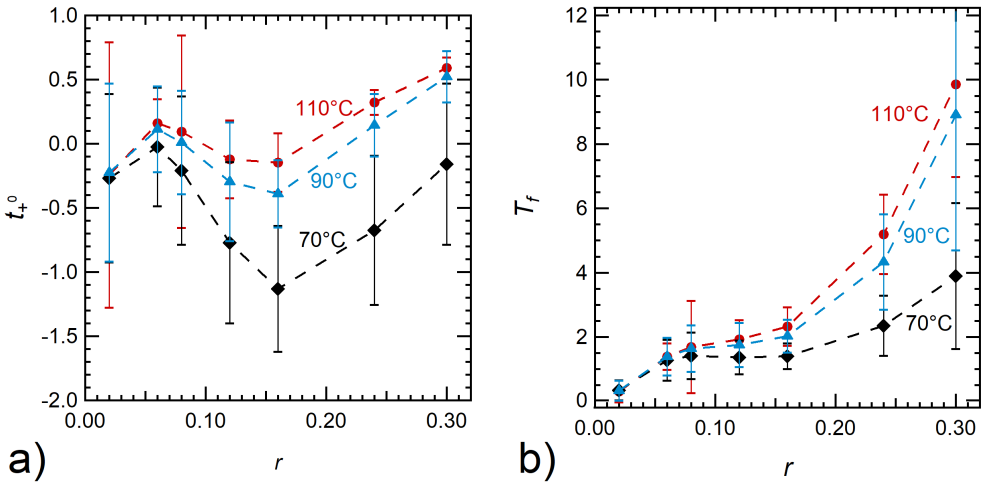

Figure 2.7: (a) Cationic transference number with respect to the solvent velocity and (b) thermodynamic factor plotted as a function of salt concentration, r at 70, 90, and 110 °C.

carbonate, and $LiPF_6$, Landesfeind and Gasteiger[23] report that t_+^0 increases with increasing temperature, while Reimers et al.[44] infer that t_+^0 is independent of temperature in mixtures of ethylene carbonate, dimethyl carbonate, and polycarbonate. T_f shows a similar temperature dependence as t_+^0, where at a given salt concentration T_f will increase as temperature is changed from 70 to 90 °C, and increase less from 90 to 110 °C.

The full characterization of an electrolyte provides information that can be used to model the salt concentration profiles inside a lithium-lithium symmetric cell as a function of applied current density, i, using concentrated solution theory.[33] We define x as the distance from the positive electrode and assume that the negative electrode is located at $x = L$, where L is the thickness of the lithium-lithium symmetric cell. The dependence of r on x is given in Reference 34,

$$\int_{r(x=0)}^{r(x)} \frac{D(r)c(r)}{r(1-t_+^0(r))}\,dr = -\frac{iL}{F}\left(\frac{x}{L}\right). \tag{2.20}$$

The dependence of D and t_+^0 are described by Figures 2.3a and 2.7a. This enables calculation of the integrand on the left side of Equation 2.20, $\frac{Dc}{r(1-t_+^0)}$. The integrand is approximated by polynomial expression,

$$\frac{D(r)c(r)}{r(1-t_+^0(r))} = ar^4 + br^3 + cr^2 + dr + e, \tag{2.21}$$

and the constants a through e are obtained by a least squares fit through the experimental data. The values of these parameters at each temperature are given in Table 2.5. We present

results for a constant current density of 0.2 mA/cm^2, and for average salt concentrations, r_{av}, of 0.065 and 0.10. Equation 2.20 is solved iteratively to obtain $r(x)$ such that the calculated r_{av} agrees with the targeted value. The results for $r_{av} = 0.065$ are shown in Figure 2.8a. Considerable concentration polarization is seen at 70 °C: $r(x/L = 0) = 0.13$, while $r(x/L = 1) = 0.02$. Increasing the temperature to 90 °C reduces the magnitude of concentration polarization, and increasing the temperature to 110 °C reduces the magnitude of concentration polarization further. The qualitative trend is not surprising as the rate of ion transport is often improved by increasing temperature. The results for r_{av} of 0.10 are shown in Figure 2.8b. Larger concentration gradients are seen in this case when compared to $r_{av} = 0.065$ at all temperatures. Increasing the temperature to 110 °C reduces concentration polarization by a factor of about 3 at $r = 0.065$ and a factor of 5 at $r = 0.10$. This is surprising because the conductivity at $r_{av} = 0.10$ is higher than that at $r_{av} = 0.065$, pointing to the importance of complete electrochemical characterization.

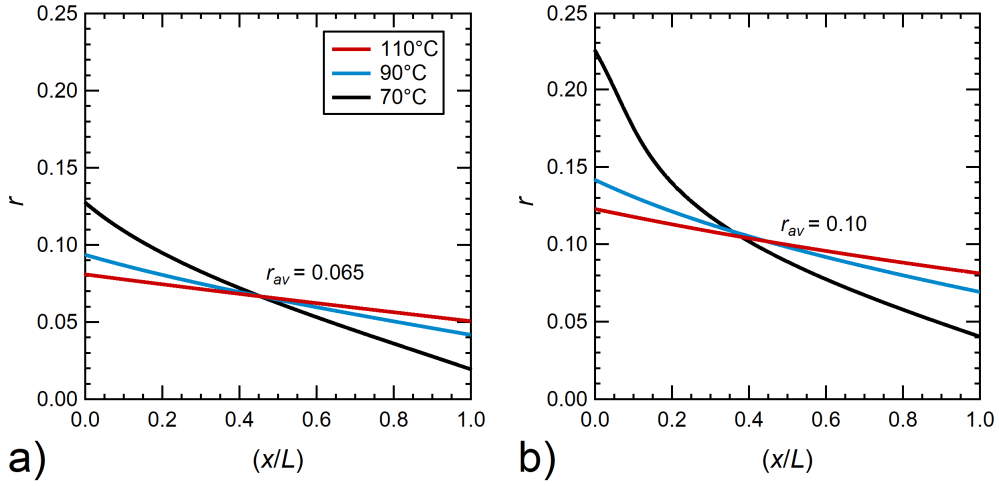

Figure 2.8: LiTFSI concentration profiles modeled using concentrated solution theory at 70, 90, and 110 °C in lithium-PEO/LiTFSI-lithium cells with average salt concentrations of (a) $r_{av} = 0.065$ (b) $r_{av} = 0.10$ at a fixed current density of 0.2 mA/cm^2. $x/L = 0$ corresponds to the anode and $x/L = 1$ corresponds to the cathode, where L is the electrolyte thickness of 500 μm

2.5 Conclusions

In this study we have performed the first investigation of the temperature effects on full electrochemical characterization of a standard polymer electrolyte: PEO/LiTFSI. The electrochemical properties, which included κ, D, t_+^0, and T_f, of these electrolytes were measured at 70, 90, and 110 °C. κ and D increase monotonically with temperature. t_+^0 shows a mini-

mum at $r = 0.16$ for all temperatures and has a monotonic dependence on temperature and a non-monotonic dependence on concentration. T_f increases with increasing salt concentration at all temperatures. We used the measured transport parameters to predict concentration polarization in symmetric lithium-lithium cells at different temperatures. We find that concentration polarization decreases by factors between 3 and 5 in our temperature window, depending on salt concentration.

2.6 Acknowledgements

This work was intellectually led by the Joint Center for Energy Storage Research (JCESR), an Energy Innovation Hub funded by the U.S. Department of Energy, Office of Science, Office of Basic Energy Science, under Contract No. DE-AC02-06CH11357, which supported characterization work conducted by Z.J.H. and D.B.S. under the supervision of N.P.B. The authors thank Louise Frenck and Kevin Gao for useful discussion related to this work.

2.7 Supporting Information

Table 2.1: Constants for Equation 2.12

Temperature	K(T)	K(T) Error	r_{max}	r_{max} Error
70	0.030714	0.00298	0.060292	0.00381
75	0.034987	0.0033	0.063643	0.00405
80	0.039574	0.00403	0.066046	0.00448
85	0.04401	0.00438	0.069334	0.00464
90	0.049425	0.00513	0.071483	0.00503
95	0.054141	0.00751	0.077843	0.00746
100	0.059221	0.00817	0.080841	0.00778
105	0.064569	0.00834	0.083199	0.00754
110	0.070448	0.00916	0.086292	0.00794

Table 2.2: Constants for Equation 2.11

r	A	A Error	E_a	E_a Error
0.02	0.1042	0.0104	7.9320	0.169
0.06	0.1566	0.0106	7.4776	0.109
0.08	0.2551	0.0139	8.2628	0.0862
0.12	0.8282	0.183	9.2822	0.337
0.16	0.7524	0.119	9.4814	0.234
0.24	0.5617	0.0418	9.6430	0.105
0.30	1.8754	0.842	11.281	0.615

Table 2.3: Glass Transition Temperatures of PEO/LiTFSI Electrolytes

r	T_g (°C)
0	-60
0.04	-56.0
0.06	-50.0
0.08	-44.9
0.095	-41.9
0.12	-36.0
0.16	-28.9
0.20	-24.7
0.24	-18.8
0.33	-9.5

Table 2.4: Salt Concentration Profile Modeling Parameters

$\frac{D(r)c(r)}{r(1-t_+^0(r))} = ar^4 + br^3 + cr^2 + dr + e$						
Temperature	$a \times 10^5$	$b \times 10^5$	$c \times 10^5$	$d \times 10^6$	$e \times 10^7$	$f \times 10^9$
70	2.894	-2.451	0.755	-0.998	0.452	0.725
90	5.097	-4.383	1.380	-1.884	0.932	0.965
110	-3.914	3.869	-1.524	3.043	-3.1467	14.325

Table 2.5: Constants for Equation 2.12 for Non-Blocking Conductivity

Temperature	K(T)	K(T) Error	r_{max}	r_{max} Error
70	0.024503	0.00203	0.059231	0.00318
90	0.045316	0.00674	0.067754	0.00675
110	0.06697	0.00757	0.07769	0.00607

2.8 Nomenclature

Table 2.6: List of Symbols and Abbreviations

Symbol	Meaning
PEO	poly(ethylene oxide)
LITFSI	lithium bis(trifluoromethanesulfonyl)imide
D	salt diffusion coefficient (cm^2/sec)
κ	conductivity (S/cm)
ρ_+	current fraction
$1 + \frac{d\ln\gamma\pm}{d\ln m}$	thermodynamic factor
t_0^+	fully defined transference number
r	molar ratio of lithium ions to ethylene oxide
L	electrolyte thickness
A_E	electrolyte area
$R_{b,0}$	initial bulk resistance of electrolyte (Ω)
$R_{b,ss}$	steady state bulk resistance of electrolyte (Ω)
$i_s s$	steady state current (mA)
i_Ω	calculated initial current (mA)
ΔV	potential drop (mV)
$R_{i,0}$	initial interfacial resistance (Ω)
$R_{i,ss}$	steady state interfacial resistance (Ω)
U	Open-Circuit Potential (mV)
a, b	fit parameters for equation 2.6
k_0	offset voltage (mV)

3: Comparing Theoretical Salt Concentration Profiles in a Polymer Electrolyte with Experimental Measurements using *Operando* Raman Spectroscopy*

3.1 Abstract

Concentrated solution theory has furthered our understanding of ion transport in electrolytes. This theory can be used to predict salt concentration profiles under an applied current if the transport properties of the electrolyte (conductivity (κ), restricted diffusion coefficient (D), and the cation transference number with respect to the solvent velocity (t_+^0), and the thermodynamic factor (T_f)) are known. In this work, we provide the first study comparing the predicted salt concentration profiles with measurements based on *operando* Raman spectroscopy. Concentration polarization is asymmetrical; the increase in salt concentration near the positive electrode is a factor of two greater than the decrease in salt concentration near the negative electrode. We find qualitative agreement between theory and experiment. Further work is needed to resolve the quantitative differences.

3.2 Introduction

There is great interest in replacing the conventional rechargeable battery electrolytes, mixtures of organic solvents and a metal salt, for the next generation of rechargeable batteries. These electrolytes provide superior performance; however their flammability provides significant safety concerns, and they are unstable against high capacity electrodes such as lithium metal.[19,67,68] Additionally, these liquid electrolytes provide no physical resistance to the growth of lithium dendrites which can grow under fast charging conditions and lead to catastrophic failure.[69–71] Polymer electrolytes have the potential to address some of the limitations of liquid electrolytes.[72]

When current is drawn across an electrolyte, salt concentration gradients will develop, resulting in depletion of salt at the negative electrode and accumulation of salt at the positive electrode.[73] These salt concentration gradients limit cell safety and performance. Theoretical models suggest that the propensity for lithium dendrite growth is accentuated by large salt concentration gradients.[74] The fastest rate of charging a cell is determined by the magnitude of salt concentration gradients. As larger values of current are drawn across the cell, these gradients grow. At a sufficiently large current, the salt concentration throughout the negative electrode is zero (or nearly so); this is defined to be the limiting current of the

*This chapter is adapted from Hoffman, Z. J.; Galluzzo, M. D.; Gordon, M. P.; Urban, J. J.; Balsara N. P. *Journal of The Electrochemical Society*, Under review.

electrolyte. Drawing currents larger than the limiting current will result in decomposition of the electrolyte and failure of the cell.

The salt concentration profile through an electrolyte at a given current density, i, can be calculated using concentrated solution theory.[28,34]. This calculation requires knowledge of three transport parameters, conductivity (κ), restricted diffusion coefficient (D), and the cationic transference number (t_+^0), along with the thermodynamic factor (T_f).[33,64]While κ can be measured by simple ac impedance experiments, determining the other 3 parameters requires considerable effort.[20,50,75] However, the performance of an electrolyte in a cell can only be predicted if all four parameters are known as a function of salt concentration.

Predictions based on concentrated solution theory have been used to explore the underpinnings of cell cycling data in several cases.[28,34,76] In typical experiments, the potential drop across the cell is measured as a function of current density. These measurements may be considered as indirect reporters of salt concentration gradients. Salt concentration gradients have been measured directly via Raman spectroscopy in some electrolytes[77–82], but they have not been interpreted in terms of concentrated solution theory. In this work we use *operando* Raman spectroscopy to determine the salt concentration profile in a polymer electrolyte at a fixed current density. The measured profiles are compared with predictions based on concentrated solution theory with no adjustable parameters.

3.3 Experimental Methods

3.3.1 Electrolyte Preparation

Poly(ethylene oxide) (PEO) with a molecular weight of 275 kg/mol (Polymer Source) and Lithium bis(trifluoromethanesulfonyl)imide (LiTFSI) (Sigma Aldrich) were dried under active evacuation for three days at 120 °C. They were then combined and dissolved in anhydrous tetrahydrofuran (THF) (Sigma Aldrich) at 60 °C in a capped vial, and then once dissolved, the cap is removed to evaporate off the THF. The electrolytes were then dried at 90 °C under active evacuation for a day to remove any remaining solvent. Preparation of electrolytes was performed in an argon-filled glovebox with water levels below 1 ppm and oxygen levels below 2 ppm. The electrolytes used in this study all have the same salt concentration, r, the ratio of lithium ions to ethylene oxide moieties ($r = [Li^+]/[EO]$). The r value chosen was $r = 0.08$.

3.3.2 Electrochemical Cell Preparation

A custom electrochemical cell was developed for these experiments and is shown below in Figures 3.4a-3.4c. Reflective tape was placed against the bottom of the cell where the electrolyte is placed to help increase the measured Raman signal. Lithium foil is then pressed against the stainless-steel electrodes and then inserted into the cell. The area of

the electrode in contact with the electrolyte is 0.035 cm^2. Then PEO/LiTFSI electrolyte is inserted between the electrodes. The channel is heated, and the electrolyte is further pressed into the channel to ensure it is filled with electrolyte. The depth of the electrolyte is 0.0875 cm, and the distance between the electrodes is 0.1 cm. The cell is then heated to 90 °C and a preconditioning cycle is applied where the cell is polarized at +10 $\mu A/cm^2$ for four hours, allowed to relax, and then polarized at -10 $\mu A/cm^2$ for four hours, then allowed to relax. These polarizations were repeated three times, and ac impedance measurements were made throughout this process to track the bulk and interfacial resistances. All the above procedures were performed within a glovebox with less than 1 ppm levels of oxygen and water.

3.3.3 Polarization Experiments

After preconditioning the electrochemical cell was sealed and removed from the glovebox. The electrochemical cell was brought to the microscope and heated to 90 °C using a custom heating stage. Throughout the initial heating and polarization experiments, an argon purge stream is used to ensure that the cell is kept free of air and water. After the cell is brought to temperature, an initial ac impedance measurement is taken, along with an initial Raman scan. Afterwards the cell is polarized with an applied current density, until the measured salt concentration profiles reach steady state.

3.3.4 Raman Measurements

The microscope used for these experiments is a WITec alpha 300 S confocal microscope with a Raman spectrometer and a UHTS-300 CCD detector. The grating used for these experiments was 1800 grooves/mm, and the laser has a wavelength of 532 nm. A Nikon E Plan lens with 20× magnification was used to focus the laser light. For each measurement point, eight 0.6 second integrations were taken. The cell was moved during measurements using a micrometer-controlled translation stage. For these experiments the cell was polarized in the x-direction (Figure 3.4), which would allow for the averaging of concentration data over both the z and y directions. However, to ensure that the intensity of the measured spectra was maximized, measurements were made at a single z value for all experiments, as deviating from this point significantly diminished the intensity of the Raman spectra. Before polarization experiments, initial Raman measurements were made to identify the z and y values for the scans that results in maximized the measured Raman signal.

For calibration curve measurements, simple stainless-steel air-free cells (Kurt J. Lesker Company) were utilized. Silicone spacer material was placed inside the stainless-steel cells and filled with electrolyte. These cells were then sealed before being removed from the glovebox. All the above procedures were performed within a glovebox with less than one ppm levels of oxygen and water. The cells were then brought to the Raman microscope and heated with a custom heating stage to 90 °C, at which point the Raman spectra was measured.

3.4 Results and Discussion

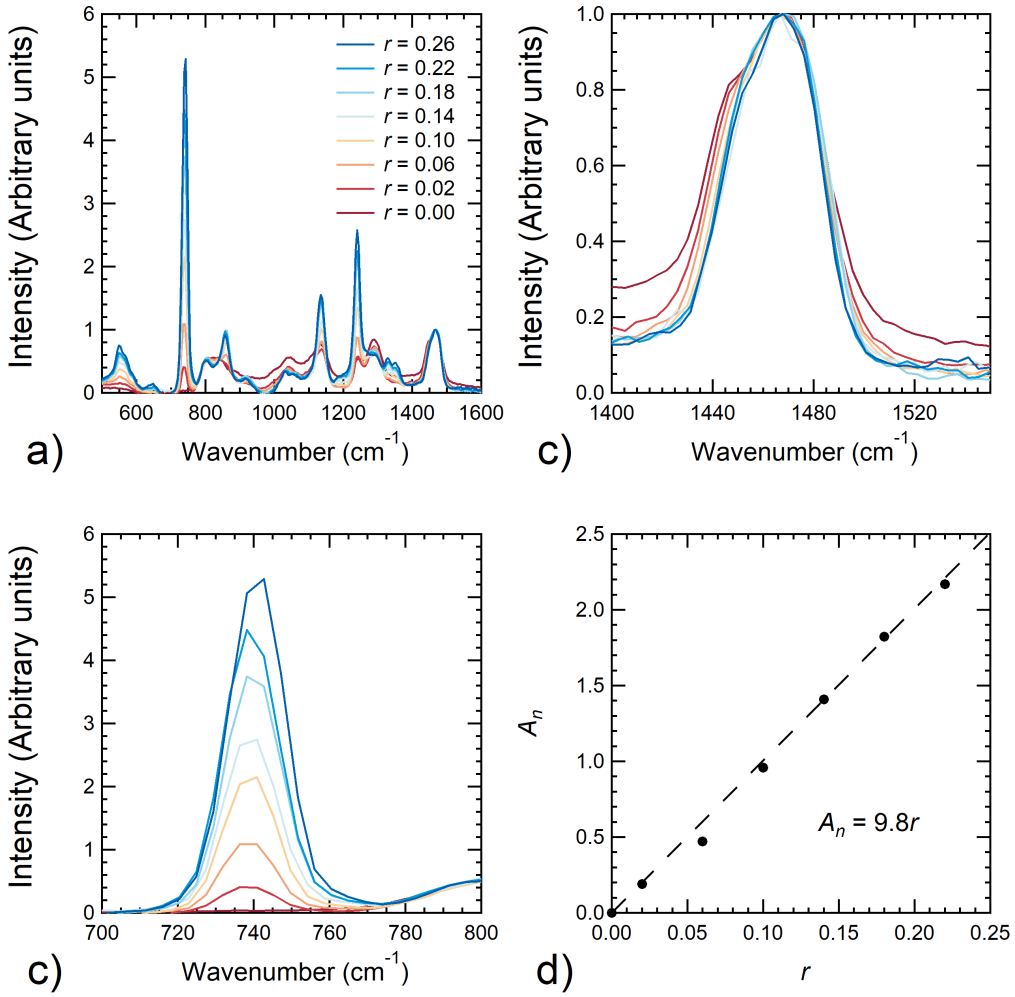

Figure 3.1: (a) Raman spectra of PEO/LiTFSI electrolytes with salt concentrations $0 \leq r \leq 0.26$, where $r = [Li^+]/[EO]$. Raman peaks corresponding to vibrations of (b) the PEO backbone, and (c) the $TFSI^-$ anion. (d) The ratio of the fitted area of the anion peak normalized by the PEO peak, plotted as a function of r. The dashed black line represents a linear fit through the data. We use this linear fit as a calibration to determine the spatial dependence of salt concentration in the *operando* Raman cell.

Previous studies have shown that Raman spectra of PEO/LiTFSI and other electrolytes are sensitive functions of salt concentration.[77,78,81–84] Our approach builds upon these studies. In Figure 3.1a the Raman spectra of PEO/LiTFSI mixtures with different salt concentrations

are shown. Due to fluorescence in the measured Raman spectra, background subtraction was required for interpreting all the measured spectra. In our work, background subtraction was performed using a Python program, following the iterative approach proposed by Lieber et al.[85] In this study, establishing the background required about 30 iterations. Figures 3.2a and 3.2b give an example of an original spectrum and the background. The background-subtracted spectra are shown in Figure 3.1a.

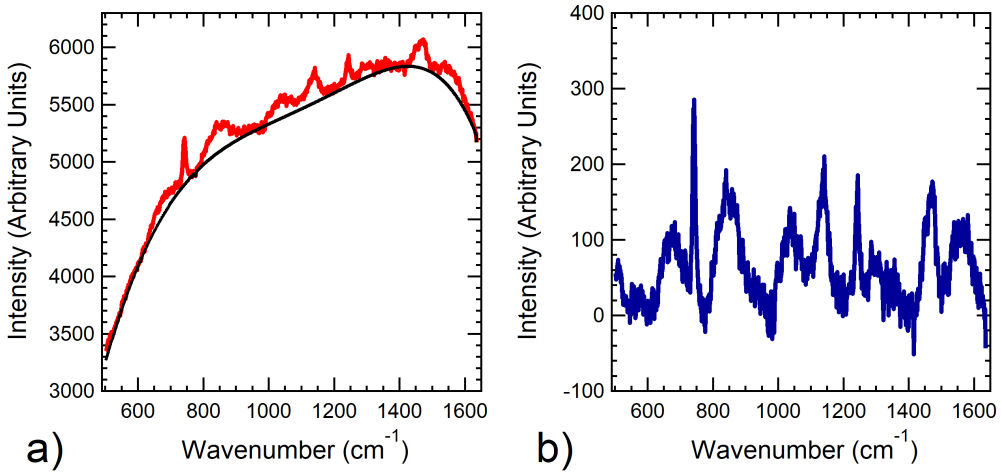

Figure 3.2: Raw Raman spectra and background subtracted spectra of a PEO/LiTFSI electrolyte. (a) The red spectrum is the raw data, the black line shows the fitted background, and (b) the purple spectrum is the background subtracted spectra similar to those shown in Figure 3.1a.

We focus on two spectral peaks, centered around 1470 cm^{-1} and 745 cm^{-1}. In the literature, the 1470 cm^{-1} peak arises from vibrations in the polymer backbone, and the 745 cm^{-1} peak arises from vibrations in the anion.[77,78,83] The 1470 cm^{-1} peak obtained at different salt concentrations is shown in Figure 3.1b, and the 745 cm^{-1} peak obtained at different salt concentrations is shown in Figure 3.1c. Figure 3.1b shows that the polymer backbone peak is a weak function of salt concentration. Figure 3.1c shows that the anion peak is strongly correlated with salt concentration. We define A_n to be the area under the anion peak normalized by the area under the polymer backbone peak.[77,78] The spectral data were fit to pseudo-Voigt functions (1400 to 1520 cm^{-1} for the polymer backbone peak and 720 to 780 cm^{-1} for the anion peak), and the peak area was determined by analytical integration of the fitted functions. An example of our fitting procedure is provided in Figures 3.3a and 3.3b. A_n is plotted as a function of salt concentration r in Figure 3.1d. A least squares linear fit through the data with the intercept held at 0 is represented by the dashed line in Figure

3.1d, $A_n = 9.8r$. We use this equation as a calibration to determine local salt concentration from *operando* Raman spectra.

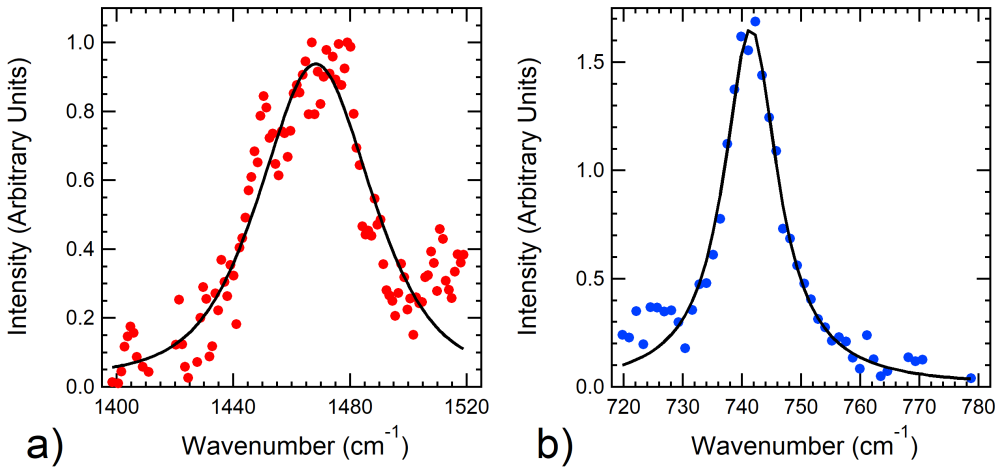

Figure 3.3: Demonstrative curve fitting using Pseudo-Voigt fits of (a) the PEO backbone and (b) the $TFSI^-$ anion.

Measuring the Raman spectra of PEO/LiTFSI electrolytes (Figures 3.1a-3.1d) is simple. However, obtaining Raman spectra in a polarized electrochemical cell required construction of a custom electrochemical cell. Most importantly, this cell required a transparent window through which the laser could pass, along with ensuring the electrodes and electrolyte remain air-free throughout the experiment. Figures 3.4a-3.4c show the electrochemical cell used in this study. The cell is made of polyether ether ketone (PEEK), and contains a channel used to flush argon through the cell during polarization, keeping it air-free. The channel holding the electrolyte and electrodes was machined separately from the base of the cell. This allowed for easy removal and cleaning between experiments. The channel holding the electrolyte is 0.1 cm thick (x-direction shown in Figures 3.4b and 3.4c), 0.4 cm long (y-direction), and 0.0875 cm deep (z-direction).

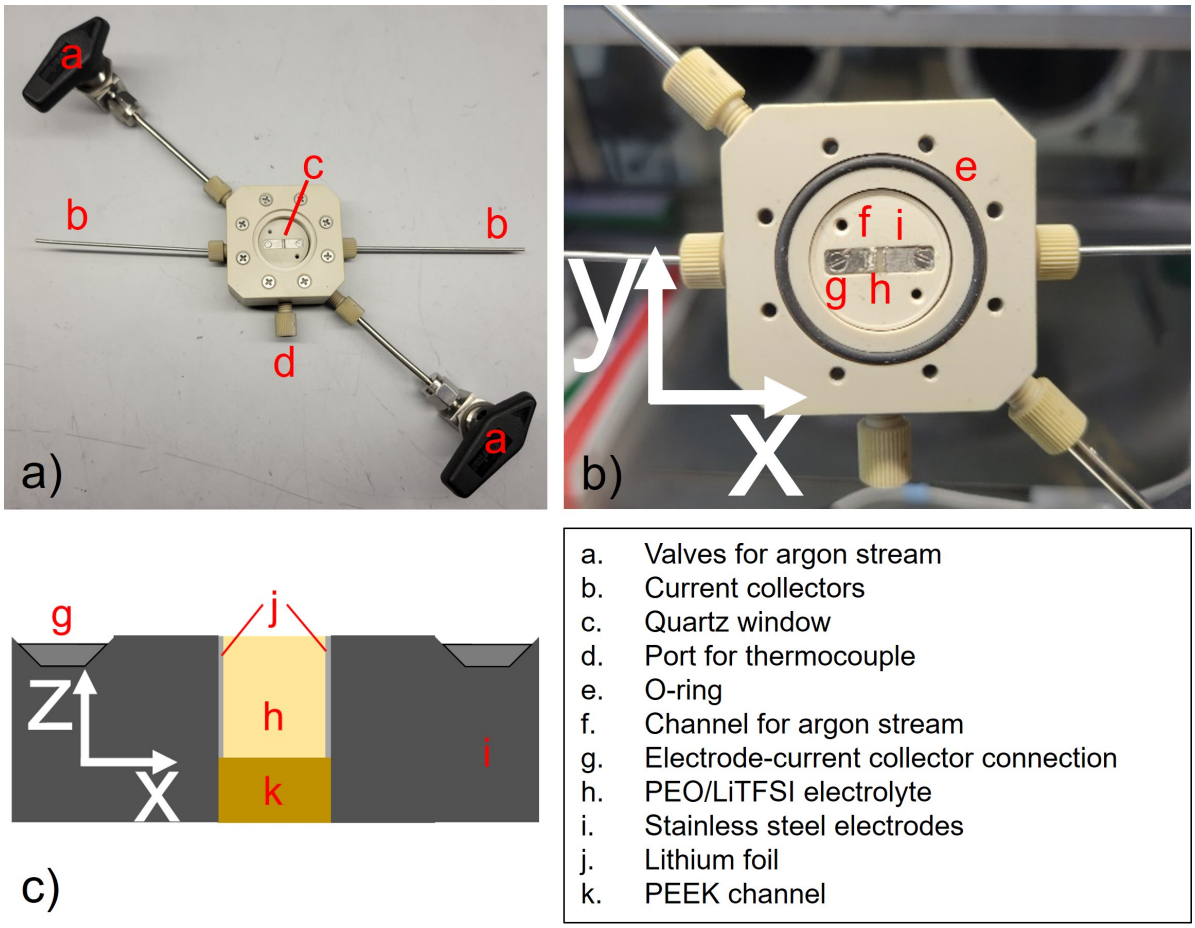

Figure 3.4: The electrochemical cell used for *operando* Raman spectroscopy. (a) View of entire cell from above. (b) View of the experimental channel with the electrodes and electrolyte. (c) Diagram of the side view of the experimental channel.

Polarization experiments were performed in a Li-PEO/LiTFSI-Li symmetric cell at current density $i = 0.18$ mA/cm^2. This current density was found to be the upper limit of applied current densities that resulted in stable polarization without significant dendrite growth. In the interest of maximizing the magnitude of concentration gradients across the electrolyte, this upper limit of stable current was utilized. Using the values of κ, D, t_+^0, and T_f we predict, using the methodology described in References 28 and 34, that the limiting current density of this cell is 0.4 mA/cm^2. The current density used in this study lies well below the limiting current. The experiment was performed three times and data obtained from one experiment is shown in Figures 3.5a and 3.5b. Figure 3.5a shows the time dependence of the potential drop across the cell during polarization. Small abrupt changes in the measured voltage occur at times when Raman spectra were measured. We posit that this is due to

heating of the electrolyte by the laser beam. As the time approaches 5 hours, the voltage data begins to vary drastically over short periods of time. This voltage behavior is indicative of dendrite growth, and this was verified by noticeable dendrite formation after 4 hours as shown by the optical micrograph of the cell in Figure 3.6.

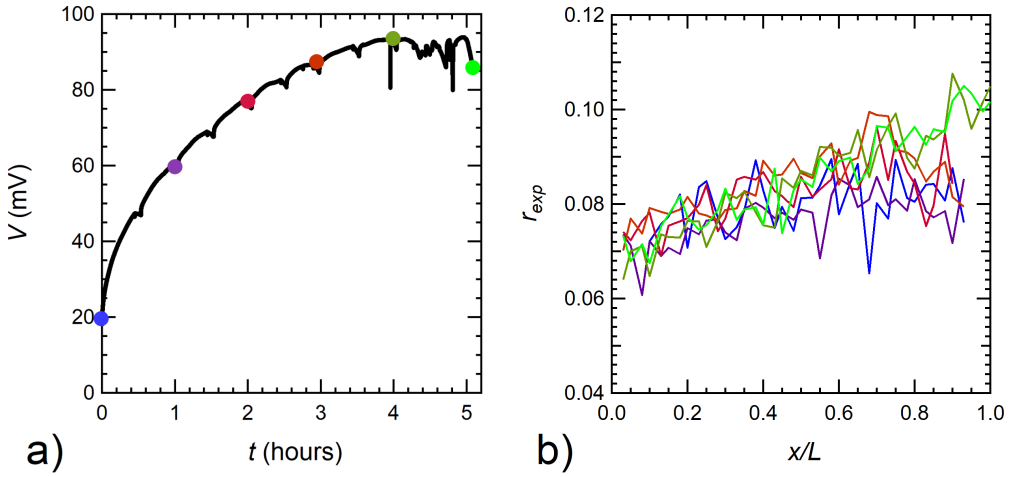

Figure 3.5: (a) Measured voltage as a function of time in the electrochemical cell during polarization, under an applied current density of 0.18 mA/cm^2. Colored circles correspond to time points at which salt concentration profiles were determined from *operando* Raman spectra. (b) Experimentally measured salt concentration, r_{exp}, as a function of normalized distance along the electrolyte, x/L, where $L = 1000$ μm. Colors indicate the time points at which the data were acquired; see (a).

Figure 3.5b shows the measured salt concentration as a function of position, x/L ($L = 0.1$ cm.), where the negative electrode is at $x/L = 0$ and the positive electrode is at $x/L = 1$, at selected times. These data reflect measured Raman spectra collected at 40 points separated by 25 μm. The measured values of A_n were recast in terms of r using the calibration curve (Figure 3.1d). The colors of the concentration profiles in Figure 3.5b correspond with the colored markers in Figure 3.5a which show the time points at which the concentration profiles were obtained. The time required for a single line scan was around 5 minutes which is small relative to the time scale required for significant changes in the local salt concentration profiles. After Raman measurements were recorded, micrographs were taken of the electrochemical channel. These micrographs were useful for observing dendrite growth within the cells. At early times we see the salt concentration oscillating around the average salt concentration value of $r_{avg} = 0.08$. As the cell is polarized, changes in concentration are most clearly seen at the positive electrode. It should be noted that while there was significant dendrite formation beginning after 4 hours of polarization, the measured salt concentration

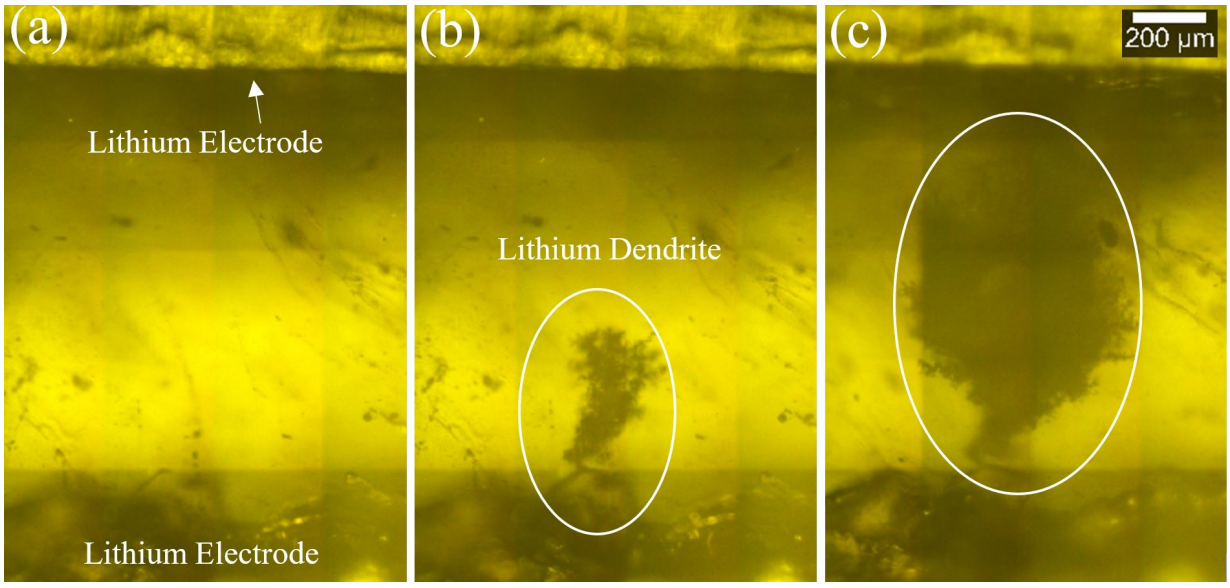

Figure 3.6: Micrographs of a portion of the lithium-polymer-lithium symmetric cell used in the *operando* Raman spectroscopy experiments at a current density, i = 0.18 mA/cm^2 (data presented in Figures 3.5a and 3.5b of main text). (a) 4.00, (b) 4.25, and (c) 4.75 h. Lithium dendrites are evident in (b) and (c). Steady state salt concentration profiles were measured at 4 hours, before significant dendrite growth.

gradients at 4 and 5 hours essentially overlap, which would indicate a steady state has been reached within the electrolyte. This can also be inferred from the measured voltage as while there is oscillation in the voltage it remains relatively constant when compared to the change seen at earlier time periods. We note that salt concentration measurements are challenging close to the lithium electrodes, and thus at times the salt concentration around $x/L = 0$ and $x/L = 1$ could not be measured reliably. For the data shown in Figures 3.5a and 3.5b, the relative position of the line scan was shifted 200 μm in the y direction according to Figure 2.2c between three and four hours to provide better data close to the electrodes. Due to the relatively small change in position of the line scan we do not expect that this change would result in any changes to the measured salt concentration compared to the previous position.

While the local salt concentration can vary during polarization, the average salt concentration must remain fixed at $r_{avg} = 0.08$. To check the validity of our measurements, the average salt concentration, r_{avg}, was calculated for each line scan. In Figure 3.7 we plot δr ($\delta r = r_{avg} - 0.08$) as a function of polarization time for all three experiments. The data in this figure are scattered around $\delta r = 0$, indicating that within experimental error the average salt concentration remains constant during polarization.

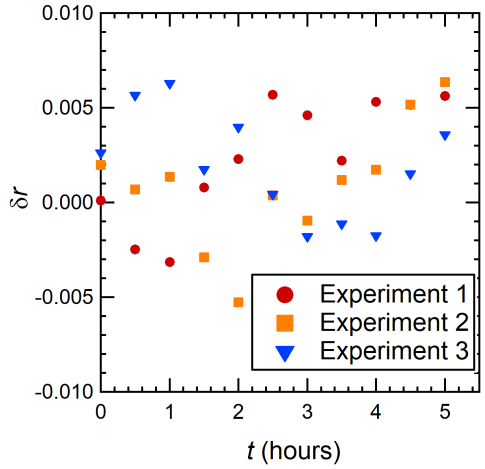

Figure 3.7: The deviation between the average salt concentration in the cell measured by *operando* Raman spectroscopy and the initial salt concentration (0.08), δr, as a function of polarization time for the 3 different experiments. In the absence of experimental error, we expect $\delta r = 0.08$.

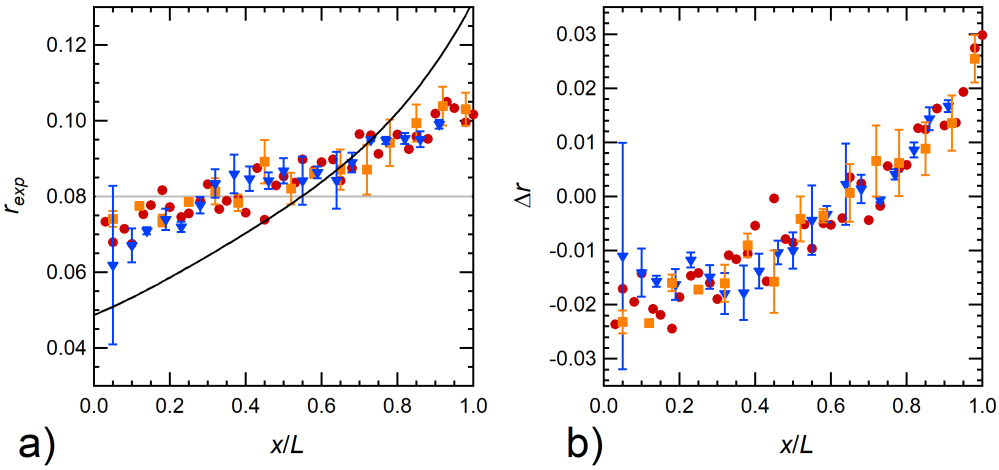

Figure 3.8: (a) Steady state salt concentration profiles of three independent experiments are plotted as a function of x/L. Three cells each with an r value of 0.08 were polarized using an applied current density of 0.18 mA/cm^2. The solid black line represents the theoretically predicted salt concentration profile, r_{theory} using concentrated solution theory. The solid gray line is indicative of the r_{avg} value of 0.08. (b) The difference in values of predicted and measured salt concentration as a function of x/L.

We are interested in understanding the difference between predicted salt concentration profiles and those that we measure using Raman spectroscopy. Figure 3.8a shows the steady state concentration profiles obtained from the three different experiments, $r = 0.08$ and $i = 0.18$ mA/cm^2. For Experiment 1, measurements were made with 40 data points in a single line scan across the width of the electrolyte. For Experiments 2 and 3, 30 data points were taken over 3 different line scans separated by about 150 μm to account for any variations that might be present within the electrolyte in the y-direction. For these experiments, the plotted data point represents the average for the 3 lines scans and the error bars correspond to the standard deviation of the 3 lines. Data from the three experiments are consistent with each other.

The solid curve in Figure 3.8a is the predicted salt concentration profile utilizing methods developed by Pesko et al. and Frenck et al. which are based on concentrated solution theory.[28,34] This prediction is made without resorting to any adjustable parameters. The steady state concentration profile, $r(x)$, is related to the current density and properties of the PEO/LiTFSI electrolyte. This relationship may be expressed as,

$$\int_{r(x=0)}^{r(x)} \frac{D(r)c(r)}{rt_-^0(r)}\,dr \;=\int_{r(x=0)}^{r(x)} \frac{\kappa(dU/d\ln m)}{(1-1/\rho_+)(z_+\nu_+)rF}\,dr \;=\int_{r(x=0)}^{r(x)} J(r)dr \;=-\frac{iL}{F}\left(\frac{x}{L}\right) \quad (3.1)$$

where $c(r)$ is the molar salt concentration, $t_-^0(r)$ is the transference number of the anion with respect to the solvent velocity, ρ_+ is the current fraction, z_+ is the charge of the cation, v_+ is the number of cations produced when the salt dissociates, F is the Faraday constant, and $dU/d\ln m$ is the change in open circuit potential with respect to the natural log of molality. We utilized transport parameters measured for PEO/LiTFSI mixtures (PEO molecular weight of 275 kg/mol) reported in Reference 34. The resulting expression $J(r)$ was fit to a 5th order polynomial,

$$J(r) = ar^5 + br^4 + cr^3 + dr^2 + er + f\left[\frac{\text{mol}}{\text{cm}-\text{sec}}\right] \quad (3.2)$$

with $a = 1.03\times10^{-4}, b = -9.02\times10^{-5}, c = 2.86\times10^{-5}, d = -3.91\times10^{-6}, e = 1.96\times10^{-7}, f = 6.36\times10^{-10}$. $r(x)$ is determined by using an initial guess of $r(x=0)$ and using Equation 3.1 to solve for $r(x)$ where $0 \le x \le L$. Then r_{avg} is calculated, and if it does not match 0.08, a new $r(x=0)$ is chosen. This process is repeated iteratively until the $r_{avg} = 0.08$. The modeled concentration profile was fit to a polynomial,

$$r_{theory} = 0.0807\left(\frac{x}{L}\right)^4 - 0.0982\left(\frac{x}{L}\right)^3 + 0.0596\left(\frac{x}{L}\right)^2 - 0.0487\left(\frac{x}{L}\right) + 0.0487 \quad (3.3)$$

The solid curve in Figure 3.8a represents Equation 3.3 Using these same procedures, the limiting current of an electrolyte can be predicted by determining the current density which results in a salt concentration of 0 at the negative electrode. For this experiment that

value was found to be 0.4 mA/cm^2, which is well above the current density utilized in our experiments.

For an electrolyte with physical properties that are independent of salt concentration, the r versus x/L prediction would be a straight line. The curvature of the black line in Figure 3.8a reflects the concentration dependence of transport and thermodynamic parameters of PEO/LiTFSI. The curvature is more pronounced near $x/L = 1$ (positive electrode) relative to $x/L = 0$ (negative electrode). At $x/L = 0$, the r_{theory} is 0.05, while that at $x/L = 1$ is 0.13. The departure of $r_{theory}(x)$ from 0.08 is thus highly asymmetrical: the departure at the positive electrode is about a factor of two smaller than that at the negative electrode. As can be seen in Figure 3.8a, the asymmetrical departures from $r = 0.08$ are also observed in the experiments, but the magnitude of the departures are significantly smaller than the theoretical predictions. In addition, the dependence of r_{exp} on x/L exhibits less curvature than r_{theory}. To better quantify the difference between theory and experiments, we define:

$$\Delta r = r_{theory} - r_{exp}. \tag{3.4}$$

In Figure 3.8b we plot Δr as a function of x/L. The values of Δr range from about -0.02 to $+0.02$.

We conclude this section by summarizing efforts in other studies to use *operando* Raman spectroscopy to measure salt concentration profiles in the presence of an applied current. In 1998 Rey et al. designed an optical cell, and demonstrated for the first time that Raman spectroscopy could be used to measure salt concentration profiles in a PEO electrolyte.[78] In a subsequent paper, Georen et al. determined salt concentration profiles near the electrodes of a polarized symmetric cell with a statistical copolymer electrolyte comprising ethylene oxide and propylene oxide monomers (75 wt% ethylene oxide). They were specifically interested in understanding how concentration gradients develop close to the electrodes, and the experimental data were compared with theoretical predictions based on concentrated solution theory.[79] In this pioneering study, the authors found that the experimentally observed concentration polarization was less than that predicted by theory. However, the theory was based on transport and thermodynamic parameters which were assumed to be independent of salt concentration. In recent studies, Fawdon et al. measured concentration profiles by Raman spectroscopy, and used these measurements to backout the thermodynamic and transport parameters in liquid electrolytes. To our knowledge, Figure 3.8a is the first comparison of experimental and theoretical results wherein the concentration dependence of transport and thermodynamic parameters used for the theoretical predictions was obtained from independent experiments using Raman spectroscopy.

3.5 Conclusions

We have measured salt concentration profiles in a model polymer electrolyte (PEO/LiTFSI) using *operando* Raman spectroscopy. These measurements are compared with predicted salt concentration profiles based on concentrated solution theory. Our main conclusion is that concentration polarization is asymmetrical - the reduction of salt concentration near the negative electrode is smaller in magnitude than the increase of salt concentration near the positive electrode. This asymmetry arises from the concentration dependence of thermodynamic and transport parameters of PEO/LiTFSI.

3.6 Acknowledgements

This work was intellectually led by the Joint Center for Energy Storage Research (JCESR), an Energy Innovation Hub funded by the U.S. Department of Energy, Office of Science, Office of Basic Energy Science, under Contract No. DE-AC02–06CH11357, which supported work conducted by Z. J. H. under the supervision of N.P.B. Work at the Molecular Foundry was supported by the Office of Science, Office of Basic Energy Sciences, of the U.S. Department of Energy under Contract No. DE-AC02-05CH11231.

3.7 Nomenclature

Table 3.1: List of Symbols and Abbreviations

Symbol	Meaning
A_n	Normalized area of PEO and Anion Raman peaks
c	Molar salt concentration, mol/L
D	Restricted diffusion coefficient, cm^2/sec
$dU/d\ln m$	Change in open circuit potential with respect to the natural log of molality
F	Faraday constant, C/mol
r	Salt Concentration ($r = [Li+]/[EO]$)
r_{avg}	Average salt concentration
r_{exp}	Experimentally measured salt concentration
r_{theory}	Salt concentration predicted from theory
t_+^0	Cationic transference number
t_-^0	Anionic transference number
T_f	Thermodynamic Factor
v_+	Number of cations
x/L	Normalized distance across the electrolyte
z_+	Charge of cation
δr	Difference between calculated and expected ravg
Δr	Difference between predicted and experimentally measured salt concentration
κ	Conductivity, S/cm
ρ_+	Current fraction

4: Comparing Experimentally Measured Sand's Times with Concentrated Solution Theory Predictions in a Polymer Electrolyte*

4.1 Abstract

We compare the electrochemically measured Sand's time, the time required for the cell potential to diverge when the applied current density exceeds the limiting current, with theoretical predictions for a 0.47 M poly(ethylene oxide) (5 kg/mol)/LiTFSI electrolyte. The theoretical predictions are made using concentrated solution theory which accounts for both concentration polarization and polymer motion, using independently measured parameters that depend on concentration, c: conductivity (κ), salt diffusion coefficient (D), and the cation transference number with respect to the solvent velocity (t_+^0), the thermodynamic factor ($1 + \frac{dlnf_\pm}{dlnc}$), and partial molar volume of the salt ($\bar{V}$); $f_\pm$ is the mean molar activity coefficient of the salt. We find quantitative agreement between experimental data and theoretical predictions.

4.2 Introduction

As current passes through a battery, salt concentration gradients develop within the electrolyte.[73] These gradients affect overall battery performance and can lead to cell failure. Understanding these salt concentration gradients is essential for identifying suitable electrolytes for various battery applications. Newman's concentrated solution theory provides a framework for predicting concentration gradients within an electrolyte.[33,64] For binary electrolytes comprising a salt that dissociates into cations and anions, and a solvent (which can either be a low molecular weight compound or a polymer), predicting concentration gradients requires knowledge of three transport parameters: conductivity (κ), salt diffusion coefficient (D), and the cation transference number with respect to the solvent velocity (t_+^0), along with two thermodynamic properties, the thermodynamic factor ($1 + \frac{dlnf_\pm}{dlnc}$), where c is the molar salt concentration and $f_\pm$ is the salt activity coefficient, and the molar volume of the salt ($\bar{V}$).[32,33,64,86] The experiments required to determine these parameters are challenging. It is perhaps not surprising that full electrochemical characterization, wherein the concentration dependence of all five parameters has been determined, is limited to relatively few electrolytes.[48,64,75,87,88]

*This chapter is adapted from Hoffman, Z. J.; Mistry, A; Srinivasan, V.; Balsara, N. P. 2023, In preparation.

The experiments required for full electrochemical characterization utilize small applied current densities (in the range of μA/cm^2). While the results of these experiments give values for the relevant transport and thermodynamic parameters, they do not provide any direct information on the electrolyte performance at high current densities relevant for battery applications. At sufficiently high current densities (in the range of mA/cm^2), the salt concentration in the vicinity of the negative electrode can reach zero. The current density at which this condition is obtained is called the limiting current density of the electrolyte.[36,76,86,89–91] If the thermodynamic and transport properties of an electrolyte are independent of concentration, then the limiting current density is given by

$$i_L = \frac{2C_b DF}{(1-t_+)L}, \tag{4.1}$$

where i_L is the limiting current density, F is Faraday's constant, ρ_+ is the current fraction, defined as the ratio of the final to initial current when the electrolyte is polarized in a symmetric cell, and L is the electrolyte thickness.[33] The importance of ρ_+ was established by Bruce and Vincent who showed that $\rho_+ = t_+^0$ in the limit of infinite dilution.[60] In this work, our efforts are focused on characterizing electrolytes at current densities above the limiting current density. In this regime, the measured electric potential diverges at a time that is referred to as Sand's time.[92–94] This is the time required for the salt concentration at the negative electrode to approach zero. In early work, Sand and coworkers showed that this time was related to both the salt diffusion coefficient and the transference number.[94] If the thermodynamic and transport properties of an electrolyte are independent of concentration, then Sand's time is given by

$$t_{Sand} = \pi D \left(\frac{Fc}{2i(1-\rho_+)} \right)^2, \tag{4.2}$$

where i is an applied current density above i_L.[94–96]

In this paper, we present data on measurements of Sand's time in a mixture of poly(ethylene oxide) (PEO), with number average molecular weight of 5 kg/mol, and lithium bis(trifluoromethanesulfonyl)imide (LiTFSI). The transport and thermodynamic parameters for this electrolyte have been reported in References 34, 48, 97. This enables explicit calculation of Sand's time with no adjustable parameters. In a noteworthy publication, Lee et al. measured the Sand's time in a PEO/LiTFSI electrolyte (4,000 kg/mol) and interpreted their data in terms of a simplified theory.[98] In their theory, the transport and thermodynamic properties were treated as constants (some were adjusted and some were not), and the motion of the solvent molecules was ignored.[99] It is however well established that an applied electric field results in the motion of solvent molecules (PEO in our case) which in turn affects the motion of ions.[100] Rigorous solution of the relevant transport equations required determining both solvent velocity and concentration as a function of space and time. The analysis presented below is the first to include the effect of solvent motion on Sand's time. We compare predictions and experimental data with no adjustable parameters.

4.3 Methods

4.3.1 Electrolyte Preparation

Poly(ethylene oxide) (PEO) with a molecular weight of 5 kg/mol (Polymer Source) was dried under active evacuation for 2 days at 90 °C. Lithium bis(trifluoromethanesulfonyl)imide (LiTFSI) (Sigma Aldrich) was dried under active evacuation for three days at 120 °C. Predetermined amounts of PEO and LiTFSI were combined and mixed in anhydrous tetrahydrofuran (THF) (Sigma Aldrich) in a capped vial at 60 °C under active stirring until fully dissolved. The cap was then removed, and the THF evaporated off. The electrolytes were then dried at 90 °C under active evacuation overnight to remove any remaining solvent. Preparation of electrolytes was performed in an argon-filled glovebox with water and oxygen levels below 2 ppm. The electrolytes used in this study all have the same salt concentration, r, the ratio of lithium ions to ethylene oxide moieties ($r = [Li^+]/[EO]$). The r value chosen was $r = 0.02$, or 0.47 M.

4.3.2 Lithium Symmetric Cells and Sand's Time Measurements

Lithium symmetric cells were constructed inside an argon-filled glovebox with water and oxygen levels below 1 PPM. Lithium electrodes were prepared using lithium foil (MTI Corp.) that was first brushed then pressed with a mechanical press. The thickness of these electrodes was measured using a micrometer. Next silicone spacer material (VWR) of thicknesses 250 and 500 μm and an inner diameter of 3.175 mm, was filled with PEO/LiTFSI electrolyte. The lithium electrodes were pressed on each side of the electrolyte and the total thickness of the stack was measured, and the thickness of the electrolyte was calculated by subtracting the electrode thicknesses from the total stack thickness. Nickel tabs were attached on each side of the stack, and the cell was sealed in laminated pouch material.

Before electrochemical experiments were conducted, the cells were annealed on a custom heating stage at 90 °C for three hours. All electrochemical experiments were performed at 90 °C using a VMP3 Biologic potentiostat. Cells were first preconditioned by applying a current density of 0.02 mA/cm^2 for 3 hours then allowing the cells to relax at open circuit voltage (OCV) for 3 hours, followed by impedance measurements. The same current density was then applied in the opposite direction followed by another period of relaxation and an impedance measurement. This process was performed for 5 cycles to form a stable solid electrolyte interface, which was determined by observing the interfacial resistance of each cell and ensuring it reached a constant value after multiple cycles. The resistance of the cell was measured using electrochemical impedance spectroscopy (EIS) with a frequency range of 1 MHz to 100 mHZ, and a sinus amplitude of 40 mV.

Sand's time measurements were performed by first taking an impedance measurement, then polarizing the cell with an applied current density, followed by an OCV step, and ending

with an impedance measurement. Each cell was polarized with length-normalized current densities, iL, of 0.0075, 0.010, 0.0125, 0.015, 0.0175, and 0.020 mA/cm.

4.3.3 Modeling

We use Newman's concentrated solution theory to theoretically understand concentration and potential evolution in a 0.47 M PEO(5kg/mol)/LiTFSI electrolyte when polarized at different current densities.[33,100,101] The concentration dependence of the relevant thermodynamic and transport properties have been previously measured for this electrolyte (Table 4.1) and their continuous concentration-dependent functions (as plotted in Figure 2 of Reference 100) are used for the theoretical calculations.[22,34,48,97] The governing equations describing the evolution of ionic concentration are:

$$\frac{dc}{dt} = \frac{d}{dx}\left(D\left(1 - \frac{d\ln c_0}{d\ln c}\right)\frac{dc}{dx}\right) - \frac{i}{F}\frac{dc}{dx} - \frac{d}{dx}(cv_0), \tag{4.3}$$

$$\frac{dv_0}{dx} = \bar{V}\left\{\frac{d}{dx}\left(D\left(1 - \frac{d\ln c_0}{d\ln c}\right)\frac{dc}{dx}\right) - \frac{i}{F}\frac{dc}{dx}\right\}. \tag{4.4}$$

Note that x represents a moving interface attached to the left lithium-electrolyte interface which strips when the ionic current flows in the $+x$ direction. The velocity of this moving interface is linked to the applied current density, i, and constant when the Li-electrolyte-Li cell is polarized at constant current densities. Based on the $c\,(x,t)$ profile obtained by solving the aforementioned equations, the electrolyte potential, $\Delta\phi$, can be computed using concentration-dependent conductivity, κ, cation transference number, t_+^0, and thermodynamic factor, $\left(1 + \frac{d\ln f_\pm}{d\ln c}\right)$, as per the following expression:

$$\Delta\phi = \Delta\phi_{x=0} - \Delta\phi_{x=L} = \int_L^0 \frac{1}{\kappa}\,dx + \frac{2RT}{F}\int_{c_{x=L}}^{c_{x=0}} (1 - t_+^0)\left(1 + \frac{d\ln f_\pm}{d\ln c}\right)\frac{dc}{c}. \tag{4.5}$$

Notice that the first term on the right is the ohmic drop, i.e., related to finite conductivity of the electrolyte, and the second term represents the overpotential related to the concentration polarization across the electrolyte thickness,

$$\Delta\phi_{ohmic} = i\int_0^L \frac{1}{\kappa}\,dx, \tag{4.6}$$

$$\Delta\phi_{concentration} = \frac{2RT}{F}\int_{c_{x=L}}^{c_{x=0}} (1 - t_+^0)\left(1 + \frac{d\ln f_\pm}{d\ln c}\right)\frac{dc}{c}. \tag{4.7}$$

These expressions are numerically solved using the Finite Volume Method (details are provided in Reference 92). The current density, i, at which the electrolyte is polarized explicitly

appears in these equations and additionally in the concentration boundary conditions at both lithium-electrolyte interfaces:

$$-D\left(1-\frac{d\ln c_0}{d\ln c}\right)=(1-t_+^0)\frac{i}{F}. \tag{4.8}$$

We assume that reaction overpotentials are negligible, an assumption that is appropriate for the thick electrolytes used in this study.[92]

4.4 Results and Discussion

Sand's time measurements are made by applying a constant current density to a lithium-electrolyte-lithium cell and measuring the resulting electric potential. The experimentally measured potential includes the potential drop across the solid electrolyte interphase (SEI). Since we are only interested in the potential drop across the electrolyte, this contribution is subtracted. The potential of interest is defined as

$$\Delta\phi(t)=V(t)-R_i i A, \tag{4.9}$$

where $V(t)$ is the measured voltage, R_i is the interfacial resistance, and A is the interfacial area. The resistance used for these calculations is the interfacial resistance measured by ac impedance after polarization. The interfacial resistance of our electrolytes was typically an order of magnitude smaller than the bulk resistance.

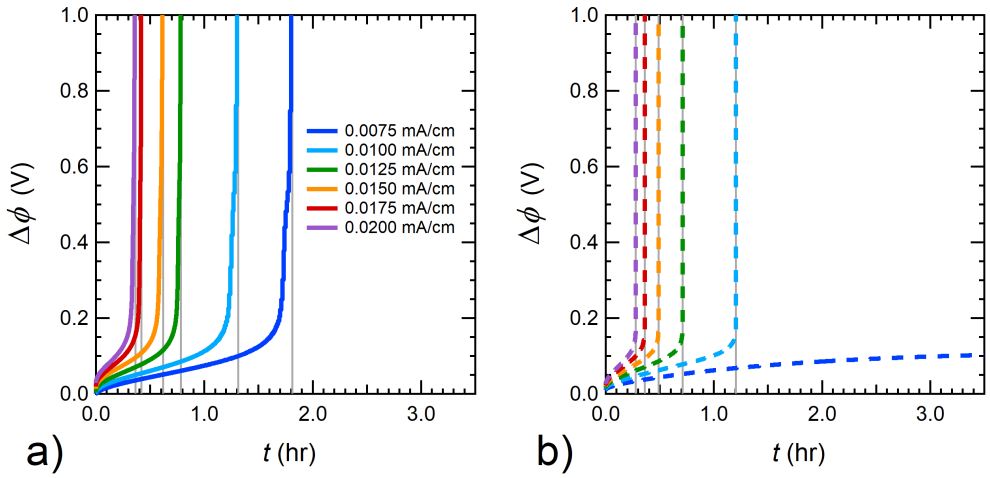

Figure 4.1: Electric potential, $\Delta\phi$, plotted as a function of time, t, in response to length normalized current densities, iL. (a) Measured data from a 0.47 M PEO/LiTFSI electrolyte with a thickness, L, of 576 μm and (b) predicted using concentrated solution theory for a 0.47 M PEO/LiTFSI electrolyte with $L = 500$ μm. The colors of the curves in (b) correspond with the same values of iL listed in (a). Gray lines indicate the time at which the potential diverged each value of iL for experiments and theory. All experimental measurements were made at 90 °C, and predictions utilize PEO/LiTFSI properties measured at 90 °C (Table 4.1).

In Figures 4.1a and 4.1b, we show $\Delta\phi$ as a function of time, t, at various values of iL, the length normalized current density. We prefer iL to i to account for the fact that the electrolyte thickness in each of our cells is not identical, and the characteristics of our symmetric cells are governed by the product, iL. Figure 4.1a shows characteristic data collected from our electrochemical experiments, for a cell with an electrolyte thickness of 576 μm. At each value of iL the electric potential increases gradually at early times. Beyond a characteristic time that decreases with increasing current density, the potential rapidly approaches the cut-off potential of 1.5 V. Equations 4.3-4.8 were solved using parameters for our PEO/LiTFSI electrolyte. These parameters are given in Table 4.1. Figure 4.1b shows the calculated potential as a function of time modeled for a salt concentration of 0.47 M and a thickness L = 500 μm.[100] The current density used in the calculations were chosen to match the iL used for the experimental measurements. At $iL \leq 0.01$ mA/cm, the correspondence between theory and experiment is nearly quantitative. At the highest current density, experiments show a divergence of cell potential while theory does not. This discrepancy is well within the uncertainty of the transport and thermodynamic parameters. The gray lines in Figures 4.1a and 4.1b were used to determine Sand's time. These lines reflect the time at which the cell potential diverges in both theory and experiment.

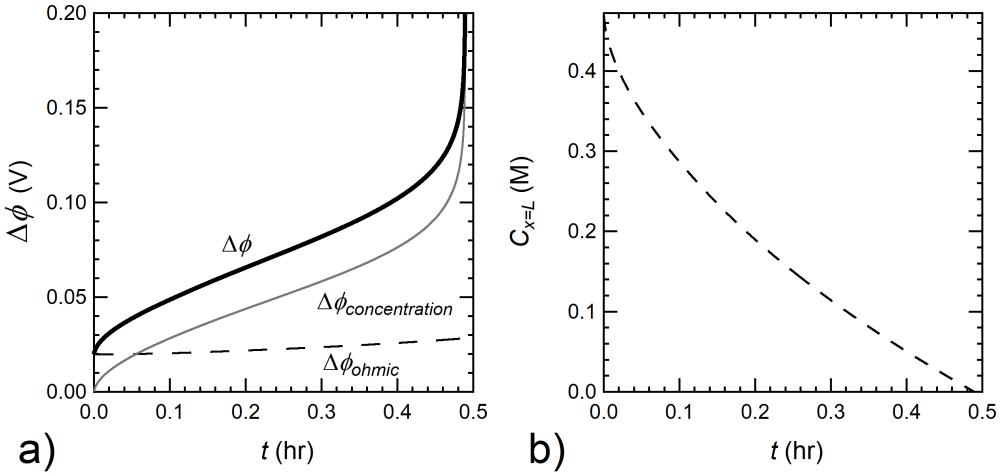

Figure 4.2: (a) Predicted electric potential (solid black line), $\Delta\phi$, and the components of the potential due to ohmic effects (dashed black line), $\Delta\phi_{ohmic}$, and concentration polarization (solid gray line), $\Delta\phi_{concentration}$, as functions of time, t. (b) Predicted lithium salt concentration at the negative electrode, $c_{x=L}$, versus t. These predictions are for a 0.47 M PEO/LiTFSI electrolyte, $L = 500$ μm, polarized at $iL = 0.015$ mA/cm. Predictions utilize PEO/LiTFSI properties measured at 90 °C (Table 4.1).

Figure 4.2a shows the time dependence of $\Delta\phi$ for a typical calculation (iL = 0.015 mA/cm, L = 500 μm). The electric potential contains two contributions: $\Delta\phi = \Delta\phi_{ohmic} + \Delta\phi_{concentration}$. $\Delta\phi_{ohmic}$ is the component of the potential due to the resistance of the electrolyte, which is related to κ by Ohm's law. Equation 4.6 can be written as

$$\Delta\phi_{ohmic} = i\frac{L}{\kappa_{avg}} \tag{4.10}$$

As the cell is polarized, the concentration varies across the cell, and κ_{avg} reflects the average conductivity of the electrolyte. $\Delta\phi_{concentration}$ is obtained by subtracting $\Delta\phi_{ohmic}$ from $\Delta\phi$. In Figure 4.2a, $\Delta\phi$ (solid black line), $\Delta\phi_{ohmic}$ (dashed black line), and $\Delta\phi_{concentration}$ (solid gray line) are plotted as a function of time. At $t = 0^+$, $\Delta\phi = \Delta\phi_{ohmic}$. Salt concentration gradients grow with increasing time, but this has a minimal effect on $\Delta\phi_{ohmic}$. At $t = 0^+$, $\Delta\phi_{concentration}$ is zero. However, the growth of salt concentration gradients is reflected in the increase in $\Delta\phi_{concentration}$. Figure 4.2b shows the salt concentration at the negative electrode, $c_{x=L}$, as a function of time. As $c_{x=L}$ smoothly approaches a value close to zero at $t = 0.5$ hours, $\Delta\phi_{concentration}$ diverges. This connection between potential divergence and concentration was first recognized by Sand.[94]

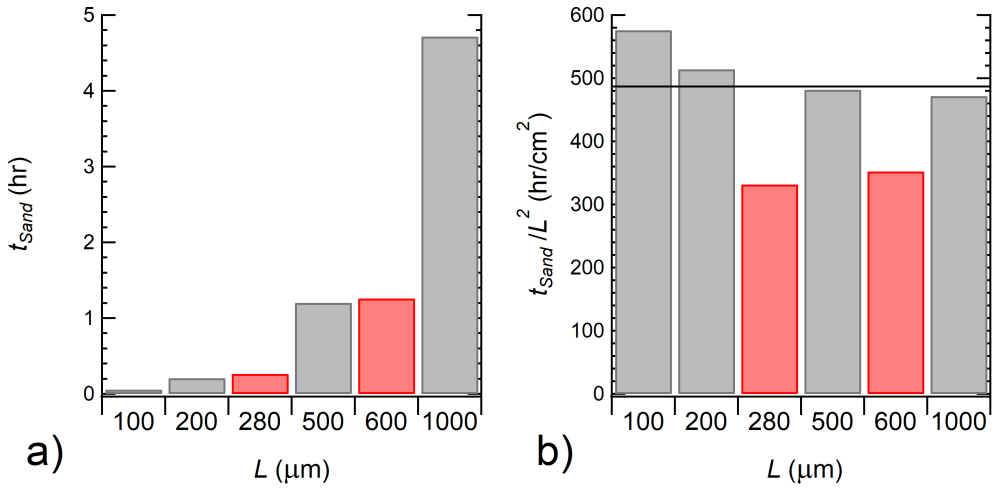

Figure 4.3: (a) Sand's times, t_{Sand}, plotted for various 0.47 M PEO/LiTFSI electrolyte thicknesses in response to polarization at $iL = 0.010$ mA/cm. (b) Length normalized Sand's times, t_{Sand}/L^2, plotted for various 0.47 M PEO/LiTFSI electrolyte thicknesses. The black line indicates the value of t_{Sand}/L^2 predicted from Equation 4.11. Gray bars indicate predictions from concentrated solution theory, and red bars indicate the average Sand's time from experimental measurements. All experimental measurements were made at 90 °C, and predictions utilize PEO/LiTFSI properties measured at 90 °C (Table 4.1)

Sand's time depends on two parameters, the applied current density, i, and electrolyte thickness, L. Rearranging Equation 4.2 gives

$$\frac{t_{Sand}}{L^2} = \pi D \left(\frac{Fc}{2(iL)(1-\rho_+)} \right)^2, \tag{4.11}$$

which shows that it is convenient to consider the dependence of the Sand's time on the length normalized current density, iL, and L. We use the model to predict the effect of L on t_{Sand} at $iL = 0.010$ mA/cm. These results are shown in Figure 4.3a. As expected, t_{Sand} increases with increasing L. At $L = 100$ μm, t_{Sand} is 0.3 hours, while at $L = 1000$ μm, $t_{Sand} = 4.7$ hours. In Figure 4.1a we reported the Sand's time at $iL = 0.01$ mA/cm for $L = 576$ μm. We repeated this experiment for three independent cells with an average value of $L = 600$ μm. In addition, we studied two cells with an average value of $L = 280$ μm with the same value of iL (0.01 mA/cm). The experimental results are also shown in Figure 4.3a. It is clear that the experiments and theoretical predictions are in quantitative agreement (within the uncertainty of the transport and thermodynamic parameters used in the calculations).

Figure 4.3b shows the same results but plotted in the format suggested by Equation 4.11. Here we show t_{Sand}/L^2 as a function of L for a fixed iL= 0.01 mA/cm. Also shown in

Figure 3.5b is the value from Equation 4.11, with parameters for our 0.47 M PEO/LiTFSI electrolyte ($D = 7.8 \times 10^{-8}$ cm^2/s, $\rho_+ = 0.15$). Calculations based on concentrated solution theory approach Equation 4.11 as L is increased from 100 to 1000 μm. This value of t_{Sand}/L^2 is 484 hr/cm^2. The experimental data obtained at two different thicknesses are reasonably consistent with theoretical predictions.

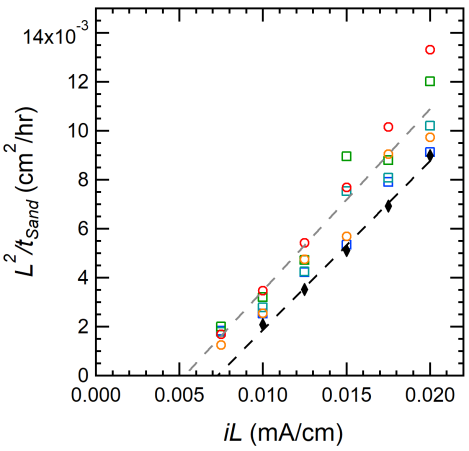

Figure 4.4: Length normalized inverse Sand's time, L^2/t_{Sand}, plotted as a function of length normalized current density, iL. The data is reported from experimental cells with nominal thicknesses of 280 μm (colored circles) and 600 μm (colored squares) and predictions from concentrated solution theory for a cell with a thickness of 500 μm (black rhombuses). The gray dashed line is a linear fit of all experimental data, and the black dashed line is a linear fit of predicted Sand's time. All experimental measurements were made at 90 °C, and predictions utilize PEO/LiTFSI properties measured at 90 °C (Table 4.1)

The Sand's time experiments were conducted at different values of iL. Figure 4.4a shows these results on a plot of L^2/t_{Sand} versus iL for electrolyte thicknesses in the vicinity of 280 (colored circles) and 600 μm (colored squares). Also shown in this figure are theoretical calculations for $L = 500$ μm (black rhombuses). Note that the theoretically predicted L^2/t_{Sand} is a weak function of L. We see that L^2/t_{Sand} is a linear function of iL. By fitting the data in Figure 4.4a to a line, we can identify the value of iL at which L^2/t_{Sand} approaches zero, or $iL \to i_L L$. In other words, the limiting current density is the current density at which the Sand's time approaches infinity. The slope and intercept of a linear fit of the experimental data are 0.745 and -4.00×10^{-3} respectively and 0.689 and -5.01×10^{-3} for concentrated solution theory predictions. This calculation results in $i_L L$ values of 0.0054 mA/cm for the experimental data and 0.0073 mA/cm for the theoretical predictions. It is challenging to directly measure iL in 5 kg/mol PEO/LiTFSI electrolytes, as the low molecular weight provides little resistance to the growth of dendrites. The large polarization times required for

limiting current density measurements correspond with high cell failure rates.[35,36,75,76,90,91] The methodology based on Sand's time provides a convenient approach for measuring limiting current as it uses much shorter polarization times which are less likely to be affected by dendrite growth.

4.5 Conclusions

We present an approach for calculating Sand's time in electrolytes using concentrated solution theory. The theory is rigorous and accounts for both concentration polarization and motion of all three species, the cation, the anion, and the solvent (a polymer in our case). Using this theory requires the knowledge of three transport parameters: κ, D, t_+^0, and two thermodynamic parameters: $1 + \frac{d\ln f_\pm}{d\ln c}$ and $\bar{V}$. All five parameters depend on concentration. We present a limited test of the theory using experimentally determined Sand's time of a 0.47 M PEO(5 kg/mol)/LiTFSI electrolyte. We examine the effects of both current density and electrolyte thickness on Sand's time. The experimental data are in excellent agreement with theoretical calculations. This agreement is obtained without resorting to any adjustable parameters. However, this electrolyte is sufficiently dilute, and results obtained using the rigorous theory are not very different from simplified models based on dilute solution theory. In the future, we plan to test the theory using experiments on more concentrated electrolytes. These experiments are challenging due to the formation of lithium dendrites at currents exceeding the limiting current. Efforts to resolve these challenges are currently underway.

4.6 Acknowledgements

This work was intellectually led by the Joint Center for Energy Storage Research (JCESR), an Energy Innovation Hub funded by the U.S. Department of Energy, Office of Science, Office of Basic Energy Science, under Contract No. DE-AC02–06CH11357, which supported work conducted by Z. J. H. under the supervision of N.P.B. A.M. and V.S. acknowledge the support by UChicago Argonne, LLC, Operator of Argonne National Laboratory ("Argonne"). Argonne, a U.S. Department of Energy Office of Science laboratory, is operated under Contract No. DE-AC02–06CH11357. The U.S. Government retains for itself, and others acting on its behalf, a paid-up nonexclusive, irrevocable worldwide license in said article to reproduce, prepare derivative works, distribute copies to the public, and perform publicly and display publicly, by or on behalf of the Government. The Department of Energy will provide public access to these results of federally sponsored research in accordance with the DOE Public Access Plan: http://energy.gov/downloads/doepublic-access-plan

4.7 Supporting Information

Table 4.1: Properties of PEO/LiTFSI electrolytes at 90 ° C, taken from References 48, 65, 97

c (M)	ρ (g/cm^3)	t_+^0	κ (S/cm)	D (cm^2/sec)	$1+\frac{d\ln f_\pm}{d\ln c}$	ρ_+
0.25	1.160	0.07	2.7×10^{-4}	6.0×10^{-8}	0.45	0.18
0.47	1.180	0.23	7.5×10^{-4}	7.8×10^{-8}	0.75	0.15
0.87	1.210	0.40	1.8×10^{-3}	1.0×10^{-7}	1.93	0.11
1.20	1.230	0.33	2.0×10^{-3}	1.3×10^{-7}	2.69	0.11
1.59	1.330	0.43	2.2×10^{-3}	1.1×10^{-7}	4.24	0.10
1.87	1.365	0.20	1.3×10^{-3}	8.4×10^{-8}	3.78	0.09
2.11	1.38	0.08	1.1×10^{-3}	7.0×10^{-8}	3.92	0.08
2.38	1.43	-0.08	9.9×10^{-4}	5.8×10^{-8}	3.93	0.07
2.58	1.45	-0.38	1.3×10^{-3}	9.4×10^{-8}	3.51	0.06
2.76	1.47	0.10	1.6×10^{-3}	9.0×10^{-8}	6.03	0.07
3.05	1.52	0.41	1.2×10^{-4}	6.5×10^{-8}	10.84	0.10
3.36	1.58	0.33	6.4×10^{-4}	6.3×10^{-8}	10.89	0.16
3.49	1.57	0.18	4.0×10^{-4}	5.9×10^{-8}	10.06	0.18

4.8 Nomenclature

Table 4.2: List of Symbols and Abbreviations

Symbol	Meaning
A	Interfacial area (cm^2)
c	Salt concentration (mole/liter)
c_0	Solvent concentration (mole/liter)
D	Salt diffusion coefficient (cm^2/sec)
F	Faraday's constant (C/mol)
i	Current density (mA/cm^2)
i_L	Limiting current density (mA/cm^2)
L	Electrolyte thickness (μm)
R	Gas constant (J/mol-K)
r	Molar ratio of lithium ions to ethylene oxide units ($r = [Li^+]/[EO]$)
R_i	Interfacial resistance (Ω)
T	Temperature (K)
t_{Sand}	Sand's time (min)
t_+^0	Cationic transference number with respect to the solvent velocity
V	Measured voltage (volts)
$\bar{V}$	Partial molar volume (cm^3/mol)
z_+	Charge number of cation
$1 + \frac{d\ln f_\pm}{d\ln c}$	Thermodynamic factor
$f_\pm$	Activity coefficient
κ	Conductivity (S/cm)
ν	Total number of ions
ν_+	Number of cations produced from salt dissociation
ν_-	Number of anions produced from salt dissociation
ν_0	Solvent velocity (nm/sec)
$\Delta\phi$	Electric potential corrected for interfacial effects (volts)
ρ_+	Current fraction

5: Limiting Current Density in Single-Ion-Conducting and Conventional Block Copolymer Electrolytes*

5.1 Abstract

The limiting current density of a conventional polymer electrolyte (PS-PEO/LiTFSI) and a single-ion-conducting polymer electrolyte (PSLiTFSI-PEO) was measured using a new approach based on the fitted slopes of the potential obtained from lithium-polymer-lithium symmetric cells at a constant current density. The results of this method were consistent with those of an alternative framework for identifying the limiting current density taken from the literature. We found the limiting current density of the conventional electrolyte is inversely proportional to electrolyte thickness as expected from theory. The limiting current density of the single-ion-conducting electrolyte was found to be independent of thickness. There are no theories that address the dependence of the limiting current density on thickness for single-ion-conducting electrolytes.

5.2 Introduction

Lithium-ion batteries are common energy sources for many applications, and as their use grows there is increasing interest in developing the next generation of rechargeable batteries.[67,102,103]Conventional lithium-ion batteries utilize a liquid electrolyte that is a mixture of organic solvents and a lithium salt. These electrolytes are highly flammable and this contributes to safety concerns.[104]A potential solution to resolve this issue is the use of polymer electrolytes which have reduced flammability.[20,105] Polymer electrolytes, particularly block copolymer electrolytes, are also of interest because of their chemical stability against lithium metal anodes.[20,21,76,106,107] Polymer electrolytes are generally prepared by mixing a lithium salt into the polymer.

The adoption of polymer electrolytes is dependent on their electrochemical performance and the limits under which they can operate. When current is passed through polymer electrolytes, salt accumulates near the anode and is depleted near the cathode. In this respect, polymer electrolytes are no different from conventional liquid electrolytes; these systems are referred to as binary electrolytes. The largest sustainable current density that can be passed through the electrolyte is known as the limiting current density.[33,94,101,108] At this value of current density the concentration of lithium salt at the cathode is zero, and operating at current densities above this value results in cell failure.[33] Measurements of the limiting current density of electrolytes are uncommon, with few historical examples in the

*This chapter is adapted from work reported in Hoffman, Z. J.; Ho, A. S.; Chakraborty, S.; Balsara, N. P. *Journal of The Electrochemical Society*, **2022**, 169, 043502.

literature.[99,109,110] However, there have been several recent reports of measurements of the limiting current density in polymer electrolytes.[35,36,76,90,111,112]

Newman derived a simple expression for the limiting current density of an electrolyte of thickness, L, placed between two planar electrodes:

$$i_L = \frac{2C_b DF}{(1-t_+)L}, \tag{5.1}$$

where iL is the limiting current, C_b is the salt concentration, D is the salt diffusion coefficient, F is Faraday's constant, t_+ is the cationic transference number, and L is the thickness of the electrolyte.[33] This equation applies to mixtures of salts and a solvent (either a liquid or a polymer) wherein the transport coefficients are independent of salt concentration. Note that the limiting current density is inversely proportional to L.

Single-ion-conducting polymer electrolytes are systems wherein the anions are covalently bound to the polymer chain; the unbound counterions (cations) are, in principle, free to move. If we neglect chain mobility, then the only mobile species are the counterions. There are no liquid analogs of single-ion-conducting polymer electrolytes. However, all inorganic ceramic and glass electrolytes are single-ion-conductors.[113] Concentration gradients cannot develop in these systems without disrupting charge neutrality across the electrolyte.[55,61] In the absence of concentration gradients, the lithium salt concentration cannot reach zero at the cathode, and traditional approaches for defining limiting current density fail. It is also worth noting that as $t_+ \to 1$, Equation 5.1 predicts that $i_L \to \infty$.

To our knowledge, the dependence of limiting current density on electrolyte thickness has not been measured in either binary electrolytes or single-ion-conducting electrolytes. It is convenient to quantify limiting current density in a lithium-electrolyte-lithium cell as the distance between the electrodes is well-defined. It is well known that the passage of high current densities results in the formation of dendrites at lithium metal anodes,[114–116] and this complicates determination of limiting current density. Dendrite growth is suppressed in block copolymer electrolytes due to their high elastic modulus.[69,72] We therefore use a block copolymer (polystyrene–*b*–polyethylene oxide (PS-PEO)) with added lithium bis(trifluoromethanesulfonyl)imide (LiTFSI) salt to experimentally determine the relationship between limiting current density and electrolyte thickness in binary electrolytes. For consistency, our single-ion-conductor is also a block copolymer (polystyrene–LiTFSI–*b*–polyethylene oxide (PSLiTFSI-PEO)). Our main goal is to contrast the thickness dependence of the limiting current density in these two systems. This required the development of a new framework for quantifying limiting current density in single-ion-conducting systems. We show that the same framework also applies to the conventional binary polymer electrolyte.

5.3 Experimental Methods

5.3.1 Polymer Synthesis

For this study two polymers were used, polystyrene–*b*–polyethylene oxide (PS-PEO) and polystyrene–LiTFSI–*b*–polyethylene oxide (PSLiTFSI-PEO). The synthesis of both these polymers is well documented in the literature.[117,118] For PS-PEO the molecular weight of the polystyrene and polyethylene oxide blocks are 200 and 222 kg mol^{-1} respectively. With PSLiTFSI-PEO the molecular weight of the polystyrene–LiTFSI and polyethylene oxide blocks are 2.1 and 5 kg mol^{-1} respectively.

5.3.2 Preparation of Electrolytes

For this study we define salt concentration r as the molar ratio of LiTFSI to ethylene oxide units. The r value of the PS-PEO/LiTFSI and PSLiTFSI-PEO electrolytes were 0.085 and 0.059 respectively. PS-PEO/LiTFSI electrolytes were prepared by adding LiTFSI salt to PS-PEO polymer according to the procedures outlined by Maslyn et al.[90]

5.3.3 Electrochemical characterization and limiting current density measurements

The current fraction, ρ_+, of the PSLiTFSI-PEO electrolyte was found to be 0.96 $\pm$ 0.01 following procedures reported previously.[75] Strictly speaking, a single-ion-conductor would exhibit $\rho_+ = t_+ = 1.0$. It is clear that to a good approximation, the PSLiTFSI-PEO polymer is a single-ion-conductor.

Limiting current density measurements for PS-PEO/LiTFSI electrolytes were performed according to procedures outlined by Maslyn et al.[90] After an initial impedance measurement, a constant current was applied while measuring the potential, and after allowing the cell to relax another impedance measurement was made. The two impedance measurements ensure that the passage of current did not result in irreversible changes in either the bulk or interfacial impedances. The limiting current density was determined by systematically increasing the applied current density and noting the nature of the cell potential vs time data. The data presented in this paper is entirely consistent with previously published comprehensive studies on the limiting current density of PS-PEO/LiTFSI electrolytes.[90,91] We thus only made one cell at each electrolyte thickness.

For PSLiTFSI-PEO, limiting current density cells were made using lithium symmetric cells with silicone spacer material (McMaster-Carr) with thicknesses of 300, 400, 550, and 840 μm according to the procedures outlined in Reference 75. The standard deviation of these electrolyte thicknesses is below 10% of the total thickness. These measurements were made during construction of the cells inside the glovebox, using methods described in Reference 75.

The PS-PEO/LiTFSI electrolytes were molded to give free-standing films. The thicknesses of the PSLiTFSI-PEO cells were much larger because the polymer could not be processed to give free-standing films. The limiting current density experiments were performed after being preconditioned with ± 0.02 mA cm^{-2}, following Reference 75. After preconditioning, the cells were subjected to various current densities while measuring the resulting potential. For the PSLiTFSI-PEO electrolytes, three to six cells were used for each measurement.

5.3.4 X-ray Microtomography

After experimentation, these pouch cells with PS-PEO/LiTFSI electrolytes were opened inside a glovebox, and a portion of the symmetric cell was cut out and repouched. The repouched cells were imaged using hard X-ray microtomography at Beamline 8.3.2 at the Advanced Light Source at Lawrence Berkeley National Laboratory, following the procedures of Reference 90. Cells were imaged at 4 $\times$ magnification, corresponding to a pixel size of approximately 1.625 μm. The attenuation-based tomograms were reconstructed using TomoPy.[119] Electrolyte thickness, L, corresponds to the average distance between approximately parallel electrodes and was determined by measuring at least 10 points within the cell using the software ImageJ on tomographic cross-sections of each cell. The PS-PEO/LiTFSI films in this study had thicknesses of 33.5, 53.0, 67.7, and 74.3 μm. The standard deviation of each thickness measurement ranged from 2%-6% of the total thickness.

5.4 Results and Discussion

Limiting current density is measured in experiments where a steady current density is drawn across a lithium-electrolyte-lithium symmetric cell and the potential drop across the cell is measured as a function of time. Typical data obtained from the PS-PEO/LiTFSI electrolyte are shown in Figure 5.1a, where Φ/L is plotted as a function of time for an average electrolyte thickness, L, of 53.0 μm. Φ represents the potential drop across the electrolyte after correcting for the potential drop across the electrolyte-electrode interfaces as described in Reference 36. This correction, which is the product of the applied current and interfacial resistance of the electrolyte, ranges from 10%-40% of the total measured potential for PSLiTFSI-PEO and 30%-50% for PS-PEO/LiTFSI. Characteristic impedance data for both electrolytes can be found in the Supporting Information. In this work we plot Φ/L to remove the potential drop due to interfacial resistances, and so that cells of different thicknesses can be compared on the same scale; the limiting current density of an electrolyte is a bulk property and thus removing interfacial effects is necessary. When the applied current density is below the limiting current density, the potential reaches a steady state value at long times; the data obtained at current densities well below the limiting current density are shown in the inset of Figure 5.1a. When current densities above the limiting current density are applied, the potential never stabilizes and at high enough current densities, the potential increases exponentially. Responses below and above the limiting current density are shown in Figure

5.1a. The time dependence of Φ/L reflects the formation of salt concentration gradients under the applied current.

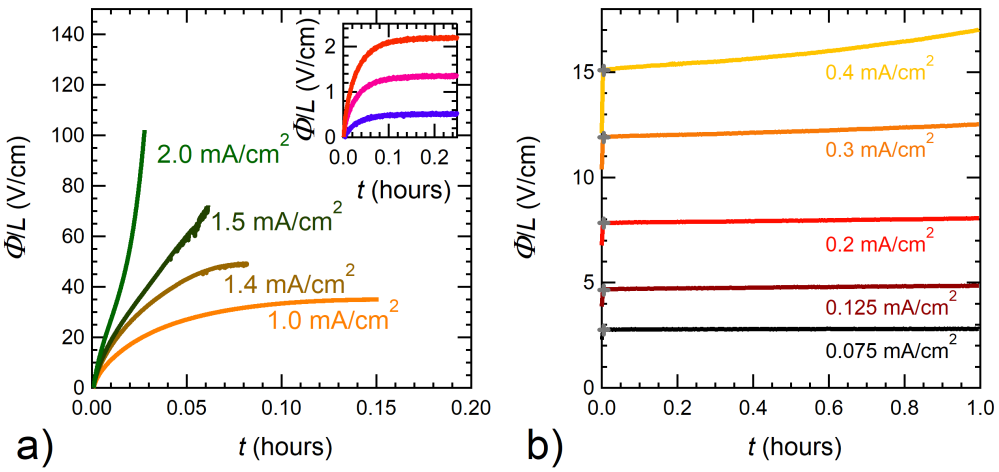

Figure 5.1: Electric potential response to various applied current densities for the (a) PS-PEO/LiTFSI electrolyte and (b) PSLiTFSI-PEO electrolyte plotted as a function of time. Φ, the electric potential, is normalized by electrolyte thickness, L. Inset of (a) shows potential responses at current densities of 0.02, 0.05, and 0.08 mA/cm^2.

Figure 5.1b shows a series of Φ/L vs time plots, when a steady current density is drawn across a symmetric cell with PSLiTFSI-PEO electrolyte, with L of 400 μm. The applied current densities in this experiment are about an order of magnitude lower than those given in Figure 5.1a. The main reason for this is the difference in electrolyte thicknesses; the product iL is similar for both electrolyte types discussed in this work. At low current densities, the potential is independent of time. This constant potential is unsurprising as no concentration gradients are expected to develop in single-ionconducting electrolytes. As larger values of current density are applied, the potential increases with time. This increase is most clear at $i = 0.4$ mA cm^{-2} , the highest current density used in this series of experiments. The Φ/L vs time behaviors at low and high current densities in a block copolymer with added salt and a single-ion conductor differ qualitatively as shown in Figures 5.1a and 5.1b. Thus, analyzing these data sets in a consistent manner to determine the limiting current density is non-trivial.

Our analysis method focuses on the time dependence of Φ/L during the final 20% of the measurement time (Δt). When the limiting current density is exceeded in a binary electrolyte, the potential shoots up toward the end of the experiment. In contrast, when the applied current density is below the limiting current, the potential approaches a time-independent

constant plateau. The distinction between these two regimes can readily be seen when the long-time behavior is examined. For consistency we use the final 20% of the measurement time to analyze both the conventional polymer electrolytes and the single-ion-conducting electrolytes. We fit the Φ/L vs time data in this regime to linear functions and examine the slopes.

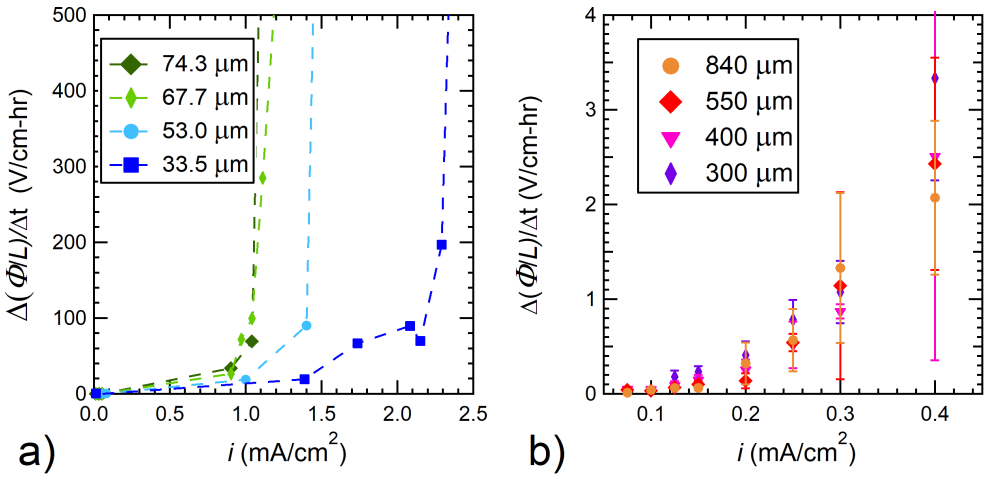

Figure 5.2: Plots of the fitted slopes, $(\Delta\Phi/L)/\Delta t$, obtained from final 20% of measurement time as a function of applied current density, i, for the (a) PS-PEO/LiTFSI electrolyte and (b) PS LiTFSI-PEO electrolyte.

Figures 5.2a and 5.2b show the results of our analysis. Here we plot the slopes, $(\Delta\Phi/L)/\Delta t$, vs the applied current density, i. Figure 5.2a shows data obtained from PS-PEO/LiTFSI electrolytes. It can be clearly seen for each thickness that at low current densities $(\Delta\Phi/L)/\Delta t$ changes minimally with increasing current, until a threshold is reached. For $L = 74.3$ μm, the threshold is in the vicinity of $i = 1.0$ mA cm^{-2} , while for $L = 33.5$ μm, the threshold is in the vicinity of $i = 2.4$ mA cm^{-2} . It is clear that the threshold is thickness-dependent for PS-PEO/LiTFSI electrolytes. This analysis was repeated for four different thicknesses of PSLiTFSI-PEO electrolytes, and the results are shown in Figure 5.2a. The data in Figure 5.2b also exhibit two regimes, wherein $(\Delta\Phi/L)/\Delta t$ changes minimally with increasing current density until a threshold is reached in the vicinity of $i = 2.3$ mA cm^{-2} . However, there is a modest change in $(\Delta\Phi/L)/\Delta t$ when this threshold is crossed. More importantly, changing the electrolyte thickness from 300 to 840 μm has no effect on the threshold current. In Figure 5.2b, the error bars reflect the standard deviation of the obtained values.

We posit that the value of current density at which the slope $(\Delta\Phi/L)/\Delta t$ begins to increase rapidly is indicative of the limiting current density of that electrolyte. To quantify the actual value of the limiting current, each data set in Figures 5.2a and 5.2b was separated into two

regimes, and data within each regime were fit to a straight line. The demarcation between the two regimes (current density) was systematically changed to minimize the sum of squared error. The point of intersection of the two-lines fit was defined as the limiting current.

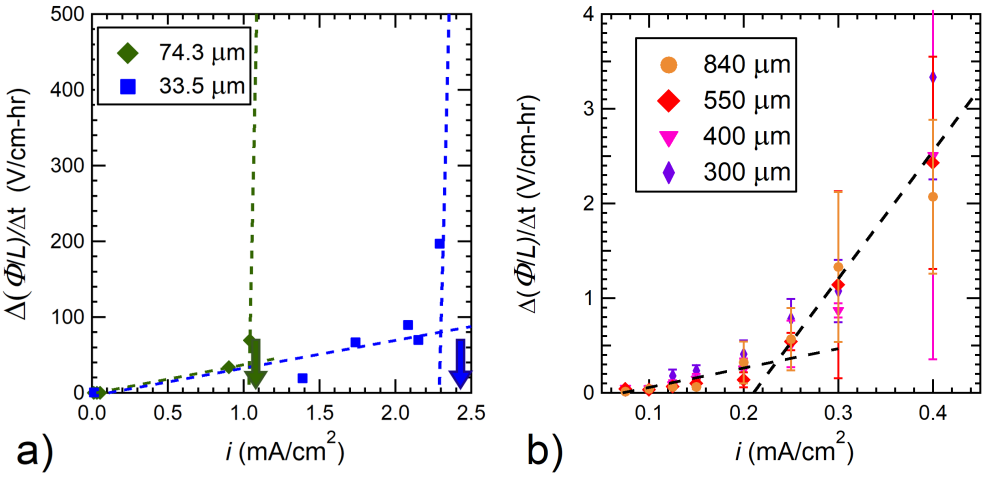

Figure 5.3: Linear fits of data from Figures 5.2a and 5.2b used to determine limiting current. (a) Two-line fits through data obtained from PS-PEO/LiTFSI electrolytes with the largest and smallest thicknesses. Arrows indicate the value of limiting current density determined by the approach from Reference 35 for PS-PEO/LiTFSI. (b) Two-line fit through the data obtained from PSLiTFSI-PEO electrolytes. The data obtained from all four electrolyte thicknesses are consistent with the fit shown.

The distinction between the two regimes was much clearer in the PS-PEO/LiTFSI electrolytes, and this led to unambiguous determination of the limiting current. Example fits obtained for the thinnest and thickest PS-PEO/LiTFSI electrolytes are shown in Figure 5.3a. In these electrolytes, following Reference 35, one could also determine limiting current density by averaging the highest sustainable current, where a steady potential is reached, and the lowest unsustainable current, where no steady state is reached. We refer to this approach as the conventional approach. This value is shown by arrows in Figure 5.3a. It is clear that both approaches give consistent estimates of the limiting current density. The result of our fitting procedure for PSLiTFSI-PEO is shown in Figure 5.3b. We conclude from this analysis that the limiting current density of PSLiTFSI-PEO is 0.235 mA cm^{-2} , and it is the same for all four thicknesses.

In Figure 5.4 we plot the limiting current density (iL) as a function of $1/L$, where the top axis corresponds to PS-PEO/LiTFSI and the bottom corresponds to PSLiTFSI-PEO. Figure 5.4 contains the results of both the conventional method for determining limiting current

density in PS-PEO/LiTFSI (purple circles) along with the slopes method proposed in this work (pink circles). For PS-PEO/LiTFSI, the horizontal error bars reflect the standard deviations of L recorded from a given cell, using X-ray microtomography as described in the experimental section. For the conventional method, iL was plotted as the midpoint of the largest sustainable current density and the smallest unsustainable current. The vertical error bars represent these bounds.

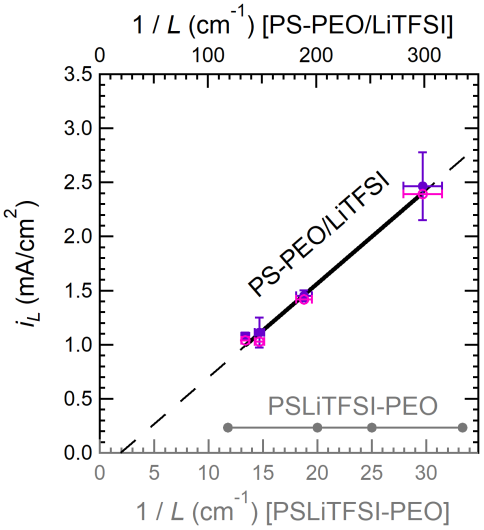

Figure 5.4: Limiting current density plotted as a function of $1/L$, where L is the electrolyte thickness. The top axis is for PS-PEO/LiTFSI, and the bottom axis is for PSLiTFSI-PEO. The two different x-axes are required because the average thicknesses of the electrolytes used in the symmetric cell experiments on the two systems were different. Dark purple data points correspond to the limiting current density determined using the conventional method, and the pink circles correspond to the limiting current density determined using the slopes method.

As seen in Figure 5.4, the limiting current density of PS-PEO/LiTFSI is a linear function of $1/L$. Extrapolation of the linear fit through all 8 data points gives an intercept that is very close to zero. Both facts are consistent with Equation 5.1, indicating that our data are consistent with the conventional definition of limiting current density, defined as the current density at which the LiTFSI concentration at the negative electrode approaches zero. Electrolyte failure occurs when the limiting current density is exceeded; the rapid increase in cell potential is due to irreversible reactions between the electrode and the LiTFSI-free electrolyte. However, the fact that the limiting current density of PSLiTFSI-PEO is independent of electrolyte thickness indicates that electrolyte failure must occur due to some other reason. We posit that beyond the limiting current density the cell potential increases more steeply than expected due to irreversible reactions between the electrode and

the single-ion-conducting electrolyte. Which portion of the polymer chain participates in these reactions (charged or neutral moieties) remains an open question.

The limiting current density of PSLiTFSI-PEO is independent of electrolyte thickness over the range of thicknesses covered in this work. This is a novel result that has not been reported in the literature. This independence with respect to thickness is further indication of the lack of concentration gradients within this electrolyte. Further studies are required to directly identify the physical underpinnings of this result.

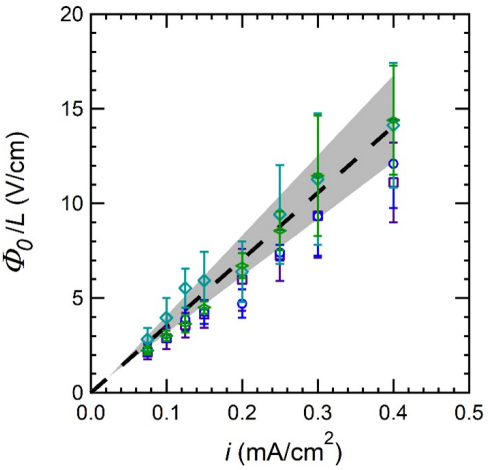

Figure 5.5: Initial values of the normalized potential, Φ_0/L, as a function of applied current for PSLiTFSI-PEO. Each symbol represents the thickness of the electrolyte, L. (Purple squares = 300 μm, Blue circles = 400 μm, Blue rhombuses = 550 μm, Green rhombuses = 840 μm) The dashed black line has a slope $1/\kappa$, and error in conductivity is shown by the gray shading.

We conclude this section by reexamining the voltage vs time curves obtained from the single-ion-conducting electrolyte, PSLiTFSI-PEO, shown in Figure 5.1b. Our analysis thus far has focused on the behavior at long times, the final 20% of our time window. For completeness, in Figure 5.5 we examine the initial potential, Φ_0/L, obtained after the potentiostat has stabilized. These values are marked by crosses in Figure 5.1b. In separate experiments this electrolyte was studied in symmetric cells using AC impedance and the conductivity, κ, thus obtained was $2.85 \times 10^{-5} \pm 4.78 \times 10^{-6}$ S cm^{-1} . A single-ion conductor must obey Ohm's law, due to the absence of concentration polarization at all values of applied current.[66] The line in Figure 5.5 has a slope $1/\kappa$. The error bars in Figure 5.5 represent the standard deviation of the initial potential for each thickness at the corresponding applied currents. The experimentally measured values of Φ_0 are in reasonable agreement with expectations, irrespective of whether the applied current density was above or below the limiting current.

5.5 Conclusions

We have examined the time dependence of potential obtained from lithium-polymer-lithium symmetric cells at constant current density. We have shown that for a conventional polymer electrolyte (PS-PEO/LiTFSI), the limiting current density is proportional to the inverse of the electrolyte thickness. While this behavior is expected and consistent with theory, we were unable to find any other studies of the effect of electrolyte thickness on limiting current density in the literature. We propose a new approach for consistently determining limiting current density in both conventional electrolytes and single-ion-conducting electrolytes. The measured limiting current density of a single-ion-conducting electrolyte (PSLiTFSI-PEO) was found to be independent of electrolyte thickness. This phenomenon has not been documented before in the literature. It has interesting implications for developing electrolytes to increase the lifetime of rechargeable batteries, as increasing electrolyte thickness has no effect on the window of current densities that can be drawn across the electrolyte. Further studies are needed to better understand what causes this failure within the PSLiTFSI electrolytes, and to determine if our framework can be used to determine the limiting current density of other single-ion-conductors such as inorganic crystals and glasses.

5.6 Acknowledgements

This work was intellectually led by the Joint Center for Energy Storage Research (JCESR), an Energy Innovation Hub funded by the U.S. Department of Energy, Office of Science, Office of Basic Energy Science, under Contract No. DE-AC02–06CH11357, which supported characterization work conducted by Z. J. H. under the supervision of N.P.B. A.S.H was supported by a National Science Foundation Graduate Research Fellowship DGE-2020294884. The authors thank Kevin Gao and Louise Frenck for useful discussion related to this work.

5.7 Supporting Information

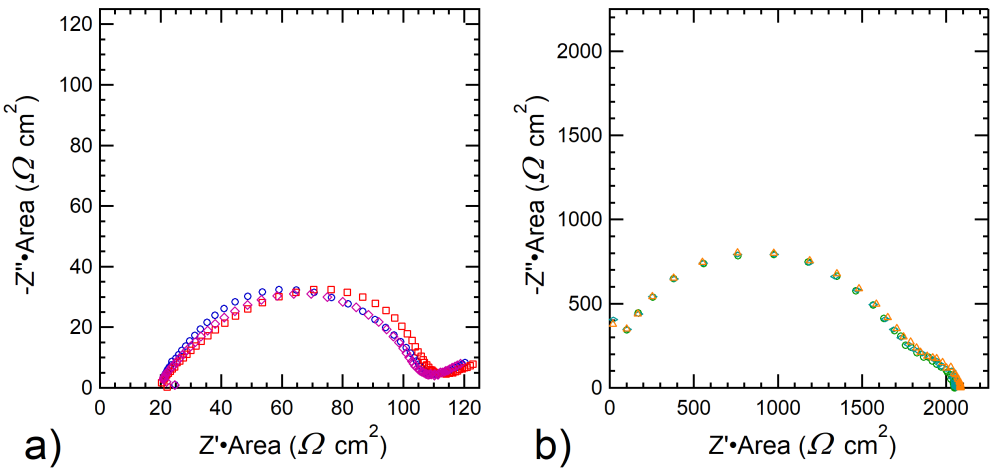

Figure 5.6: Characteristic impedance data collected between limiting current density experiments for (a) PS-PEO/LiTFSI electrolyte with a thickness of 67.7 μm, and (b) PSLiTFSI-PEO electrolyte with a thickness of 550 μm. The complex impedance is Z'+iZ". Minimal changes are observed in impedance data between measurements indicating no significant changes to the electrolyte.

5.8 Nomenclature

Table 5.1: List of Symbols and Abbreviations

Symbol	Meaning
C_b	salt concentration (mol/cm^3)
D	salt diffusion coefficient (cm^2/s)
F	Faraday's constant (C/mol)
i	applied current density (mA/cm^2)
i_L	limiting current density (mA/cm^2)
L	electrolyte thickness (μm)
LiTFSI	lithium bis(trifluoromethanesulfonyl)imide
PS-PEO	polystyrene–b–polyethylene oxide
PSLiTFSI-PEO	polystyrene-LiTFSI-b-polyethylene oxide
r	molar ratio of lithium ions to ethylene oxide units (r = [Li$^+$]/[EO])
t_+	cationic transference number
t	measurement time (hr)
κ	conductivity (S/cm)
Φ	potential (mV)
Φ_0	initial potential (mV)
ρ_+	current fraction

6: Complete Electrochemical Characterization of a Beyond-PEO Polymer Electrolyte*

6.1 Abstract

Typical liquid electrolytes are comprised of a lithium salt dissolved in a mixture of organic solvents. Conventional polymer electrolytes (typically poly(ethylene oxide) (PEO) based) have comparatively lackluster performance which prevents their widespread adoption, however they are nonflammable and stable against lithium metal anodes. Recently, our group published work on a new polymer electrolyte, lithium bis(trifluoromethanesulfonyl)imide salt (LiTFSI) dissolved in poly(pentyl malonate) (PPM), with the potential to surpass PEO as the benchmark polymer electrolyte [X. Yu et al., *ACS Energy Lett.* 2022, 3791-3797]. In this study we present a synthetic method that results in improved purity of PPM. Additionally, we have completed the full electrochemical characterization of PPM, including determination of the cationic transference number with respect to the solvent velocity, t_0^+, and the thermodynamic factor, T_f. We find PPM's measured t_0^+ is significantly higher than that of PEO, which explains the higher limiting current density measured in our previous study on PPM. The thermodynamic factor is lower in PPM than PEO, and interestingly shows that PPM electrolytes demonstrate ideal interactions within a range of salt concentration $0.04 \leq r \leq 0.10$. Using our results from full electrochemical characterization, salt concentration profiles and electric potential drops across the electrolyte are modeled with Newman's concentrated solution theory. We find that salt concentration polarization is significantly reduced in PPM, and that our predicted values of the limiting current density agree with those measured previously. We also provide a comparison of PPM and PEO to demonstrate the practical benefits in performance for PPM over PEO.

6.2 Introduction

Demand for lithium-ion batteries is only growing as electric vehicle production increases, and the use of rechargeable batteries in consumer products grows.[120–122] Recently, increases in lithium-ion performance have begun to decline, and as we strive for the next generation of rechargeable lithium-ion batteries, new electrode materials are required to provide significant performance gains over conventional lithium-ion technologies.[24,123–125] Electrolyte compatibility is a major barrier for the adoption of these promising electrode materials such as silicon or lithium metal anodes. Conventional lithium-ion battery electrolytes are comprised of metal salts dissolved in mixtures of organic solvents. These electrolytes react

*This chapter is adapted from Lee, J.†; Hoffman, Z. J.†; Chakraborty, S.; Patel, V.; Balsara, N. P. 2023, In preparation. † denotes equal contribution

against high energy electrode materials and show the need for alternative materials to enable next-generation battery technologies.[24,26]

Polymer electrolytes have great potential for replacing conventional battery electrolytes. Metal salts dissolved in poly(ethylene oxide) (PEO) were first hypothesized for battery electrolyte applications by M. Armand.[18] While, PEO's potential as an electrolyte material was discovered decades ago, only recently have there been polymeric electrolyte materials that show promise to outperform PEO electrolytes. Jones et al. have reported polymeric zwitterionic electrolytes that show conductivity and current fraction values, transport parameters that can be used to compare electrolyte performance in the regimes of small applied current densities, that surpass those of PEO electrolytes.[126] Our group has recently published work on a polymer electrolyte, poly(pentyl malonate) (PPM), which shows great potential to surpass the electrochemical performance of PEO electrolytes.[127]

The product of κ and ρ_+, known as the electrolyte efficacy, provides a basis to compare electrolyte performance in the regimes of small current densities where these parameters are measured. Our preliminary study showed PPM to have a greater electrolyte efficacy over PEO. However, superior electrolyte efficacy is not always an indicator of improvements in practical performance, and of more interest is PPM's larger measured limiting current density.[89,127] The limiting current density, i_L, is the maximum current density which can be stably applied across an electrolyte. This limitation is driven by the concentration gradients that develop within an electrolyte, as larger current densities are applied salt concentration gradients grow until the salt concentration at the negative electrode reaches zero at the limiting current density. Materials with high values of limiting current density are of great interest for use in high power battery applications.

So far, our study of the electrochemical properties of PPM has been limited to measurements of κ, ρ_+, and i_L. Following Newman's concentrated solution theory, fully characterizing ion transport in an electrolyte allows for determination of the thermodynamic factor along with three transport parameters, κ, salt diffusion coefficient, D, and the cationic transference number with respect to the solvent velocity, t_+^0.[33] Completing measurements of all these parameters is rare in the literature, and to our knowledge there are few studies where polymer electrolyte aside from PEO have been fully characterized.[29,87,89] Full electrochemical characterization allows for the prediction of steady-state salt concentration profiles and electric potential gradients that result when an electrolyte is polarized in response to an applied current density.

In this study we report synthetic methods for improved purity and control of functional end groups of PPM compared to the framework previously reported.[127] The results of the full electrochemical characterization of our "well-defined" PPM are reported here, including a comparison of the modeled limiting current densities to our experimental results. We also provide a framework for comparing the practical performance of electrolytes, reinforcing the

promise of PPM electrolytes.

6.3 Experimental Methods

6.3.1 Polymer Synthesis

All chemicals were purchased from commercial sources and used as received: dimethyl malonate (98%), 1,5-pentanediol (purum, ≥97.0% (GC)), titanium(IV) isopropoxide (99.999% trace metals basis) and lithium bis(trifluoromethanesulfonyl)imide (LITFSI, 99.95% trace metals basis) were purchased from Aldrich.

Dimethyl malonate (13.85 grams, 105 mmol) and 1,5-pentanediol (10.4 grams, 100mmol) were placed in a 100 mL round-bottom flask equipped with a magnetic stir bar. Then, the flask was purged with Nitrogen gas at 120 °C for 2 hours to remove the moisture in the reactor. After that, titanium isopropoxide (30 μL, 0.1 mmol) was added to the flask, and the flask was equipped with a 30 cm air reflux condenser at 120 °C for 12 hours. Methanol was formed and evaporated throughout the course of the reaction. The reactor was maintained at 120 °C and connected to moderate vacuum (250 mmHg) for 24 hours followed by high vacuum (0.3 mmHg) for 48 hours. After cooling down the flask to room temperature, the crude product was purified by re-precipitation in methanol solvent after adding dichloromethane (DCM). After collecting the precipitated polymer, the polymer was re-dissolved DCM and re-precipitated in diethyl ether solvent. The pale-yellow viscous polymer was dried in a vacuum oven for 24 hours without heat, and then further dried for 24 hours at 60 °C.

6.3.2 Electrolyte Preparation

Electrolytes were prepared within an argon glovebox with oxygen and water levels below 2 and 1 ppm respectively. Poly(pentyl malonate) (PPM) polymer with a molecular weight of 14.5 kg/mol was dried in a heated glovebox antechamber at 90 °C for 1 day under active evacuation, to remove any solvent from synthesis. Lithium bis(trifluoromethanesulfonyl)imide salt (LiTFSI) (Sigma Aldrich) was dried in a heated glovebox antechamber at 120 °C for 3 days under active evacuation. Predetermined amounts of PPM and LiTFSI were dissolved in anhydrous THF (Sigma Aldrich) and stirred at 60 °C in a capped vial. Once fully dissolved, the vial was uncapped and the THF evaporated overnight. The electrolytes were then thoroughly dried in a heated glovebox antechamber at 90 °C for 1 day. We use r as a measure of salt concentration which is defined as the molar ratio of lithium atoms to oxygen atoms in the polymer unit, where $r = [Li^+]/[O]$. The range of salt concentrations studied in this work was from $r = 0.005$ to 0.15. The PPM electrolytes were amorphous across the range of salt concentrations studied. At low concentrations the electrolytes flowed readily, however at high salt concentrations the electrolytes were significantly more viscous.

The density, ρ, of our electrolytes was directly measured by filling an aluminum pan (TA Instrument) with a set volume of 40 μl. The pans were sealed, and then the mass was measured. This measurement was made for three different samples of each electrolyte. The error of these measurements was found to be below 3%. This data can be found in Figure 6.7. These density measurements were used to calculate the salt concentration, c, using the equation,

$$c = \frac{\rho r}{M_{PM} + r M_{LiTFSI}}, \tag{6.1}$$

where M_{PM} and M_{LiTFSI} are 172.2 and 287.09 g/mol, respectively. The values of r, ρ, c, and m are reported in Table 6.1.

Table 6.1: Values of density and salt concentration of PPM electrolytes as a function of r.

r	ρ (g/L)	c (mol/L)	m (mol/kg)
0	1273	0.00	0.00
0.005	1276	0.14	0.12
0.01	1286	0.28	0.23
0.02	1339	0.54	0.46
0.04	1386	1.01	0.93
0.06	1429	1.43	1.39
0.08	1465	1.82	1.86
0.10	1567	2.17	2.32
0.12	1646	2.51	2.79
0.14	1691	2.82	3.25
0.15	1710	2.98	3.48

6.3.3 Electrochemical Characterization

All electrochemical cells were prepared within an argon glovebox with oxygen and water concentrations below 1 ppm. Stainless-steel symmetric cells were used to measure the conductivity, κ, of our electrolytes. These cells were constructed by filling silicone spacer material (McMaster Carr) (internal diameter of 3.175 mm) with our electrolytes and sandwiching them between two 200 μm thick stainless-steel electrodes. The thickness of the stack was measured with a micrometer to find the electrolyte thickness, L. Nickel tabs (MIT Corp.) were attached to the electrodes and the cells were vacuum sealed in laminated pouch material (MTI Corp.). Lithium symmetric cells were used for measurements of the salt diffusion coefficient, D, current fraction, ρ_+, and limiting current density, i_L. These cells were constructed similarly to the stainless-steel symmetric cells. Lithium foil (MTI Corp.) was brushed and pressed using a pneumatic press, then the thickness was measured using a micrometer. The silicone spacer material (McMaster Carr) (internal diameter of 3.175 mm) was placed on one

lithium electrode, and the electrolyte was loaded into the cell. The second lithium electrode was placed on top and stainless-steel shims were placed on top of each lithium electrode. The thickness of the stack was measured with a micrometer, and the electrolyte thickness was calculated by subtracting the thickness of the electrodes and stainless-steel shims from the total thickness. Nickel tabs were then attached, and the stack was vacuum sealed in laminated pouch material.

Conductivity measurements were made using stainless-symmetric cells. The cells were annealed at 90 °C for 3 hours before experiments were performed. Conductivity measurements were made at various temperatures from 30 to 90 °C. To measure the conductivity electrochemical impedance spectroscopy (EIS) was used. Measurements were made from 1 MHz to 100 mHz with a sinus amplitude of 40 mV to identify the bulk resistance, R_{bulk}. The conductivity was calculated by,

$$\kappa = \frac{L}{aR_{bulk}}, \tag{6.2}$$

where a is the electrochemically active area, and L is the electrolyte thickness.

The current fraction was measured using lithium symmetric cells following previously described methods.[48,60,75] All measurements with lithium symmetric cells were performed at 90 °C. These cells were first preconditioned with 3-hour polarizations of $\pm$ 0.02 mA/cm^2 followed by 3 hours of OCV. The resistance of the electrolyte was measured during preconditioning to track changes in the bulk and interfacial resistances, R_{int}. This process was repeated 4 times until the resistances stabilized and a stable solid electrolyte interface (SEI) layer was formed. After preconditioning, a potential was applied to the cell until the measured current reached a steady state value, i_{ss}. During this polarization, impedance measurements were made to track R_{bulk} and R_{int}. A modified version of the equation developed by Bruce and Vincent can be used to calculate the current fraction:

$$\rho_+ = \frac{i_{ss}(\Delta V - i_\Omega R_{int,0})}{i_\Omega(\Delta V - i_{ss}R_{int,ss})}. \tag{6.3}$$

i_Ω is the calculated initial current ($i_\Omega = \frac{\Delta V}{R_{bulk,0}+R_{int,0}}$), where subscripts 0 and ss indicate the initial and stead state values respectively. For these experiments ΔV values of $\pm$10 and $\pm$20 mV were used.

After polarization, the cells are allowed to relax, and the resulting decline in potential can be fit to an exponential equation,

$$V(t) = k_0 + k_1 e^{-k_2 t}, \tag{6.4}$$

where k_0 is the fitted offset voltage and k_1 and k_2 are fit parameters. The salt diffusion coefficient is calculated using equation 6.5,

$$D = \frac{L^2 k_2}{\pi^2}. \tag{6.5}$$

The determination of the time range over which this data is fit is significant and is discussed in previous works.[55,75]

Concentration cells were used to measure the electric potential resulting in salt concentration differences between electrolytes. Their construction follows previously reported methods.[48,75] It is worth noting that due to the low viscosity of PPM electrolytes compared to PEO or PEO-based electrolytes, the spacer material used to construct these cells included an adhesive backing to ensure the electrolyte did not leak out of the cell during experiments. For these cells, half of the channel was filled with a reference electrolyte, $r = 0.06$, and the other half was filled with the electrolyte of interest. Lithium electrodes with nickel current collectors were placed on the end of each channel, and the cell was sealed in laminated pouch material. The cells were heated to 90 °C and the electric potential, U, of the electrolyte was measured until it reached a plateau, typically at around 10 hours.

6.3.4 Limiting Current Density Measurements

Lithium symmetric cells were used to measure the limiting current density of our electrolytes. The cells were constructed and preconditioned exactly as described for the measurements ofρ_+ and D. For limiting current density measurements an initial impedance measurement was taken, followed by a constant current polarization. After a stable plateau in potential was reached, or the potential diverged, the cell was allowed to relax at OCV, and then a final impedance measurement was taken. The limiting current density was taken as the average of the highest stable current density, where a plateau in potential is reached, and lowest unstable current density, where no plateau is reached.[35]

6.4 Results and Discussion

A comparison of κ and ρ_+ of the well-defined PPM in this study, and the PPM previously reported can be found in Figure S2.[127] Slight differences arise in our measurements, which we attribute to the improved purity of our well-defined PPM. For the remainder of this work, the PPM discussed is the well-defined PPM synthesized for this study unless otherwise specified. Results of our full electrochemical characterization of PPM are shown below. The measured electrochemical properties of PPM are shown in Figures 6.1a-6.1d and both experimentally collected data and their fits are reported. We also compare the results of our electrochemical characterization of PPM to that of PEO/LiTFSI electrolytes. The reported data for PEO in this work came from the compilation of data from studies of PEO/LiTFSI electrolytes at various molecular weights above the entanglement threshold of PEO, unless stated otherwise.[22] The black lines indicate a fit through the entire PEO data set compiled in Reference 22, and the gray shading is indicative of 95% confidence intervals for each fit. Further explanation of the data and processes to compile them can be found in Reference 22.

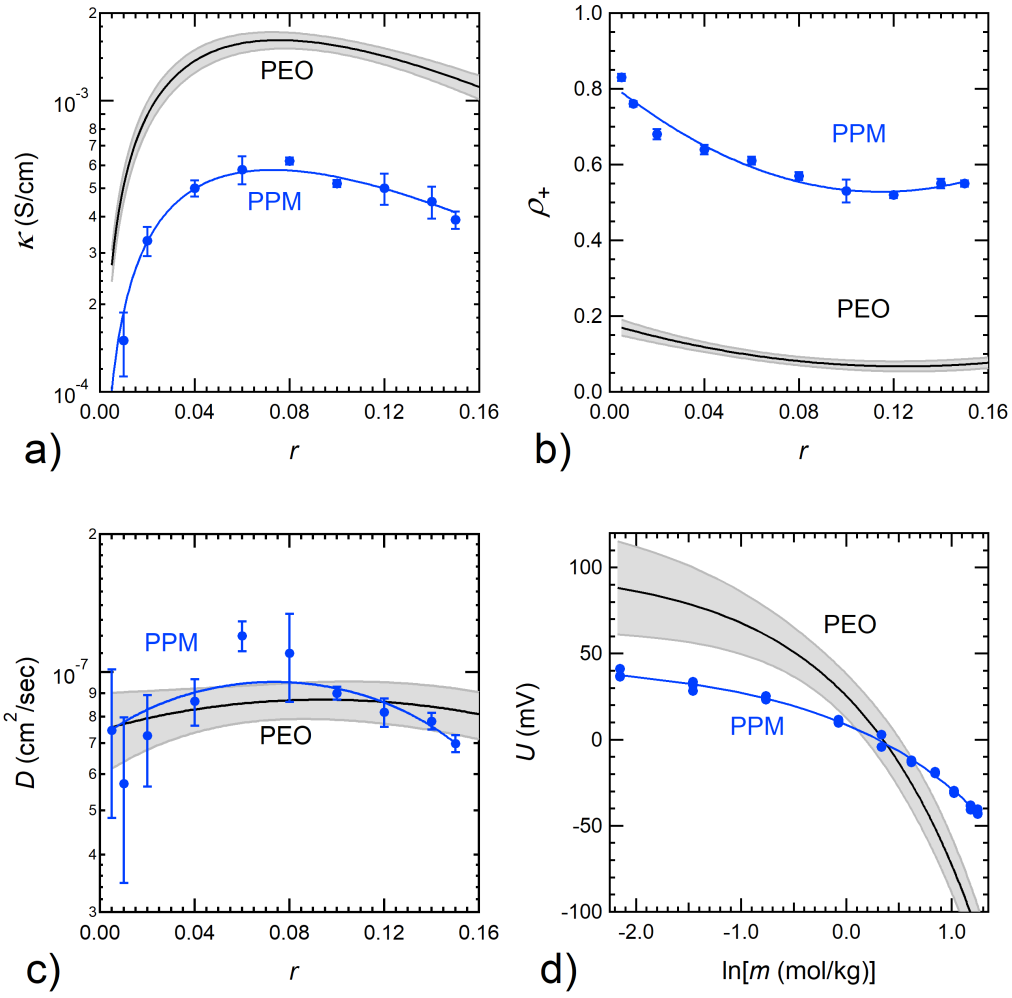

Figure 6.1: (a) Conductivity, κ, (b) current fraction, ρ_+, and (c) salt diffusion coefficient, D, plotted as a function of salt concentration, r.(d) Open circuit potential measured using concentration cells, U, as a function of the natural log of molality, ln$m$. All measurements were made at 90 °C. The blue data points are the average of the measured values at each salt concentration for PPM/LiTFSI, and the error bars represent the standard deviation of each measurement. The blue lines are the fits of this data, Equations 6.5-6.9. The black lines in each plot represent the values of PEO/LiTFSI electrolytes for each parameter, with the gray shading representing the 95% confidence interval. This data is taken from Reference 22

Figure 6.1a shows the conductivity, κ, as a function of salt concentration, r. At low salt concentrations, $r < 0.08$, the conductivity increases with salt concentration due to increases in the concentration of charge carriers. At high salt concentrations, $r > 0.08$, the conductivity steadily declines as the addition of salt results in restriction of the segmental motion of the

polymer. We use a fit proposed by Mongcopa et al.,

$$\kappa = A_1 r e^{-\frac{r}{r_{max}}} \tag{6.6}$$

where A_1 is a fitted parameter, equal to 0.0216 for PPM, and r_{max} is a fitted value that corresponds to salt concentration at which conductivity is maximized, equal to 0.0729 for PPM.[58] This result is consistent with the analysis for PEO/LiTFSI electrolytes, where r_{max} = 0.075.[22,75] This consistency in r_{max} is not universal across polymer electrolytes.[89,128] Across the range of salt concentrations studied, the conductivity of the PPM electrolytes is approximately three times smaller than that of PEO electrolytes.

Figure 6.1b shows the current fraction, ρ_+, as a function of r. The current fraction decreases steadily with increasing salt concentration until a minimum value is reached around r = 0.12, after which point it increases as salt concentration increases. The PPM data fit was fit to a polynomial function,

$$\rho_+ = 21.9r^2 - 5.01r + 0.815. \tag{6.7}$$

The maximum value of current fraction in PPM/LiTFSI is over four times greater than that of PEO/LiTFSI. As with the conductivity data, the trends in current fraction with respect to salt concentration are very similar between PEO and PPM.

Figure 6.1c shows the salt diffusion coefficient, D, as a function of r. The salt diffusion increases slightly with salt concentration until it reaches a maximum at r = 0.08, where it then decreases with increasing salt concentration. The PPM data set was fit to a polynomial function,

$$D = (-4.29 \times 10^{-6})r^2 + (6.32 \times 10^{-7})r + (7.20 \times 10^{-8}). \tag{6.8}$$

Across the range of salt concentrations in this study, D of PPM lies within error of PEO.

Figure 6.1d shows the open-circuit potential across concentration cells, U, as a function of electrolyte of a salt concentration r = 0.06. U decreases monotonically with increasing salt concentration as expected. The data is fit to the equation,

$$U = 45.9 - 37.3m^{0.691}. \tag{6.9}$$

The analytical zero of Equation 6.9 lies at r = 0.059, which matches the salt concentration of our reference electrolyte, r = 0.06. This monotonic decrease in U with respect to ln$m$ matches with PEO, though we note that the dependence of U on ln$m$ is weaker in PPM than in PEO.

The thermodynamic factor, T_f, can be calculated using the equation,

$$T_f = 1 + \frac{dln\gamma_{\pm}}{dln\mathrm{m}} = \frac{\kappa}{\nu RTDc(\frac{1}{\rho_+} - 1)} \left(\frac{dU}{dln\mathrm{m}}\right)^2, \tag{6.10}$$

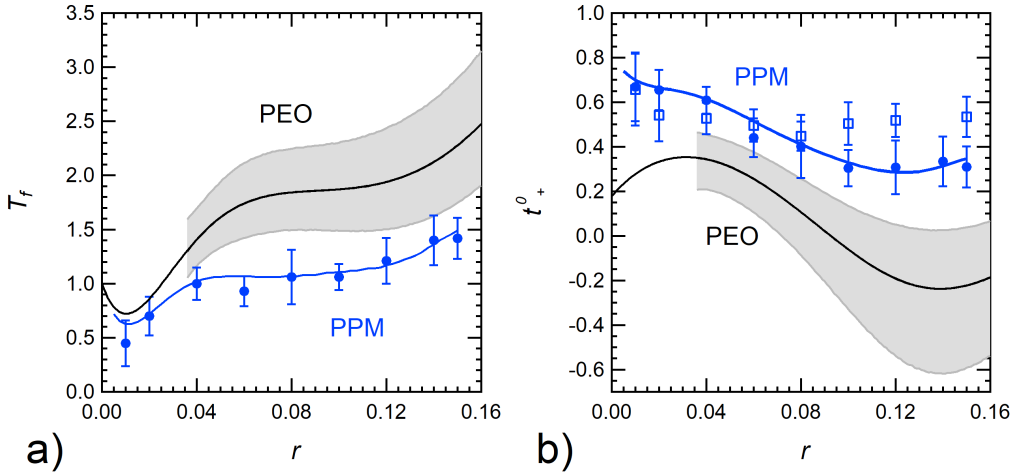

Figure 6.2: (a) Thermodynamic factor, T_f, (b) cationic transference number with respect to the solvent velocity, t_+^0, plotted as a function of salt concentration, r. The filled blue circles indicate the results of Equation 6.11 and 6.12 using experimentally measured values of each parameter for PPM/LiTFSI with the error bars representing the cumulative error of the calculation following the procedures discussed in Reference 22. The blue line indicates the results of Equation 6.11 and 6.12 using fits of experimental values, Equations 6.6-6.10. The PEO curves below $r = 0.035$ comes from a polynomial fit of the data for $r < 0.035$, constrained so that as $r \to 0$, $T_f \to 1$, and $t_+^0 \to \rho_+$. The PPM curves below $r = 0.02$ comes from a polynomial fit of the data for $r < 0.02$, constrained so that as $r \to 0$, $T_f \to 1$, and $t_+^0 \to \rho_+$. The blue hollow squares in (b) are t_+^0 values of PPM/LiTFSI electrolytes predicted from MD simulations from Reference 129. The black lines in each plot represent the values of PEO/LiTFSI electrolytes for each parameter, with the gray shading representing the 95% confidence interval. This data is taken from Reference 22.

where $\gamma_\pm$ is the mean molal activity coefficient of the salt, ν is the stoichiometric parameter, $\nu = \nu_+ + \nu_-$, where ν_+ and ν_- are the number of cations and anions respectively formed when the salt dissociates, R is the gas constant, and T is the temperature. Figure 6.2a shows the results of these calculations for PPM and PEO electrolytes. The blue data points are the values of the thermodynamic factor calculated from the experimentally determined values of κ, ρ_+, D, and U in Figures 6.1a-6.1d with the error bars representing the cumulative error of the calculation following the procedures discussed in Reference 75, and the blue line is the thermodynamic factor calculated using Equations 6.6-6.10. Thermodynamics dictates that $T_f = 1$ at $r = 0$ for all electrolytes, thus the solid curves in Figure 6.2a below a cutoff r value, 0.02 and 0.035 for PPM and PEO respectively, comes from a polynomial fit of the data above the cutoff concentration, constrained so that $T_f = 1$ at $r = 0$.[33,130] As seen in Figure 6.2a, T_f initially decreases for both PPM and PEO, which is consistent with studies of other

electrolytes.[29,87–89] From $0.04 \leq r \leq 0.10$, T_f remains close to a value of one. This indicates $\frac{dln\gamma_{\pm}}{dlnm} \rightarrow 0$ across this range of salt concentrations, meaning that changes in salt concentration have little effect on the interactions between ions within the electrolyte, characteristic of ideal behavior.[33,130] For $r > 0.10$, T_f increases with salt concentration. While the trend in T_f with respect to r is very similar between PPM and PEO, the magnitude of T_f in PPM is smaller than that of PPM. As discussed in previous work, the lowered value of T_f indicates more favorable interactions between polymer and salt which may stem from an increased density of oxygen atoms in the PPM polymer compared to PEO.[89] Initial studies of PPM with MD simulations have been performed and will be discussed below, but further MD simulations are necessary to understand the T_f results in PPM electrolytes.

The cationic transference number with respect to the solvent velocity can be determined with the equation,

$$t_+^0 = 1 + \left(\frac{1}{\rho_+} - 1\right) \frac{FDc}{\kappa} \left(\frac{dlnm}{dU}\right). \tag{6.11}$$

Figure 6.2b shows the results of these calculations for PPM and PEO electrolytes. The blue data points are the values of t_+^0 calculated from the experimental measurements of κ, ρ_+, D, and U with the error bars representing the cumulative error of the calculation following the procedures discussed in Reference 75, and the blue line is t_+^0 calculated using Equations 6.1a-6.1d and Equation 6.10. Following Newman's concentrated solution theory, in the dilute limit, $r \rightarrow 0$, $t_+^0 \rightarrow \rho_+$.[33,38,59] Thus, the solid curves in Figure 6.2b below a cutoff r value, 0.02 and 0.035 for PPM and PEO respectively, are produced from a polynomial fit of the data above the cutoff concentration, constrained so that $t_+^0 \rightarrow \rho_+$ as $r \rightarrow 0$. t_+^0 decreases with increasing r, until a minimum is reached around $r = 0.12$. For $r > 0.12$, t_+^0 increases with r. For PEO electrolytes, $t_+^0 < 0$ over a range of salt concentrations, but for PPM it remains positive throughout the concentrations studied in this work.

Recent MD simulations have predicted t_+^0 for PPM electrolytes.[129] These results are plotted in Figure 6.2b as hollow blue squares. At $r \leq 0.08$, our experimentally determined values of t_+^0 match within error with those from MD predictions. At $r > 0.08$, there is still qualitative agreement between simulations and experimental results. These MD simulations suggest the high values of t_+^0 in PPM stem from the involvement of 2 or 3 chains within the solvation cage, compared to PEO which typically has 1 or 2 chains involved.[129]

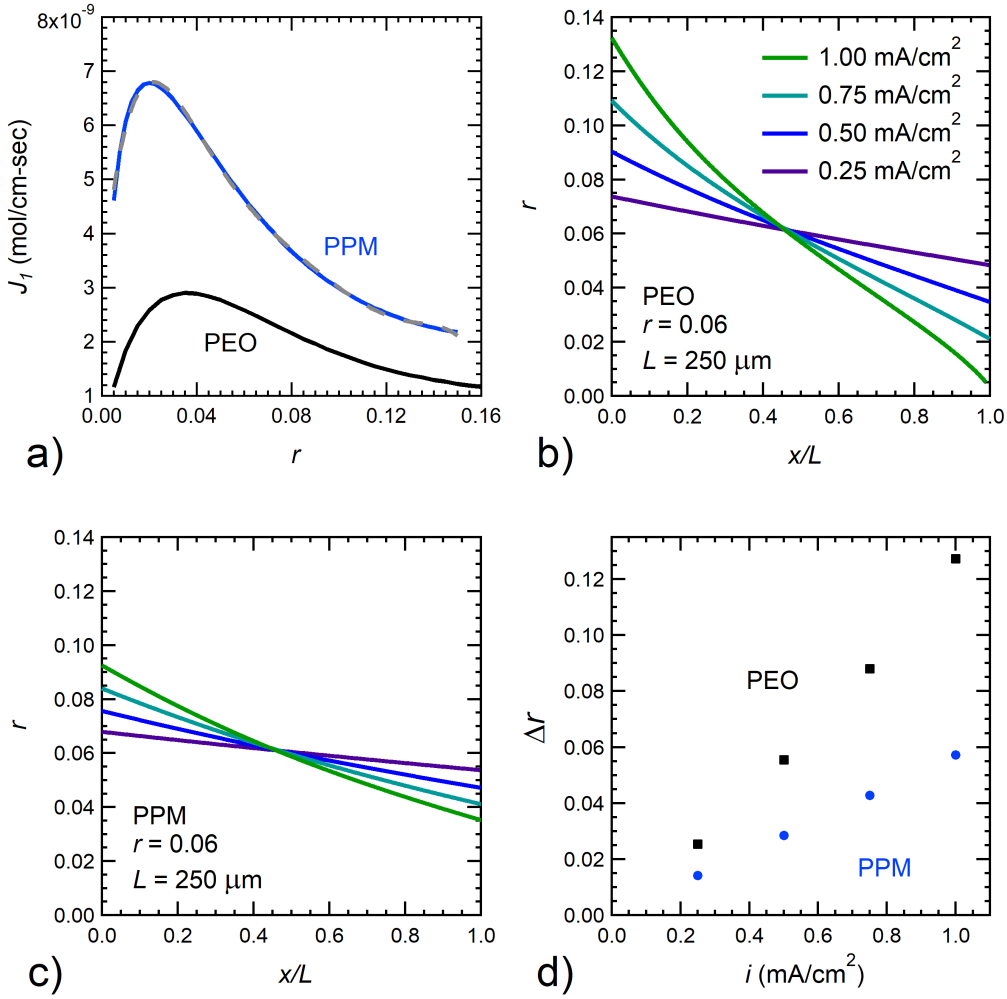

Figure 6.3: (a) J_1 plotted as a function of r for PPM (blue solid line), using Equations 6.6, 6.7, 6.9, and 6.12, and PEO (black solid line), using data from Reference 22 and Equation 6.12. The gray dashed line indicates the polynomial fit (Equation 6.14) of J_1 of PPM. (b) Predicted salt concentration profiles from concentration solution theory in a $r = 0.06$ PEO electrolyte of $L = 250$ μm, at four different applied current densities. (c) Predicted salt concentration profiles from concentration solution theory in a $r = 0.06$ PPM electrolyte of $L = 250$ μm, at the four current densities used in (b). (d) Predicted concentration polarization, Δr ($\Delta r = r_{x=0} - r_{x=L}$), plotted as a function of the applied current density for $r = 0.06$ PPM and PEO electrolytes with $L = 250$ μm.

Salt concentration gradients can be predicted using the results of full electrochemical char-

acterization. The equation,

$$\int_{r(x=0)}^{r(x)} J_1 \, dr = -\frac{iL}{F}\left(\frac{x}{L}\right), \tag{6.12}$$

where,

$$J_1 = \frac{\kappa\left(\frac{dU}{dln\mathrm{m}}\right)}{\left(1-\frac{1}{\rho_+}\right)rF}, \tag{6.13}$$

is used to make these predictions following methods developed previously using concentrated solution theory.[28,34] Figure 6.3a shows J_1 plotted as a function of r for PPM, along with J_1 for PEO electrolytes using data from Reference 22. Equations 6.6, 6.7, and 6.8, are combined to produce J_1 curve for PPM (solid blue line). The PPM curve was fit to a polynomial equation (dashed gray line),

$$\begin{aligned} J_1 = \ & (-2.71\times10^{-2})r^6 \ + \ (1.45\times10^{-2})r^5 + (-3.11\times10^{-3})r^4 + \\ & (3.36\times10^{-4})r^3 + \ (-1.90\times10^{-5})r^2 + (4.60\times10^{-7})r \ + \ \left(2.94\times10^{-9}\right). \end{aligned} \tag{6.14}$$

Figure 6.3b shows steady-state salt concentration profiles generated using Equations 6.12 and 6.13, along with data from Reference 22, for a PEO electrolyte with r = 0.06 and L = 250 μm. Four different applied current densities were modeled: 0.25, 0.50, 0.75, and 1.00 mA/cm^2. Larger applied current densities result in larger salt concentration gradients. Figure 6.3c shows steady-state concentration profiles generated using Equations 6.12-6.14 for a PPM electrolyte with r =0.06 and L = 250 μm, for applied current densities: 0.25, 0.50, 0.75, and 1.00 mA/cm^2. The colors of the curves in Figure 6.3c correspond with the same current densities indicated in the legend of Figure 6.3b. The concentration polarization for PPM at each modeled current density is clearly smaller than that of PEO. To quantify the difference in predicted concentration polarization we can calculate the difference in salt concentration between the two electrodes,

$$\Delta r = \ r_{x=0} - r_{x=L}. \tag{6.15}$$

Figure 6.3d shows Δr as a function of applied current density for our modeled predictions for PPM and PEO electrolytes with r = 0.06 and L = 250 μm. At each applied current density, the concentration polarization in PEO is two times greater than in PPM.

Concentrated solution theory allows for predictions of the electric potential drop across an electrolyte, in addition to the salt concentration profiles that develop in response to an applied current density. Following the equations and methods developed by Pesko et al.,

$$\int_{r(x=0)}^{r(x)} J_2 \, dr = -\frac{\Phi_{ss}(x)}{F}, \tag{6.16}$$

where,

$$J_2 = \frac{\frac{dU}{dln\mathrm{m}}}{(\rho_+ - 1)\, rF}, \tag{6.17}$$

are used to predict the potential drop across an electrolyte at steady state.[34] Figure 6.4a shows J_2 plotted as a function of r for PPM, along with J_2 for PEO electrolytes using data from Reference 22. Equations 6.8 and 6.9 are combined to produce the J_2 curve for PPM (solid blue line). This curve was fit to a double exponential equation (dashed gray line),

$$J_2 = (9.09 \times 10^{-6}) + (3.54 \times 10^{-5})e^{-33.1r} + (4.48 \times 10^{-5})e^{-176.1r}. \tag{6.18}$$

Figure 6.4b shows the comparison of the modeled steady-state potential drops that occur in the electrolytes from Figures 6.3b and 6.3c in response to the applied current densities: 0.25, 0.50 0.75, and 1.00 mA/cm^2. As with the concentration polarization, at each applied current density the resulting potential drop in the PEO electrolyte is two times larger than in the PPM electrolyte.

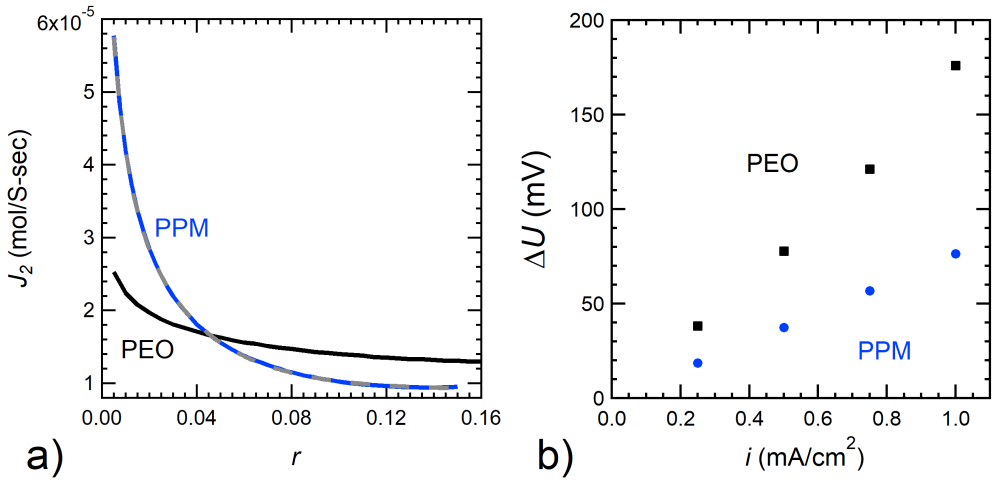

Figure 6.4: (a) J_2 plotted as a function of r for PPM (blue solid line), using Equations 6.8, 6.9, and 6.17, and PEO (black solid line), using data from Reference 22 and Equation 6.17. The gray dashed line indicates the double exponential fit (Equation 6.18) used to fit J_2 of PPM. (b) Predicted cell potential drops, ΔU, plotted as a function of the applied current density for $r = 0.06$ PPM and PEO electrolytes with $L = 250$ μm.

Experimental validations of predicted salt concentration gradients are challenging and can require more intricate methods such as X-ray transmission, MRI, or Raman spectroscopy.[78,86,131] However, the measurement of the steady state electric potential of an electrochemical cell, and comparison with the predicted electric potential drop can provide a straightforward

method for indirectly evaluating the predicted salt concentration gradients. Work to measure cell potential as a function of salt concentration and applied current density is currently ongoing to allow for a widescale comparison with the predicted results to understand the accuracy of our modeled results. Future work is needed to make direct measurements of salt concentration profiles within PPM electrolytes to compare with those predicted from concentrated solution theory.

Previous work from our group compared the experimentally measured limiting current density of PEO electrolytes with that predicted from concentrated solution theory. This work found quantitative agreement between experiments and predictions.[36] These results are included in Figure 5, where the black square indicate experimentally determined values for a 35 kg/mol PEO electrolyte from Reference 36, and the black dashed line is the result predicted from concentrated solution theory using the data from Reference 22. In our previous study on PPM, the limiting current density of PPM electrolytes was measured for three different salt concentrations: $r = 0.02$, 0.04, and 0.06.11 We can use these results as a preliminary check of our concentrated solution theory modeling, and these results are shown in Figure 6.5, where the blue circles are indicative of the experimental values, and the blue dashed line shows the results from the concentrated solution theory modeling done in this work.

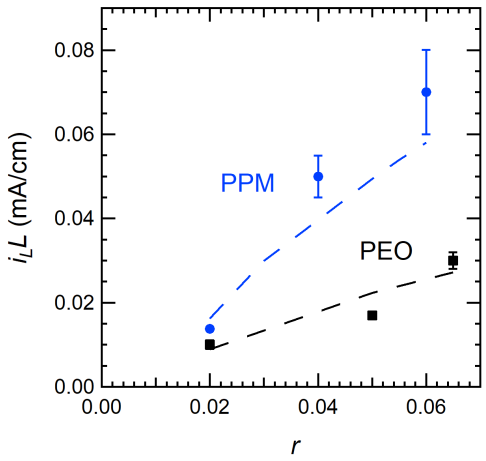

Figure 6.5: Length normalized limiting current density ($i_L L$) plotted as a function of r for PPM and PEO electrolytes. PPM data points come from Reference 22, and the blue dotted line indicates the concentrated solution theory modeling that was performed in this study. The black data points and black dotted line comes from Reference 36.

The data shown in Figure 6.5 for PPM indicates that there is quantitative agreement between experiments and concentrated solution theory predictions for PPM electrolytes. There are ongoing efforts to measure the limiting current density in the well-defined PPM described

in this work, however preliminary results indicate minimal differences between the limiting current density of the PPM studied in this work and that in Reference 127.

The magnitude of the salt concentration gradients in electrolytes controls the amount of current that can be drawn across an electrolyte and contributes to the potential drop across the electrolyte. In practice, the measured electrical potential of a battery is lower than the theoretical, due to ohmic effects of the electrolyte, side reactions, heating effects, salt concentration gradients, etc.[33] An optimal electrolyte, is one with a high value of limiting current, while also minimizing the potential drop that occurs during polarization. Thus, it is of interest to compare both the limiting current, i_L, along with the electric potential, Φ, that results from the largest current density that results in stable operation of an electrolyte. In Figure 6.6, we plot the length normalized values, or Φ/L as a function of $i_L L$. The PEO data is taken from Reference 36, and the PPM data comes from Reference 127. Further studies are ongoing to expand the range of values shown in this plot.

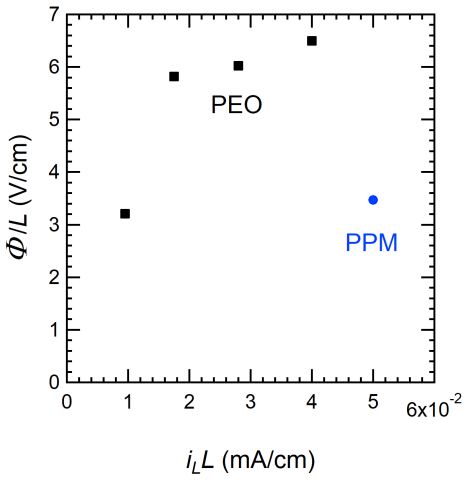

Figure 6.6: Length normalized potential drop resulting from the highest stable applied current density, Φ/L, plotted as a function of the length normalized limiting current density ($i_L L$). The PPM data point comes from Reference 127, and the black data points come from Reference 36

Galluzzo et al. provided a similarly motivated plot that compares values of κ and ρ_+, but Figure 6.6 allows for a comparison of the practical performance of different electrolytes.[66] The range of values for PEO shown in Figure 6.6 correspond with $r = 0.02$, 0.05, 0.065, and 0.085. We show a single point for PPM at $r = 0.04$. While further studies will expand the data ranges in this plot, Figure 6.6 shows a clear difference between PEO and PPM, where PPM can tolerate current densities 5 times greater than PEO, with the same resulting potential drop across the two electrolytes. Clearly, PPM shows great promise as a beyond-

PEO polymer electrolyte, and further studies are required to understand its performance in full cells along with its electrochemical properties when used to produce block copolymer electrolytes.

6.5 Conclusions

We have presented a synthetic method for producing well-defined PPM polymer. We also performed full electrochemical characterization of PPM/LiTFSI electrolytes in which the salt concentration dependence of transport and thermodynamic parameters was determined, and compared with the standard polymer electrolyte, PEO/LiTFSI. The current fraction of PPM is significantly higher than that of PEO, while the conductivity is lower for PPM than PEO, which agrees with our previous study on PPM. The salt diffusion coefficient was found to be similar between PPM and PEO, and we find that the electric potentials measured in PPM with concentration cells are smaller in magnitude than those measured in PEO. With these measurements, we calculated the thermodynamic factor and the cationic transference number with respect to the solvent velocity. The thermodynamic factor of PPM was lower than PEO at all salt concentrations studied, and from $0.04 \leq r \leq 0.10$ the thermodynamic factor remained constant at a value of 1, indicative of ideal behavior. The cationic transference number with respect to the solvent velocity was also higher than that of PEO, which can explain the higher values of limiting current density in PPM that have been previously measured by our group. These experimentally determined values of the cationic transference number match with published results from MD simulations.

Concentrated solution theory was used to model salt concentration profiles and potential drops across the electrolyte with respect to various applied current densities for a PPM and PEO electrolyte., with the concentration polarization and potential drop in PPM being almost half that of PEO at every modeled current density. Our predictions of the limiting current density in PPM agree quantitatively with experimental measurements. Finally, we provide a framework to compare the performance of various electrolytes and show that PPM has clear promise for use in batteries over PEO.

6.6 Acknowledgements

This work was supported by the Assistant Secretary for Energy Efficiency and Renewable Energy, Office of Vehicle Technologies, of the U.S. Department of Energy, under Contract DE-AC02-05CH11231 under the Battery Materials Research Program.

6.7 Supporting Information

Table 6.2: Equations 6.6-6.10 with Error of Fitted Values

Property	Equation
κ (S/cm)	$\kappa = (0.0216 \pm 0.00118) r e^{\left(-\frac{r}{(0.0729 \pm 0.00305)}\right)}$
ρ_+	$\rho_+ = (21.9 \pm 4.01) r^2 - (5.01 \pm 0.627) r + (0.815 \pm 0.0185)$
D (cm^2/sec)	$D = (-4.29 \times 10^{-6} \pm 1.16 \times 10^{-6}) r^2 + (6.32 \times 10^{-7} \pm 2.46 \times 10^{-7}) r + (7.20 \times 10^{-8} \pm 1.24 \times 10^{-8})$
U (mV)	$U = (45.9 \pm 1.72) - (37.3 \pm 2.06) m^{(0.691 \pm 0.0326)}$

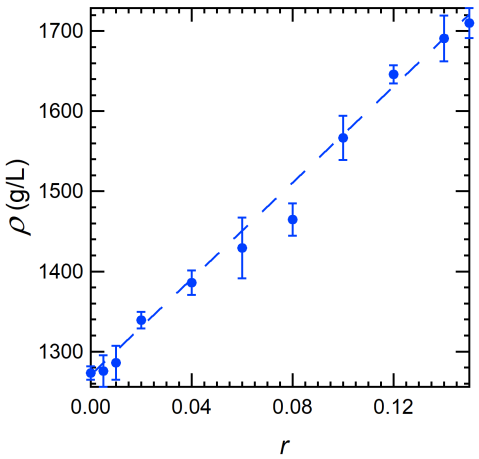

Figure 6.7: Electrolyte density, ρ, plotted as a function of r for PPM electrolytes. Error bars indicate the standard deviation of three measurements. The dashed line is a linear fit of the experimental data. All measurements were made at 90 °C.

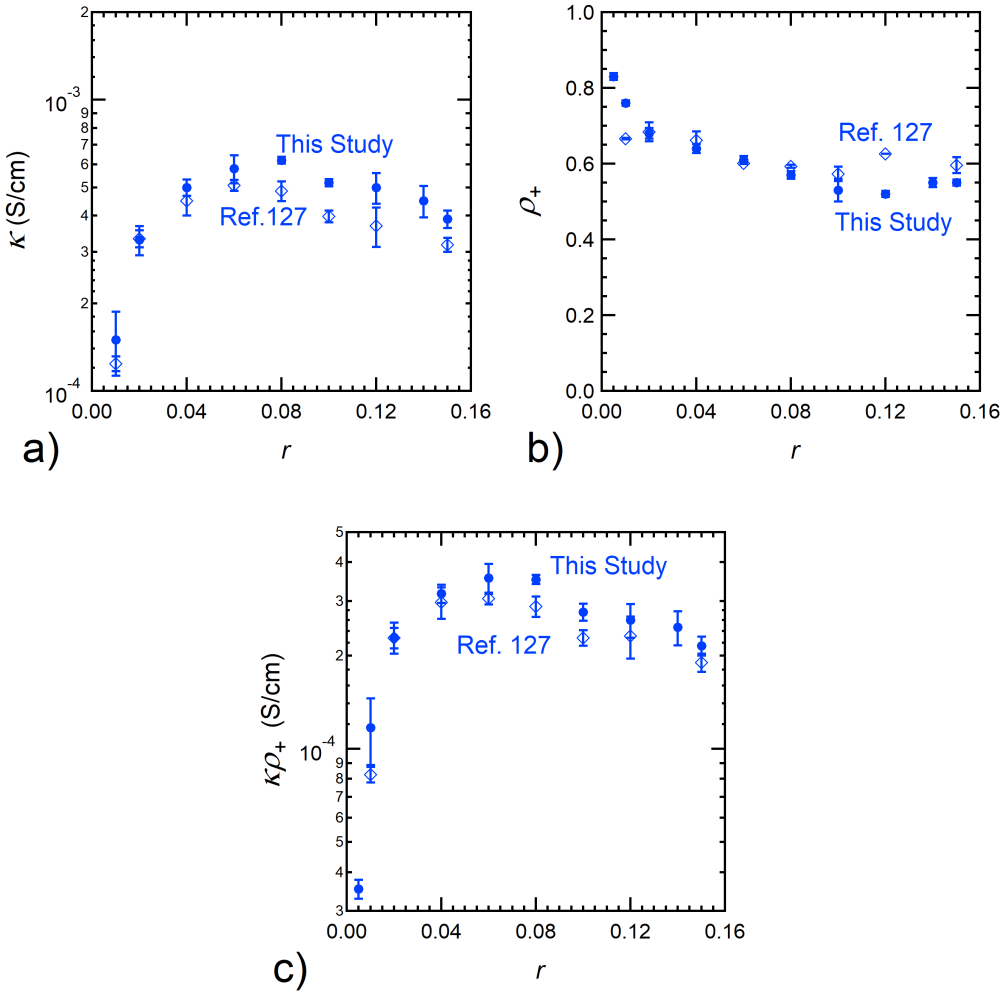

Figure 6.8: (a) Conductivity, κ, (b) current fraction, ρ_+, and (c) electrolyte efficacy, $\kappa\rho_+$, plotted as a function of r for PPM electrolytes. Data from this study are indicated by filled circles, and data from Reference 22 are indicated by the hollow diamonds. All measurements were made at 90 °C.

6.8 Nomenclature

Table 6.3: List of Symbols and Abbreviations

Symbol	Meaning
a	Electrochemically active area (cm^2)
c	Molar salt concentration (mol/L)
D	Salt diffusion coefficient (cm^2/sec)
F	Faraday's constant (C/mol)
i	Current density (mA/cm^2)
i_L	Limiting current density (mA/cm^2)
i_{ss}	Steady-state current density (mA/cm^2)
i_Ω	Calculated initial current density(mA/cm^2)
k_0	Fitted offset voltage (V)
k_1, k_2	Fit parameters for Equation 6.4
L	Electrolyte thickness (cm)
m	Molality (mol/kg)
r	Molar ratio of lithium atoms to oxygen atoms in the polymer unit
r_{max}	Salt concentration where conductivity is maximized
R	Gas constant (kJ/mol-K)
R_{bulk}	Bulk resistance (Ω-cm^2)
R_{int}	Interfacial resistance (Ω-cm^2)
T	Temperature (K)
T_f	Thermodynamic factor
t_+^0	Cationic transference number with respect to the solvent velocity
U	Open-circuit potential measured with concentration cells (mV)
V	Measured voltage
Δr	Concentration polarization
ΔU	Predicted potential drop across electrolyte (mV)
ΔV	Applied voltage (V)
κ	Conductivity (S/cm)
ν	Stoichiometric parameter
ρ	Density (g/L)
ρ_+	Current fraction
Φ	Measured electric potential drop from highest stable current density

7: Conclusions

Current lithium-ion batteries utilize an electrolyte comprised of a lithium salt dissolved in a mixture of organic solvents. Concerns about the flammability of these mixtures, along with instability against high-energy anode materials, requires the discovery of new electrolyte materials. Polymer electrolytes offer a compelling alternative to conventional electrolytes due to their safety and stability. Developing an understanding of the transport phenomena occurring within these electrolytes allows for a rigorous comparison of their performance with the aims of determining polymer materials with superior electrochemical properties. Newman's concentrated solution theory provides a framework for the measurement of transport parameters that fully describe ion transport. In this work, we seek to test the ability of concentrated solution theory to predict electrochemical performance of a standard polymer electrolyte, mixtures of poly(ethylene oxide) (PEO) and a lithium salt, LiTFSI. Additionally, next-generation polymer electrolyte materials are studied, including a single-ion-conducting block copolymer and a novel homopolymer.

In Chapter 2, we evaluate the temperature and salt concentration dependence of ion transport properties in PEO/LiTFSI electrolytes. These properties were measured across a wide range of salt concentrations at three temperatures of interest: 70, 90, and 110 °C. Both conductivity and salt diffusion coefficient increase monotonically with temperature. Both current fraction and electric potential measured with concentration cells remain constant across the measured temperatures. The cationic transference number and the thermodynamic factor monotonically increase with temperature. The change in the transference number and thermodynamic factor is substantially higher between 70 and 90 °C than 90 and 110 °C. With the measured transport parameters, salt concentration profiles were predicted using concentrated solution theory and it was found that the predicted concentration polarization, the difference in salt concentration between the two electrodes, that occurs in response to an applied current density is substantially larger at 70 °C than the higher temperatures.

In Chapter 3, we compare experimentally measured salt concentration profiles with those predicted from concentrated solution theory in a PEO/LiTFSI electrolyte. *Operando* Raman spectroscopy is used to observe salt concentration profiles during polarization of the electrolyte until a steady state is reached. The steady state concentration profiles were consistent over multiple experiments, and the measured concentration polarization was smaller than that predicted with concentrated solution theory.

In Chapter 4, the performance of a PEO/LiTFSI electrolyte above the limiting current density is evaluated and compared with predictions from concentrated solution theory. The Sand's time was measured at various applied current densities and compared with theoretical predictions. We found quantitative agreement between the measurements and predictions. Additionally, a new framework is used to estimate the limiting current density of this electrolyte using the Sand's time at various overlimiting current densities. The measured and predicted Sand's times yielded an estimated limiting current density that aligned with the

modeled limiting current density using concentrated solution theory.

In Chapter 5, the thickness dependence of the limiting current density was determined for a conventional block copolymer, poly(styrene)–*b*–poly(ethylene oxide), and a single-ion-conducting polymer, poly(styrene-LiTFSI)–*b*–poly(ethylene oxide). The limiting current was found to increase linearly with decreasing electrolyte thickness for the conventional electrolyte, as expected from theory. For the single-ion-conducting electrolyte, the limiting current was independent of electrolyte thickness.

In Chapter 6, the ion transport properties of a novel homopolymer electrolyte, mixtures of poly(pentyl malonate) (PPM) and LiTFSI salt, were determined from $0.005 \leq r \leq 0.15$. These results were compared with the properties of the standard polymer electrolyte, PEO/LiTFSI. The conductivity of PPM was lower than that of PEO, while the current fraction was significantly higher than that of PEO. The salt diffusion coefficient was found to be the same between PPM and PEO. The cationic transference number of PPM was larger than that of PEO, and positive across the range of salt concentrations investigated in this study. The thermodynamic factor was lower in PPM, and plateaued at a value of 1, indicative of ideal behavior, from $0.04 \leq r \leq 0.10$. Our experimentally determined transference numbers matched those predicted from MD simulations. The predicted concentration polarization was two times lower in PPM than in PEO.

References

[1] Mathew, M. D., "Nuclear energy: A pathway towards mitigation of global warming," *Progress in Nuclear Energy*, vol. 143, no. August 2021, p. 104 080, 2022. DOI: 10.1016/j.pnucene.2021.104080.

[2] Intergovernmental Panel on Climate Change (IPCC), "Climate Change 2021: The Physical Science Basis. Contribution of Working Group I to the Sixth Assessment Report of the Intergovernmental Panel on Climate Change," Tech. Rep., 2021. DOI: https://doi.org/10.1017/9781009157896.

[3] McKay, D. I., Staal, A., Abrams, J. F., Winkelmann, R., Sakschewski, B., Loriani, S., Fetzer, I., Cornell, S. E., Rockström, J., and Lenton, T. M., "Exceeding 1.5°C global warming could trigger multiple climate tipping points," *Science*, vol. 377, no. 6611, 2022. DOI: 10.1126/science.abn7950.

[4] King, M. D., Howat, I. M., Candela, S. G., Noh, M. J., Jeong, S., Noël, B. P., Broeke, M. R. van den, Wouters, B., and Negrete, A., "Dynamic ice loss from the Greenland Ice Sheet driven by sustained glacier retreat," *Communications Earth and Environment*, vol. 1, no. 1, pp. 1–7, 2020. DOI: 10.1038/s43247-020-0001-2.

[5] Rignot, E., Mouginot, J., Morlighem, M., Seroussi, H., and Scheuchl, B., "Widespread, rapid grounding line retreat of Pine Island, Thwaites, Smith, and Kohler glaciers, West Antarctica, from 1992 to 2011," *Geophysical Research Letters*, vol. 41, no. 10, pp. 3502–3509, 2014. DOI: 10.1002/2014GL060140.

[6] Drijfhout, S., Bathiany, S., Beaulieu, C., Brovkin, V., Claussen, M., Huntingford, C., Scheffer, M., Sgubin, G., and Swingedouw, D., "Catalogue of abrupt shifts in Intergovernmental Panel on Climate Change climate models," *Proceedings of the National Academy of Sciences of the United States of America*, vol. 112, no. 43, E5777–E5786, 2015. DOI: 10.1073/pnas.1511451112.

[7] Hughes, T. P., Barnes, M. L., Bellwood, D. R., Cinner, J. E., Cumming, G. S., Jackson, J. B., Kleypas, J., Van De Leemput, I. A., Lough, J. M., Morrison, T. H., Palumbi, S. R., Van Nes, E. H., and Scheffer, M., "Coral reefs in the Anthropocene," *Nature*, vol. 546, no. 7656, pp. 82–90, 2017. DOI: 10.1038/nature22901.

[8] O'Neill, S., "COP26: Some Progress, But Nations Still Fiddling While World Warms," *Engineering*, vol. 11, no. xxxx, pp. 6–8, 2022. DOI: 10.1016/j.eng.2022.02.004.

[9] Nascimento, L., Kuramochi, T., and Höhne, N., "The G20 emission projections to 2030 improved since the Paris Agreement, but only slightly," *Mitigation and Adaptation Strategies for Global Change*, vol. 27, no. 6, pp. 1–24, 2022. DOI: 10.1007/s11027-022-10018-5.

[10] Rekker, S., Ives, M. C., Wade, B., Webb, L., and Greig, C., "Measuring corporate Paris Compliance using a strict science-based approach," *Nature Communications*, vol. 13, no. 1, pp. 1–11, 2022. DOI: 10.1038/s41467-022-31143-4.

[11] Lamb, W. F., Wiedmann, T., Pongratz, J., Andrew, R., Crippa, M., Olivier, J. G., Wiedenhofer, D., Mattioli, G., Khourdajie, A. A., House, J., Pachauri, S., Figueroa, M., Saheb, Y., Slade, R., Hubacek, K., Sun, L., Ribeiro, S. K., Khennas, S., De La Rue Du Can, S., Chapungu, L., Davis, S. J., Bashmakov, I., Dai, H., Dhakal, S., Tan, X., Geng, Y., Gu, B., and Minx, J., "A review of trends and drivers of greenhouse gas emissions by sector from 1990 to 2018," *Environmental Research Letters*, vol. 16, no. 7, 2021. DOI: 10.1088/1748-9326/abee4e.

[12] Dunn, J. B., Gaines, L., Kelly, J. C., James, C., and Gallagher, K. G., "The significance of Li-ion batteries in electric vehicle life-cycle energy and emissions and recycling's role in its reduction," *Energy and Environmental Science*, vol. 8, no. 1, pp. 158–168, 2015. DOI: 10.1039/c4ee03029j.

[13] Arbabzadeh, M., Sioshansi, R., Johnson, J. X., and Keoleian, G. A., "The role of energy storage in deep decarbonization of electricity production," *Nature Communications*, vol. 10, no. 1, 2019. DOI: 10.1038/s41467-019-11161-5.

[14] Sisternes, F. J. de, Jenkins, J. D., and Botterud, A., "The value of energy storage in decarbonizing the electricity sector," *Applied Energy*, vol. 175, pp. 368–379, 2016. DOI: 10.1016/j.apenergy.2016.05.014.

[15] Yao, P., Yu, H., Ding, Z., Liu, Y., Lu, J., Lavorgna, M., Wu, J., and Liu, X., "Review on Polymer-Based Composite Electrolytes for Lithium Batteries," *Frontiers in Chemistry*, vol. 7, no. August, pp. 1–17, 2019. DOI: 10.3389/fchem.2019.00522.

[16] Horowitz, Y., Schmidt, C., Yoon, D. h., Riegger, L. M., Katzenmeier, L., Bosch, G. M., Noked, M., Ein-Eli, Y., Janek, J., Zeier, W. G., Diesendruck, C. E., and Golodnitsky, D., "Between Liquid and All Solid: A Prospect on Electrolyte Future in Lithium-Ion Batteries for Electric Vehicles," *Energy Technology*, vol. 8, no. 11, pp. 1–12, 2020. DOI: 10.1002/ente.202000580.

[17] Fenton, D. E., Parker, J. M., and Wright, P. V., "Complexes of alkali metal ions with poly(ethylene oxide)," *Polymer*, vol. 14, no. 11, p. 589, 1973. DOI: 10.1016/0032-3861(73)90146-8.

[18] Armand, M., "Polymer solid electrolytes - an overview," *Solid State Ionics*, 1983. DOI: 10.1016/0167-2738(83)90083-8.

[19] Xu, K., "Nonaqueous Liquid Electrolytes for Lithium-Based Rechargeable Batteries," *Chemical Reviews*, vol. 104, no. 10, pp. 4303–4417, Oct. 2004. DOI: 10.1021/CR030203G.

[20] Hallinan, D. T. and Balsara, N. P., "Polymer Electrolytes," *Annual Review of Materials Research*, vol. 43, no. 1, pp. 503–525, Jul. 2013. DOI: 10.1146/annurev-matsci-071312-121705.

[21] Frenck, L., Sethi, G. K., Maslyn, J. A., and Balsara, N. P., "Factors That Control the Formation of Dendrites and Other Morphologies on Lithium Metal Anodes," *Frontiers in Energy Research*, vol. 0, p. 115, Nov. 2019. DOI: 10.3389/FENRG.2019.00115.

[22] Gao, K. W. and Balsara, N. P., "Electrochemical properties of poly(ethylene oxide) electrolytes above the entanglement threshold," *Solid State Ionics*, vol. 364, p. 115 609, Jun. 2021. DOI: 10.1016/J.SSI.2021.115609.

[23] Landesfeind, J. and Gasteiger, H. A., "Temperature and Concentration Dependence of the Ionic Transport Properties of Lithium-Ion Battery Electrolytes," *Journal of The Electrochemical Society*, 2019. DOI: 10.1149/2.0571912jes.

[24] Heubner, C., Maletti, S., Auer, H., Hüttl, J., Voigt, K., Lohrberg, O., Nikolowski, K., Partsch, M., and Michaelis, A., "From Lithium-Metal toward Anode-Free Solid-State Batteries: Current Developments, Issues, and Challenges," *Advanced Functional Materials*, vol. 31, no. 51, 2021. DOI: 10.1002/adfm.202106608.

[25] Cheng, X. B., Zhang, R., Zhao, C. Z., and Zhang, Q., *Toward Safe Lithium Metal Anode in Rechargeable Batteries: A Review*, 2017. DOI: 10.1021/acs.chemrev.7b00115.

[26] Xu, Z., Yang, J., Li, H., Nuli, Y., and Wang, J., "Electrolytes for advanced lithium ion batteries using silicon-based anodes," *Journal of Materials Chemistry A*, vol. 7, no. 16, pp. 9432–9446, 2019. DOI: 10.1039/c9ta01876j.

[27] Chintapalli, M., Le, T. N., Venkatesan, N. R., Mackay, N. G., Rojas, A. A., Thelen, J. L., Chen, X. C., Devaux, D., and Balsara, N. P., "Structure and Ionic Conductivity of Polystyrene-block-poly(ethylene oxide) Electrolytes in the High Salt Concentration Limit," *Macromolecules*, 2016. DOI: 10.1021/acs.macromol.5b02620.

[28] Frenck, L., Veeraraghavan, V. D., Maslyn, J. A., Müller, A., Ho, A. S., Loo, W. S., Minor, A. M., and Balsara, N. P., "Effect of salt concentration profiles on protrusion growth in lithium-polymer-lithium cells," *Solid State Ionics*, vol. 358, p. 115 517, Dec. 2020. DOI: 10.1016/J.SSI.2020.115517.

[29] Galluzzo, M. D., Loo, W. S., Wang, A. A., Walton, A., Maslyn, J. A., and Balsara, N. P., "Measurement of Three Transport Coefficients and the Thermodynamic Factor in Block Copolymer Electrolytes with Different Morphologies," *Journal of Physical Chemistry B*, vol. 124, no. 5, pp. 921–935, 2020. DOI: 10.1021/acs.jpcb.9b11066.

[30] Gao, K. W., Jiang, X., Hoffman, Z. J., Sethi, G. K., Chakraborty, S., Villaluenga, I., and Balsara, N. P., "Optimizing the monomer structure of polyhedral oligomeric silsesquioxane for ion transport in hybrid organic–inorganic block copolymers," *Journal of Polymer Science*, vol. 58, no. 2, pp. 363–371, Jan. 2020. DOI: 10.1002/pol.20190073.

[31] Chakraborty, S., Jiang, X., Hoffman, Z. J., Sethi, G. K., Zhu, C., Balsara, N. P., and Villaluenga, I., "Reversible Changes in the Grain Structure and Conductivity in a Block Copolymer Electrolyte," *Macromolecules*, vol. 53, no. 13, pp. 5455–5464, Jul. 2020. DOI: 10.1021/acs.macromol.0c00466.

[32] Onsager, L., "Theories and Problems of Liquid Diffusion," *Annals of the New York Academy of Sciences*, vol. 46, no. 5, pp. 241–265, 1945. DOI: 10.1111/j.1749-6632.1945.tb36170.x.

[33] Newman, J. and Thomas-Alyea, K. E., *Electrochemical systems. Third edition.* 2004. DOI: 10.1192/bjp.112.483.211-a.

[34] Pesko, D. M., Feng, Z., Sawhney, S., Newman, J., Srinivasan, V., and Balsara, N. P., "Comparing Cycling Characteristics of Symmetric Lithium-Polymer-Lithium Cells with Theoretical Predictions," *Journal of The Electrochemical Society*, 2018. DOI: 10.1149/2.0921813jes.

[35] Shah, D. B., Kim, H. K., Nguyen, H. Q., Srinivasan, V., and Balsara, N. P., "Comparing Measurements of Limiting Current of Electrolytes with Theoretical Predictions up to the Solubility Limit," *Journal of Physical Chemistry C*, 2019. DOI: 10.1021/acs.jpcc.9b07121.

[36] Gribble, D. A., Frenck, L., Shah, D. B., Maslyn, J. A., Loo, W. S., Mongcopa, K. I. S., Pesko, D. M., and Balsara, N. P., "Comparing Experimental Measurements of Limiting Current in Polymer Electrolytes with Theoretical Predictions," *Journal of The Electrochemical Society*, 2019. DOI: 10.1149/2.0391914jes.

[37] Grundy, L. S., Fu, S., Hoffman, Z. J., and Balsara, N. P., "Electrochemical Characterization of PEO/LiTFSI Electrolytes Near the Solubility Limit," *Macromolecules*, vol. 55, no. 20, pp. 9030–9038, 2022. DOI: 10.1021/acs.macromol.2c01655.

[38] Gao, K. W., Fang, C., Halat, D. M., Mistry, A., Newman, J., and Balsara, N. P., "The Transference Number," *Energy and Environmental Materials*, vol. 5, no. 2, pp. 366–369, 2022. DOI: 10.1002/eem2.12359.

[39] Shao, Y., Gudla, H., Brandell, D., and Zhang, C., "Transference Number in Polymer Electrolytes: Mind the Reference-Frame Gap," *Journal of the American Chemical Society*, vol. 144, no. 17, pp. 7583–7587, 2022. DOI: 10.1021/jacs.2c02389.

[40] Thackeray, M. M., Wolverton, C., and Isaacs, E. D., "Electrical energy storage for transportation—approaching the limits of, and going beyond, lithium-ion batteries," *Energy & Environmental Science*, vol. 5, no. 7, pp. 7854–7863, Jun. 2012. DOI: 10.1039/C2EE21892E.

[41] Choudhury, S., Stalin, S., Vu, D., Warren, A., Deng, Y., Biswal, P., and Archer, L. A., "Solid-state polymer electrolytes for high-performance lithium metal batteries," *Nature Communications 2019 10:1*, vol. 10, no. 1, pp. 1–8, Sep. 2019. DOI: 10.1038/s41467-019-12423-y.

[42] Wong, D. H. C., Thelen, J. L., Fu, Y., Devaux, D., Pandya, A. A., Battaglia, V. S., Balsara, N. P., and DeSimone, J. M., "Nonflammable perfluoropolyether-based electrolytes for lithium batteries," *Proceedings of the National Academy of Sciences*, vol. 111, no. 9, pp. 3327–3331, Mar. 2014. DOI: 10.1073/PNAS.1314615111.

[43] Harris, W. S., "Electrochemical studies in cyclic esters," Ph.D. dissertation, 1958.

[44] Valoen, L. O. and Reimers, J. N., "Transport Properties of LiPF[sub 6]-Based Li-Ion Battery Electrolytes," *Journal of The Electrochemical Society*, 2005. DOI: 10.1149/1.1872737.

[45] Lundgren, H., Behm, M., and Lindbergh, G., " Electrochemical Characterization and Temperature Dependency of Mass-Transport Properties of LiPF 6 in EC:DEC," *Journal of The Electrochemical Society*, 2015. DOI: 10.1149/2.0641503jes.

[46] Stevens, M. B., "Hybrid Fuel Cell Vehicle Powertrain Development Considering Power Source Degradation," *Design*, 2008.

[47] Teran, A. A., Tang, M. H., Mullin, S. A., and Balsara, N. P., "Effect of molecular weight on conductivity of polymer electrolytes," *Solid State Ionics*, 2011. DOI: 10.1016/j.ssi.2011.09.021.

[48] Pesko, D. M., Timachova, K., Bhattacharya, R., Smith, M. C., Villaluenga, I., Newman, J., and Balsara, N. P., "Negative Transference Numbers in Poly(ethylene oxide)-Based Electrolytes," *Journal of The Electrochemical Society*, 2017. DOI: 10.1149/2.0581711jes.

[49] Pesko, D. M., Jung, Y., Hasan, A. L., Webb, M. A., Coates, G. W., Miller, T. F., and Balsara, N. P., "Effect of monomer structure on ionic conductivity in a systematic set of polyester electrolytes," *Solid State Ionics*, 2016. DOI: 10.1016/j.ssi.2016.02.020.

[50] Devaux, D., Bouchet, R., Glé, D., and Denoyel, R., "Mechanism of ion transport in PEO/LiTFSI complexes: Effect of temperature, molecular weight and end groups," *Solid State Ionics*, 2012. DOI: 10.1016/j.ssi.2012.09.020.

[51] Hiller, M. M., Joost, M., Gores, H. J., Passerini, S., and Wiemhöfer, H. D., "The influence of interface polarization on the determination of lithium transference numbers of salt in polyethylene oxide electrolytes," *Electrochimica Acta*, 2013. DOI: 10.1016/j.electacta.2013.09.138.

[52] Pożyczka, K., Marzantowicz, M., Dygas, J. R., and Krok, F., "IONIC CONDUCTIVITY AND LITHIUM TRANSFERENCE NUMBER OF POLY(ETHYLENE OXIDE):LiTFSI SYSTEM," *Electrochimica Acta*, 2017. DOI: 10.1016/j.electacta.2016.12.172.

[53] Loo, W. S., Mongcopa, K. I., Gribble, D. A., Faraone, A. A., and Balsara, N. P., "Investigating the Effect of Added Salt on the Chain Dimensions of Poly(ethylene oxide) through Small-Angle Neutron Scattering," *Macromolecules*, 2019. DOI: 10.1021/acs.macromol.9b01509.

[54] Staunton, E., Andreev, Y. G., and Bruce, P. G., "Factors influencing the conductivity of crystalline polymer electrolytes," in *Faraday Discussions*, 2007. DOI: 10.1039/b601945e.

[55] Newman, J. and Chapman, T. W., "Restricted diffusion in binary solutions," *AIChE Journal*, 1973. DOI: 10.1002/aic.690190220.

[56] Thompson, S. D. and Newman, J., "Differential Diffusion Coefficients of Sodium Polysulfide Melts," *Journal of The Electrochemical Society*, 2019. DOI: 10.1149/1.2096451.

[57] Perrier, M., Besner, S., Paquette, C., Vallée, A., Lascaud, S., and Prud'homme, J., "Mixed-alkali effect and short-range interactions in amorphous poly(ethylene oxide) electrolytes," *Electrochimica Acta*, 1995. DOI: 10.1016/0013-4686(95)00151-4.

[58] Mongcopa, K. I. S., Tyagi, M., Mailoa, J. P., Samsonidze, G., Kozinsky, B., Mullin, S. A., Gribble, D. A., Watanabe, H., and Balsara, N. P., "Relationship between Segmental Dynamics Measured by Quasi-Elastic Neutron Scattering and Conductivity in Polymer Electrolytes," *ACS Macro Letters*, 2018. DOI: 10.1021/acsmacrolett.8b00159.

[59] Balsara, N. P. and Newman, J., "Relationship between Steady-State Current in Symmetric Cells and Transference Number of Electrolytes Comprising Univalent and Multivalent Ions," *Journal of The Electrochemical Society*, 2015. DOI: 10.1149/2.0651514jes.

[60] Bruce, P. G. and Vincent, C. A., "Steady state current flow in solid binary electrolyte cells," *Journal of Electroanalytical Chemistry*, 1987. DOI: 10.1016/0022-0728(87)80001-3.

[61] Doyle, M., Fuller, T. F., and Newman, J., "The importance of the lithium ion transference number in lithium/polymer cells," *Electrochimica Acta*, vol. 39, no. 13, pp. 2073–2081, 1994. DOI: 10.1016/0013-4686(94)85091-7.

[62] Borodin, O. and Smith, G. D., "Mechanism of ion transport in amorphous poly(ethylene oxide)/ LiTFSI from molecular dynamics simulations," *Macromolecules*, 2006. DOI: 10.1021/ma052277v.

[63] Diddens, D., Heuer, A., and Borodin, O., "Understanding the lithium transport within a rouse-based model for a PEO/LiTFSI polymer electrolyte," *Macromolecules*, 2010. DOI: 10.1021/ma901893h.

[64] Ma, Y., "The Measurement of a Complete Set of Transport Properties for a Concentrated Solid Polymer Electrolyte Solution," *Journal of The Electrochemical Society*, 1995. DOI: 10.1149/1.2044206.

[65] Pesko, D. M., Sawhney, S., Newman, J., and Balsara, N. P., "Comparing Two Electrochemical Approaches for Measuring Transference Numbers in Concentrated Electrolytes," *Journal of The Electrochemical Society*, 2018. DOI: 10.1149/2.0231813jes.

[66] Galluzzo, M. D., Maslyn, J. A., Shah, D. B., and Balsara, N. P., "Ohm's law for ion conduction in lithium and beyond-lithium battery electrolytes," *Journal of Chemical Physics*, 2019. DOI: 10.1063/1.5109684.

[67] Wang, Q., Jiang, L., Yu, Y., and Sun, J., *Progress of enhancing the safety of lithium ion battery from the electrolyte aspect*, Jan. 2019. DOI: 10.1016/j.nanoen.2018.10.035.

[68] Hess, S., Wohlfahrt-Mehrens, M., and Wachtler, M., "Flammability of Li-Ion Battery Electrolytes: Flash Point and Self-Extinguishing Time Measurements," *Journal of The Electrochemical Society*, 2015. DOI: 10.1149/2.0121502jes.

[69] Monroe, C. and Newman, J., "Dendrite Growth in Lithium/Polymer Systems : A Propagation Model for Liquid Electrolytes under Galvanostatic Conditions," *Journal of The Electrochemical Society*, vol. 150, no. 10, A1377, Sep. 2003. DOI: 10.1149/1.1606686.

[70] Aurbach, D., Zinigrad, E., Cohen, Y., and Teller, H., "A short review of failure mechanisms of lithium metal and lithiated graphite anodes in liquid electrolyte solutions," *Solid State Ionics*, vol. 148, no. 3-4, pp. 405–416, Jun. 2002. DOI: 10.1016/S0167-2738(02)00080-2.

[71] Goodenough, J. B. and Kim, Y., "Challenges for rechargeable Li batteries," *Chemistry of Materials*, vol. 22, no. 3, pp. 587–603, Feb. 2010. DOI: 10.1021/cm901452z.

[72] Monroe, C. and Newman, J., "The Impact of Elastic Deformation on Deposition Kinetics at Lithium/Polymer Interfaces," *Journal of The Electrochemical Society*, vol. 152, no. 2, A396, Jan. 2005. DOI: 10.1149/1.1850854.

[73] Choo, Y., Halat, D. M., Villaluenga, I., Timachova, K., and Balsara, N. P., *Diffusion and migration in polymer electrolytes*, Apr. 2020. DOI: 10.1016/j.progpolymsci.2020.101220.

[74] Barai, P., Higa, K., Srinivasan, V., Boz, B., Dev, T., Salvadori, A., and Kim, H.-K., "Impact of External Pressure and Electrolyte Transport Properties on Lithium Dendrite Growth You may also like Impact of Electrolyte Transference Number on Lithium Dendrite Growth Process Review-Electrolyte and Electrode Designs for Enhanced Ion Transport," 2018. DOI: 10.1149/2.0651811jes.

[75] Hoffman, Z. J., Shah, D. B., and Balsara, N. P., "Temperature and concentration dependence of the ionic transport properties of poly(ethylene oxide) electrolytes," *Solid State Ionics*, vol. 370, p. 115 751, Nov. 2021. DOI: 10.1016/J.SSI.2021.115751.

[76] Sethi, G. K., Frenck, L., Sawhney, S., Chakraborty, S., Villaluenga, I., and Balsara, N. P., "Effect of microphase separation on the limiting current density in hybrid organic-inorganic copolymer electrolytes," *Solid State Ionics*, vol. 368, p. 115 702, Oct. 2021. DOI: 10.1016/J.SSI.2021.115702.

[77] Fawdon, J., Ihli, J., Mantia, F. L., and Pasta, M., "Characterising lithium-ion electrolytes via operando Raman microspectroscopy," DOI: 10.1038/s41467-021-24297-0.

[78] Rey, I., Bruneel, J.-L., Grondin, J., Servant, L., and Lassègues, J.-C., "Raman Spectroelectrochemistry of a Lithium/Polymer Electrolyte Symmetric Cell," *Journal of The Electrochemical Society*, vol. 145, no. 9, pp. 3034–3042, Sep. 1998. DOI: 10.1149/1.1838759/XML.

[79] Georén, P., Adebahr, J., Jacobsson, P., and Lindbergh, G., "Concentration Polarization of a Polymer Electrolyte," *Journal of The Electrochemical Society*, vol. 149, no. 8, A1015, Jun. 2002. DOI: 10.1149/1.1487832/XML.

[80] Cheng, Q., Wei, L., Liu, Z., Ni, N., Sang, Z., Zhu, B., Xu, W., Chen, M., Miao, Y., Chen, L. Q., Min, W., and Yang, Y., "Operando and three-dimensional visualization of anion depletion and lithium growth by stimulated Raman scattering microscopy," *Nature Communications 2018 9:1*, vol. 9, no. 1, pp. 1–10, Jul. 2018. DOI: 10.1038/s41467-018-05289-z.

[81] Forster, J. D., Harris, S. J., and Urban, J. J., "Mapping Li+ concentration and transport via in situ confocal Raman microscopy," *Journal of Physical Chemistry Letters*, vol. 5, no. 11, pp. 2007–2011, Jun. 2014. DOI: 10.1021/jz500608e.

[82] Yamanaka, T., Nakagawa, H., Tsubouchi, S., Domi, Y., Doi, T., Abe, T., and Ogumi, Z., "InSitu Raman Spectroscopic Studies on Concentration of Electrolyte Salt in Lithium-Ion Batteries by Using Ultrafine Multifiber Probes," *ChemSusChem*, vol. 10, no. 5, pp. 855–861, Mar. 2017. DOI: 10.1002/CSSC.201601473.

[83] Fawdon, J., Rees, G. J., Mantia, F. L., and Pasta, M., "Insights into the Transport and Thermodynamic Properties of a Bis(fluorosulfonyl)imide-Based Ionic Liquid Electrolyte for Battery Applications," *J. Phys. Chem. Lett*, vol. 13, p. 27, 2022. DOI: 10.1021/acs.jpclett.1c04246.

[84] Tripathi, A. M., Su, W. N., and Hwang, B. J., "In situ analytical techniques for battery interface analysis," *Chemical Society Reviews*, vol. 47, no. 3, pp. 736–851, Feb. 2018. DOI: 10.1039/C7CS00180K.

[85] Lieber, C. A. and Mahadevan-Jansen, A., "Automated Method for Subtraction of Fluorescence from Biological Raman Spectra," *Applied Spectroscopy*, vol. 57, no. 11, pp. 1363–1367, Nov. 2003. DOI: 10.1366/000370203322554518.

[86] Bazak, J. D., Allen, J. P., Krachkovskiy, S. A., and Goward, G. R., "Mapping of Lithium-Ion Battery Electrolyte Transport Properties and Limiting Currents with In Situ MRI," *Journal of The Electrochemical Society*, vol. 167, no. 14, p. 140 518, Oct. 2020. DOI: 10.1149/1945-7111/ABC0C9.

[87] Shah, D. B., Nguyen, H. Q., Grundy, L. S., Olson, K. R., Mecham, S. J., Desimone, J. M., and Balsara, N. P., "Difference between approximate and rigorously measured transference numbers in fluorinated electrolytes," *Physical Chemistry Chemical Physics*, 2019. DOI: 10.1039/c9cp00216b.

[88] Hickson, D. T., Halat, D. M., Ho, A. S., Reimer, J. A., and Balsara, N. P., "Complete characterization of a lithium battery electrolyte using a combination of electrophoretic NMR and electrochemical methods," *Physical Chemistry Chemical Physics*, vol. 24, no. 43, pp. 26 591–26 599, Nov. 2022. DOI: 10.1039/D2CP02622H.

[89] Choo, Y., Snyder, R. L., Shah, N. J., Abel, B. A., Coates, G. W., and Balsara, N. P., "Complete Electrochemical Characterization and Limiting Current of Polyacetal Electrolytes," *Journal of The Electrochemical Society*, vol. 169, no. 2, p. 020 538, 2022. DOI: 10.1149/1945-7111/ac4f22.

[90] Maslyn, J. A., Frenck, L., Veeraraghavan, V. D., Müller, A., Ho, A. S., Marwaha, N., Loo, W. S., Parkinson, D. Y., Minor, A. M., and Balsara, N. P., "Limiting Current in Nanostructured Block Copolymer Electrolytes," *Macromolecules*, vol. 54, no. 9, pp. 4010–4022, May 2021. DOI: 10.1021/acs.macromol.1c00425.

[91] Frenck, L., Veeraraghavan, V. D., Maslyn, J. A., and Balsara, N. P., "Comparing Measurement of Limiting Current in Block Copolymer Electrolytes as a Function of Salt Concentration with Theoretical Predictions," *Electrochimica Acta*, p. 139 911, Jan. 2022. DOI: 10.1016/J.ELECTACTA.2022.139911.

[92] Mistry, A. and Srinivasan, V., "On our Limited Understanding of Electrodeposition," *MRS Advances*, vol. 4, no. 51-52, pp. 2843–2861, 2019. DOI: 10.1557/ADV.2019.443.

[93] Rosso, M., Gobron, T., Brissot, C., Chazalviel, J. N., and Lascaud, S., "Onset of dendritic growth in lithium/polymer cells," *Journal of Power Sources*, vol. 97-98, pp. 804–806, Jul. 2001. DOI: 10.1016/S0378-7753(01)00734-0.

[94] Sand, H. S., "On the concentration at the electrodes in a solution, with special reference to the liberation of hydrogen by electrolysis of a mixture of copper sulphate and sulphuric acid," *Proceedings of the Physical Society of London*, vol. 17, no. 1, pp. 496–534, Oct. 1899. DOI: 10.1088/1478-7814/17/1/332.

[95] Devaux, D., Leduc, H., Dumaz, P., Lecuyer, M., Deschamps, M., and Bouchet, R., "Effect of Electrode and Electrolyte Thicknesses on All-Solid-State Battery Performance Analyzed With the Sand Equation," *Frontiers in Energy Research*, vol. 7, p. 168, Jan. 2020. DOI: 10.3389/FENRG.2019.00168/BIBTEX.

[96] Stolz, L., Homann, G., Winter, M., and Kasnatscheew, J., "The Sand equation and its enormous practical relevance for solid-state lithium metal batteries," *Materials Today*, vol. 44, no. April, pp. 9–14, 2021. DOI: 10.1016/j.mattod.2020.11.025.

[97] Kim, H.-K., Balsara, N. P., and Srinivasan, V., "Continuum Description of the Role of Negative Transference Numbers on Ion Motion in Polymer Electrolytes," *Journal of The Electrochemical Society*, vol. 167, no. 11, p. 110 559, 2020. DOI: 10.1149/1945-7111/aba790.

[98] Lee, Y., Ma, B., and Bai, P., "Overlimiting ion transport dynamic toward Sand's time in solid polymer electrolytes," *Materials Today Energy*, vol. 27, p. 101 037, 2022. DOI: 10.1016/j.mtener.2022.101037.

[99] Lee, S. I., Jung, U. H., Kim, Y. S., Kim, M. H., Ahn, D. J., and Chun, H. S., "A study of electrochemical kinetics of lithium ion in organic electrolytes," *Korean Journal of Chemical Engineering*, vol. 19, no. 4, pp. 638–644, 2002. DOI: 10.1007/BF02699310.

[100] Mistry, A., Grundy, L. S., Halat, D. M., Newman, J., Balsara, N. P., and Srinivasan, V., "Effect of Solvent Motion on Ion Transport in Electrolytes," *Journal of The Electrochemical Society*, vol. 169, no. 4, p. 040 524, 2022. DOI: 10.1149/1945-7111/ac6329.

[101] Newman, J., "Current Distribution on a Rotating Disk below the Limiting Current," *Journal of The Electrochemical Society*, vol. 113, no. 12, p. 1235, Dec. 1966. DOI: 10.1149/1.2423795.

[102] Trahey, L., Brushett, F. R., Balsara, N. P., Ceder, G., Cheng, L., Chiang, Y. M., Hahn, N. T., Ingram, B. J., Minteer, S. D., Moore, J. S., Mueller, K. T., Nazar, L. F., Persson, K. A., Siegel, D. J., Xu, K., Zavadil, K. R., Srinivasan, V., and Crabtree, G. W., "Energy storage emerging: A perspective from the Joint Center for Energy Storage Research," *Proceedings of the National Academy of Sciences of the United States of America*, vol. 117, no. 23, pp. 12 550–12 557, Jun. 2020. DOI: 10.1073/pnas.1821672117.

[103] Zhang, X. Q., Zhao, C. Z., Huang, J. Q., and Zhang, Q., *Recent Advances in Energy Chemical Engineering of Next-Generation Lithium Batteries*, Dec. 2018. DOI: 10.1016/j.eng.2018.10.008.

[104] Arbizzani, C., Gabrielli, G., and Mastragostino, M., "Thermal stability and flammability of electrolytes for lithium-ion batteries," *Journal of Power Sources*, vol. 196, no. 10, pp. 4801–4805, May 2011. DOI: 10.1016/j.jpowsour.2011.01.068.

[105] Ngai, K. S., Ramesh, S., Ramesh, K., and Juan, J. C., *A review of polymer electrolytes: fundamental, approaches and applications*, Aug. 2016. DOI: 10.1007/s11581-016-1756-4.

[106] Ho, A. S., Barai, P., Maslyn, J. A., Frenck, L., Loo, W. S., Parkinson, D. Y., Srinivasan, V., and Balsara, N. P., "Uncovering the Relationship between Diameter and Height of Electrodeposited Lithium Protrusions in a Rigid Electrolyte," *ACS Applied Energy Materials*, vol. 3, no. 10, pp. 9645–9655, Oct. 2020. DOI: 10.1021/ACSAEM.0C01175.

[107] Veeraraghavan, V. D., Frenck, L., Maslyn, J. A., Loo, W. S., Parkinson, D. Y., and Balsara, N. P., "Evolution of Protrusions on Lithium Metal Anodes Stabilized by a Solid Block Copolymer Electrolyte Studied Using Time-Resolved X-ray Tomography," *ACS Applied Materials & Interfaces*, vol. 13, no. 23, pp. 27 006–27 018, Jun. 2021. DOI: 10.1021/ACSAMI.1C04582.

[108] Hogge, E. A. and Kraichman, M. B., "The Limiting Current on a Rotating Disc Electrode in Potassium Iodide-Potassium Triiodide Solutions," *Journal of the American Chemical Society*, vol. 76, no. 5, pp. 1431–1433, Mar. 1954. DOI: 10.1021/ja01634a088.

[109] Laoire, C. O., Plichta, E., Hendrickson, M., Mukerjee, S., and Abraham, K. M., "Electrochemical studies of ferrocene in a lithium ion conducting organic carbonate electrolyte," *Electrochimica Acta*, vol. 54, no. 26, pp. 6560–6564, Nov. 2009. DOI: 10.1016/j.electacta.2009.06.041.

[110] Park, J. W., Yoshida, K., Tachikawa, N., Dokko, K., and Watanabe, M., "Limiting current density in bis(trifluoromethylsulfonyl)amide-based ionic liquid for lithium batteries," *Journal of Power Sources*, vol. 196, no. 4, pp. 2264–2268, Feb. 2011. DOI: 10.1016/j.jpowsour.2010.09.067.

[111] Ford, H. O., Park, B., Jiang, J., Seidler, M. E., and Schaefer, J. L., "Enhanced Li+ Conduction within Single-Ion Conducting Polymer Gel Electrolytes via Reduced Cation-Polymer Interaction," *ACS Materials Letters*, vol. 2, no. 3, pp. 272–279, Mar. 2020. DOI: 10.1021/acsmaterialslett.9b00510.

[112] Chen, Z., Steinle, D., Nguyen, H. D., Kim, J. K., Mayer, A., Shi, J., Paillard, E., Iojoiu, C., Passerini, S., and Bresser, D., "High-energy lithium batteries based on single-ion conducting polymer electrolytes and Li[Ni0.8Co0.1Mn0.1]O2 cathodes," *Nano Energy*, vol. 77, p. 105 129, Nov. 2020. DOI: 10.1016/j.nanoen.2020.105129.

[113] Siegel, D. J., Nazar, L., Chiang, Y. M., Fang, C., and Balsara, N. P., "Establishing a unified framework for ion solvation and transport in liquid and solid electrolytes," *Trends in Chemistry*, vol. 3, no. 10, pp. 807–818, Oct. 2021. DOI: 10.1016/J.TRECHM.2021.06.004.

[114] Selim, R. and Bro, P., "Some Observations on Rechargeable Lithium Electrodes in a Propylene Carbonate Electrolyte," *Journal of The Electrochemical Society*, vol. 121, no. 11, p. 1457, Nov. 1974. DOI: 10.1149/1.2401708.

[115] Epelboin, I., Froment, M., Garreau, M., Thevenin, J., and Warin, D., "Behavior of Secondary Lithium and Aluminum-Lithium Electrodes in Propylene Carbonate," *Journal of The Electrochemical Society*, vol. 127, no. 10, p. 2100, Oct. 1980. DOI: 10.1149/1.2129354.

[116] Lin, D., Liu, Y., and Cui, Y., "Reviving the lithium metal anode for high-energy batteries," *Nature Nanotechnology 2017 12:3*, vol. 12, no. 3, pp. 194–206, Mar. 2017. DOI: 10.1038/nnano.2017.16.

[117] Rojas, A., Inceoglu, S., Mackay, N., Thelen, J., Devaux, D., Stone, G., and Balsara, N., "Effect of Lithium-Ion Concentration on Morphology and Ion Transport in Single-Ion-Conducting Block Copolymer Electrolytes," *Macromolecules*, vol. 48, no. 18, pp. 6589–6595, Sep. 2015. DOI: 10.1021/ACS.MACROMOL.5B01193.

[118] Hadjichristidis, N., Iatrou, H., Pispas, S., and Pitsikalis, M., "Anionic polymerization: High vacuum techniques," *Journal of Polymer Science Part A: Polymer Chemistry*, vol. 38, no. 18, pp. 3211–3234, Sep. 2000. DOI: https://doi.org/10.1002/1099-0518(20000915)38:18<3211::AID-POLA10>3.0.CO;2-L.

[119] Gürsoy, D., De Carlo, F., Xiao, X., and Jacobsen, C., "TomoPy: a framework for the analysis of synchrotron tomographic data," *Journal of Synchrotron Radiation*, vol. 21, no. Pt 5, p. 1188, 2014. DOI: 10.1107/S1600577514013939.

[120] Bae, H. and Kim, Y., "Technologies of lithium recycling from waste lithium ion batteries: a review," *Materials Advances*, vol. 2, no. 10, pp. 3234–3250, May 2021. DOI: 10.1039/D1MA00216C.

[121] Mayyas, A., Steward, D., and Mann, M., "The case for recycling: Overview and challenges in the material supply chain for automotive li-ion batteries," *Sustainable Materials and Technologies*, vol. 19, e00087, Apr. 2019. DOI: 10.1016/J.SUSMAT.2018.E00087.

[122] Costa, C. M., Barbosa, J. C., Gonçalves, R., Castro, H., Campo, F. J., and Lanceros-Méndez, S., "Recycling and environmental issues of lithium-ion batteries: Advances, challenges and opportunities," *Energy Storage Materials*, vol. 37, pp. 433–465, May 2021. DOI: 10.1016/J.ENSM.2021.02.032.

[123] Ziegler, M. S. and Trancik, J. E., "Re-examining rates of lithium-ion battery technology improvement and cost decline," *Energy & Environmental Science*, vol. 14, no. 4, pp. 1635–1651, Apr. 2021. DOI: 10.1039/D0EE02681F.

[124] Way, R., Ives, M. C., Mealy, P., and Farmer, J. D., "Empirically grounded technology forecasts and the energy transition," *Joule*, vol. 6, no. 9, pp. 2057–2082, 2022. DOI: 10.1016/j.joule.2022.08.009.

[125] Frith, J. T., Lacey, M. J., and Ulissi, U., "A non-academic perspective on the future of lithium-based batteries," *Nature Communications*, vol. 14, no. 1, 2023. DOI: 10.1038/s41467-023-35933-2.

[126] Jones, S. D., Nguyen, H., Richardson, P. M., Chen, Y. Q., Wyckoff, K. E., Hawker, C. J., Clément, R. J., Fredrickson, G. H., and Segalman, R. A., "Design of Polymeric Zwitterionic Solid Electrolytes with Superionic Lithium Transport," *ACS Central Science*, vol. 8, no. 2, pp. 169–175, Feb. 2022. DOI: 10.1021/ACSCENTSCI.1C01260/ASSET/IMAGES/LARGE/OC1C01260{_}0003.JPEG.

[127] Yu, X., Hoffman, Z. J., Lee, J., Fang, C., Gido, L. A., Patel, V., Eitouni, H. B., Wang, R., and Balsara, N. P., "A Practical Polymer Electrolyte for Lithium and Sodium Batteries: Poly(pentyl malonate)," *ACS Energy Letters*, vol. 7, no. 11, pp. 3791–3797, 2023. DOI: 10.1021/acsenergylett.2c02128.

[128] Snyder, R. L., Choo, Y., Gao, K. W., Halat, D. M., Abel, B. A., Sundararaman, S., Prendergast, D., Reimer, J. A., Balsara, N. P., and Coates, G. W., "Improved Li+Transport in Polyacetal Electrolytes: Conductivity and Current Fraction in a Series of Polymers," *ACS Energy Letters*, vol. 6, no. 5, pp. 1886–1891, 2021. DOI: 10.1021/acsenergylett.1c00594.

[129] Fang, C., Yu, X., Chakraborty, S., Balsara, N. P., and Wang, R., "Molecular Origin of High Cation Transference in Mixtures of Poly(pentyl malonate) and Lithium Salt," *ACS Macro Letters*, vol. 12, no. 5, pp. 612–618, 2023. DOI: 10.1021/acsmacrolett.3c00041.

[130] Stewart, S. and Newman, J., "Measuring the Salt Activity Coefficient in Lithium-Battery Electrolytes," *Journal of The Electrochemical Society*, vol. 155, no. 6, A458, 2008. DOI: 10.1149/1.2904526.

[131] Grundy, L. S., Galluzzo, M. D., Loo, W. S., Fong, A. Y., Balsara, N. P., and Takacs, C. J., "Inaccessible Polarization-Induced Phase Transitions in a Block Copolymer Electrolyte: An Unconventional Mechanism for the Limiting Current," *Macromolecules*, vol. 55, no. 17, pp. 7637–7649, 2022. DOI: 10.1021/acs.macromol.2c00922.

Appendices

A Dependence of PEO Salt Diffusion Coefficient on Molecular Weight

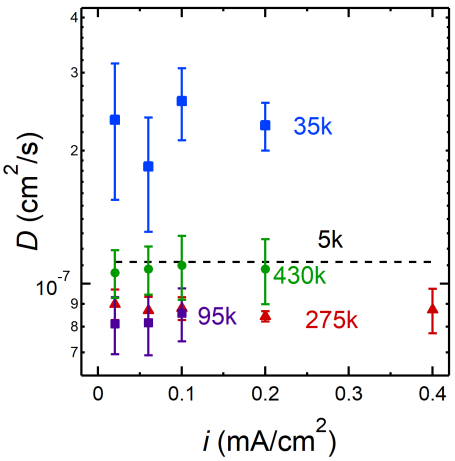

Figure A1: Salt diffusion coefficient, D, measured for $r = 0.08$ PEO/LiTFSI electrolytes with PEO molecular weights of 35 kg/mol (blue squares), 95 kg/mol (purple squares), 275 kg/mol (red triangles), and 430 kg/mol (green circles), plotted as a function of the applied current density. The dashed line shows data from Reference 48.

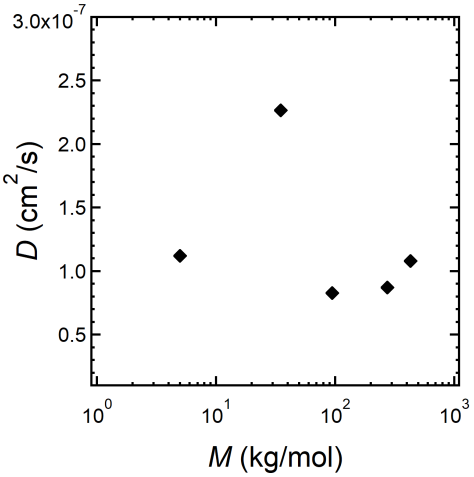

Figure A2: Salt diffusion coefficient, D, plotted as a function of molecular weight of PEO. Data points represent the average of measurements at various applied current densities. 5 kg/mol data is taken from 48.

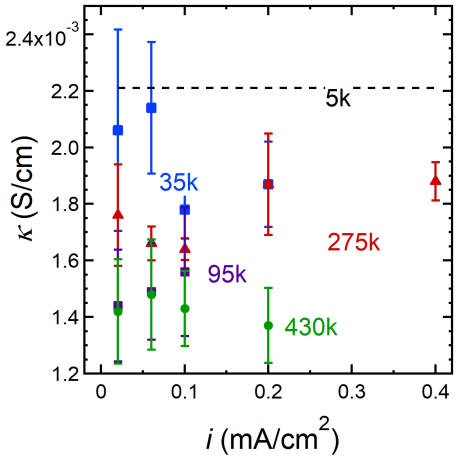

Figure A3: Conductivity, κ, measured for $r = 0.08$ PEO/LiTFSI electrolytes with PEO molecular weights of 35 kg/mol (blue squares), 95 kg/mol (purple squares), 275 kg/mol (red triangles), and 430 kg/mol (green circles), plotted as a function of the applied current density.. The dashed line shows data from Reference 48.